



ΕΘΝΙΚΟ ΜΕΤΣΟΒΙΟ ΠΟΛΥΤΕΧΝΕΙΟ
ΣΧΟΛΗ ΠΟΛΙΤΙΚΩΝ ΜΗΧΑΝΙΚΩΝ - ΤΟΜΕΑΣ ΓΕΩΤΕΧΝΙΚΗΣ
Ηρώων Πολυτεχνείου 9, Πολυτεχνειούπολη Ζωγράφου 157 80
Τηλ: 210 772 3780, Fax: 210 772 3428,
e-mail: gbouck@central.ntua.gr www.georgebouckovalas.com

ΠΡΑΞΗ:

**«ΘΑΛΗΣ- ΕΜΠ: ΠΡΩΤΟΤΥΠΟΣ ΣΧΕΔΙΑΣΜΟΣ ΒΑΘΡΩΝ
ΓΕΦΥΡΩΝ ΣΕ ΡΕΥΣΤΟΠΟΙΗΣΙΜΟ ΕΔΑΦΟΣ ΜΕ ΧΡΗΣΗ
ΦΥΣΙΚΗΣ ΣΕΙΣΜΙΚΗΣ ΜΟΝΩΣΗΣ»**

MIS 380043

Επιστημονικός Υπεύθυνος: Καθ. Γ. ΜΠΟΥΚΟΒΑΛΑΣ

ΔΡΑΣΗ 8

Εφαρμογή σε Χαλύβδινη Καλωδιωτή Γέφυρα

ΠΑΡΑΔΟΤΕΑ:

***Κριτήρια Επιτελεστικότητας
για Χαλύβδινη Καλωδιωτή Γέφυρα (Π8α)***

Ιανουάριος 2015



ΕΙΣΑΓΩΓΗ

Η παρούσα Τεχνική Έκθεση αποτελεί το Παραδοτέο Π8α της Δράσης (Επιμέρους Εργασίας) Δ8 του Ερευνητικού Προγράμματος με τίτλο:

ΘΑΛΗΣ-ΕΜΠ (MIS 380043)

Πρωτότυπος Σχεδιασμός Βάθρων Γεφυρών σε Ρευστοποιήσιμο Έδαφος με Φυσική Σεισμική Μόνωση

με Συντονιστή (Ερευνητικό Υπεύθυνο) τον Γεώργιο Μπουκοβάλα Καθηγητή ΕΜΠ, και με Επιστημονικό Υπεύθυνο της Δράσης Δ8 τον Χάρη Γαντέ, Καθηγητή ΕΜΠ.

Συγκεκριμένα, η εν λόγω Δράση Δ8, με τίτλο:

"Εφαρμογή σε Χαλύβδινη (Καλωδιωτή) Γέφυρα".

αφορά στην εφαρμογή και συγκριτική αξιολόγηση της προτεινόμενης νέας μεθοδολογίας σχεδιασμού σε χαλύβδινη γέφυρα, ενώ το αντικείμενο του εν λόγω παραδοτέου περιγράφεται στην εγκεκριμένη ερευνητική πρόταση ως ακολούθως:

"Ο σκοπός της Ερευνητικής Ομάδας είναι να διερευνήσει τη δυνατότητα εφαρμογής της προτεινόμενης μεθοδολογίας σχεδιασμού και τα προτερήματα έναντι συμβατικών μεθόδων σχεδιασμού για την περίπτωση μιας καλωδιωτής γέφυρας, με χαλύβδινους πυλώνες και σύμμικτο κατάστρωμα. Αυτός ο τύπος γέφυρας, αν και είναι λιγότερο διαδεδομένος στην Ελλάδα, μπορεί να αποτελέσει μία τεχνικά και οικονομικά καλύτερη λύση σε περιπτώσεις γεφυρών μεσαίων-μεγάλων ανοιγμάτων ανάμεσα στα μεσόβαθρα (π.χ. μεγαλύτερα από 80m). Παράλληλα, παρουσιάζει συγκεκριμένες ιδιαιτερότητες σε σχέση με τις γέφυρες από σκυρόδεμα των Δράσεων 6 και 7, λόγω των διαφορετικών υλικών κατασκευής αλλά και λόγω της πιο εύκαμπτης απόκρισης, η οποία μπορεί να οδηγήσει σε: (α) λιγότερο αυστηρά κριτήρια επιτελεστικότητας βάσει των επιτρεπόμενων μετακινήσεων της θεμελίωσης, αλλά επίσης (β) αυξανόμενο κίνδυνο συντονισμού του φορέα της ανωδομής κατά τη λειτουργία του ρευστοποιημένου εδάφους ως «φυσικού» συστήματος σεισμικής μόνωσης.

Οι κύριες δραστηριότητες που θα πρέπει να πραγματοποιηθούν για την ολοκλήρωση αυτής της Δράσης είναι οι ακόλουθες:

(α) Αρχικώς, θα πρέπει να εκτιμηθούν οι επιτρεπόμενες μετακινήσεις στη θεμελίωση (καθιζήσεις και στροφές) για διάφορους τύπους καλωδιωτών γεφυρών, και συγκεκριμένα για τύπο «άρπας» (*harp*) και ακτινωτό (*fan*), με μονόπλευρο ή αμφίπλευρους πυλώνες, καθώς και για ανηρτημένες γέφυρες με κύριο καλώδιο μεταξύ των κορυφών των πυλώνων και κατακόρυφους αναρτήρες. Θα ληφθούν υπόψη τα επιτρεπόμενα επίπεδα βλάβης και

λειτουργικότητας (π.χ. όχληση στην οδήγηση, επισκευάσιμες βλάβες, μή επισκευάσιμες βλάβες) καθώς και το αναμενόμενο επίπεδο σεισμικότητας (π.χ. σεισμική διέγερση με 90, 450 ή 900 χρόνια περίοδο επαναφοράς) και θα καθοριστούν μετά από μία συλλογική αξιολόγηση των παρακάτω:

- μία εκτεταμένη βιβλιογραφική έρευνας των συναφών κανονιστικών διατάξεων και οδηγιών (π.χ. Ευρωκώδικας 2 – Μέρος 2, Ευρωκώδικας 8 – Μέρος 2, Ευρωκώδικας 7, MCEER & FHA – κεφάλαιο 11.4),
- παραδείγματα απόκρισης από ήδη κατασκευασμένες γέφυρες κατά τη διάρκεια πρόσφατων σεισμών, και
- παραμετρικές αναλύσεις διαφόρων δομικών στοιχείων της γέφυρας (π.χ. μεσόβαθρα, καλώδια, κατάστρωμα) υπό στατικές και ανακυκλιζόμενες δυναμικές φορτίσεις.

(β) Στη συνέχεια, τα βάθρα μιας τυπικής καλωδιωτής γέφυρας, τύπου «άρπας» ή ακτινωτού, με μεσαίο άνοιγμα 80-120m μεταξύ των πυλώνων, θα σχεδιαστούν με βάση την συμβατική μεθοδολογία θεμελίωσης, με χρήση ομάδας πασσάλων και καθολική βελτίωση του εδάφους στην περιοχή της θεμελίωσης. Πρόθεσή μας είναι να επιλέξουμε μία υπαρκτή γέφυρα ή μία μελετημένη γέφυρα σε στάδιο οριστικής μελέτης σε περιοχή ποταμού, όπου οι συνθήκες του υπεδάφους είναι καθορισμένες από πλήρεις γεωτεχνικές μελέτες, ενώ προβλέπεται εκτεταμένη ρευστοποίηση κάτω από ένα ή περισσότερα βάθρα της γέφυρας.

(γ) Τέλος, η διαστασιολόγηση της γέφυρας σε στατικού και σεισμικούς συνδυασμούς φορτίσεων θα επαναληφθεί για τη νέα μεθοδολογία της «φυσικής» σεισμικής μόνωσης, εφαρμόζοντας επιφανειακή θεμελίωση και μερική βελτίωση του ρευστοποιήσιμου εδάφους με δημιουργία επιφανειακής μόνον κρούστας, σε συνδυασμό με τις επιτρεπόμενες μετακινήσεις στη θεμελίωση που θα καθοριστούν στο βήμα (α) που περιγράφηκε παραπάνω. Τα πλεονεκτήματα αλλά και οι περιορισμοί της νέας μεθοδολογίας θα συγκριθούν με τα αντίστοιχα της συμβατικής λύσης και θα αξιολογηθούν με βάση τόσο τεχνικών όσο και οικονομικών κριτηρίων.

Η παρούσα Ερευνητική Έκθεση - παραδοτέο, αφορά στην Επιμέρους Εργασία (α) ανωτέρω, ενώ οι Επιμέρους Εργασίες (β) και (γ) βρίσκονται σε εξέλιξη και θα περιγραφούν σε επόμενη Ερευνητική Έκθεση - Παραδοτέο (Π8β).

Επισημαίνεται ότι, κατά τα πρώτα βήματα αυτής της διερεύνησης, διαπιστώθηκε ότι οι τάσεις εδάφους λόγω μονίμων φορτίων στις θέσεις των βάθρων κοινών καλωδιωτών ή κρεμαστών γεφυρών ήταν μεγαλύτερες από τα όρια που θεωρήθηκαν ως αποδεκτά για την προτεινόμενη καινοτόμο λύση, για βάθρα που θεμελιώνονται σε ρευστοποιήσιμα εδάφη. Γι' αυτό αποφασίστηκε να μελετηθεί η περίπτωση μιας τοξωτής μεταλλικής γέφυρας με ανηρημένο σύμμικτο κατάστρωμα, που είναι μία συνήθης λύση γέφυρας με καλώδια για μικρότερα ανοίγματα και επομένως οδηγεί σε μικρότερες τάσεις εδάφους λόγω μονίμων φορτίων. Πέραν τούτου, ο εν λόγω τύπος γέφυρας διατηρεί πολλά από τα χαρακτηριστικά των καλωδιωτών γεφυρών (π.χ. μεγαλύτερη ανοχή σε μετακινήσεις της θεμελίωσης) και έτσι ικανοποιεί πλήρως τις απαιτήσεις του ερευνητικού προγράμματος.

ΜΕΘΟΔΟΛΟΓΙΑ ΚΑΙ ΑΠΟΤΕΛΕΣΜΑΤΑ

Όπως προαναφέρθηκε, μελετάται μία οδική τοξωτή μεταλλική γέφυρα με ανηρημένο σύμμικτο κατάστρωμα δύο αμφιέριστων τμημάτων, κατά την επιβολή μετακινήσεων και στροφών στη βάση του μεσοβάθρου λόγω ρευστοποίησης των υποκείμενων εδαφικών σχηματισμών. Η γέφυρα θεωρείται πως θεμελιώνεται επιφανειακά σε έδαφος ρευστοποιήσιμο σε μεγάλο βάθος. Στόχος της διερεύνησης είναι ο προσδιορισμός των ανεκτών καθιζήσεων και στροφών που μπορεί να παραλάβει η γέφυρα χωρίς να αστοχήσει.

Η γέφυρα που μελετάται αποτελείται από δύο αμφιέριστα ανοίγματα θεωρητικού μήκους 42.00m το καθένα, τα οποία συνδέονται μεταξύ τους με πλάκα συνέχειας. Το θεωρητικό

πλάτος του καταστρώματος ισούται με 14.70m. Το κατάστρωμα της γέφυρας είναι σύμμικτο και το κάθε άνοιγμα αποτελείται από δύο κύριες δοκούς και δεκαεφτά διαδοκίδες. Κάθε κύρια δοκός αναρτάται από ένα τόξο με τη χρήση αναρτήρων ενώ τα δύο τόξα του κάθε ανοίγματος συνδέονται μεταξύ τους με εγκάρσιους και διαγώνιους συνδέσμους δυσκαμψίας. Το ύψος των τόξων είναι ίσο με 10.00m. Οι δοκοί, οι διαδοκίδες, τα τόξα και οι σύνδεσμοι δυσκαμψίας έχουν κατασκευαστεί από δομικό χάλυβα. Το μεσόβαθρο αποτελείται από τη δοκό έδρασης και τρεις στύλους κυκλικής συμπαγούς διατομής από οπλισμένο σκυρόδεμα μορφώνοντας έτσι ένα πλαίσιο στην εγκάρσια έννοια της γέφυρας, έχει δε ύψος 10m συμπεριλαμβανομένης της δοκού έδρασης. Τα ακρόβαθρα θεωρούνται πολύ δύσκαμπτα σε σχέση με τη γέφυρα και γι' αυτό λαμβάνονται υπόψη ως ακλόνητα.

Επιβάλλονται κατακόρυφες μετακινήσεις και στροφές στο επίπεδο θεμελίωσης του μεσοβάθρου, εκπονούνται μη γραμμικές αναλύσεις, λαμβάνοντας υπόψη τη γεωμετρική μη γραμμικότητα, καθώς και τη μη γραμμικότητα των υλικών. Η μη γραμμική συμπεριφορά των στύλων του μεσοβάθρου από οπλισμένο σκυρόδεμα έχει προσομοιωθεί με τη χρήση διαγραμμάτων ρομών – καμπυλοτήτων. Καταγράφεται η συμπεριφορά όλων των κρίσιμων μελών της γέφυρας, συμπεριλαμβανομένων των μεταλλικών στοιχείων της ανωδομής, των εφεδράνων και του μεσοβάθρου, έως την πρώτη αστοχία. Ως πρώτη αστοχία ορίζεται η πρώτη διαρροή στη βάση των στύλων του μεσοβάθρου, ο σχηματισμός πλαστικών αρθρώσεων στην κορυφή των στύλων αυτών, ή η αστοχία κύριων μεταλλικών στοιχείων. Αστοχία σε στοιχεία όπως εφέδρανα, πλάκα συνέχειας ή διαγώνιοι σύνδεσμοι δυσκαμψίας μεταξύ των τόξων δεν μπορούν να προκαλέσουν κατάρρευση της γέφυρας και μπορούν να επισκευαστούν ή και να αντικατασταθούν εύκολα. Επομένως δεν λαμβάνονται υπόψη για τον καθορισμό των επιτρεπόμενων εδαφικών μετακινήσεων. Ωστόσο, στις αναλύσεις λαμβάνεται υπόψη η μεταβολή της δυσκαμψίας τους σε περίπτωση που υφίστανται βλάβες. Παράλληλα, δεν μελετάται η απόκριση της δοκού έδρασης καθώς είναι αρκετά δύσκαμπτη και δεν επηρεάζεται σημαντικά από τις επιβαλλόμενες μετακινήσεις και στροφές.

Από τις αναλύσεις προέκυψε πως κρίσιμότερη είναι η στροφή περί το διαμήκη άξονα της γέφυρας, προκαλώντας πλαστικές αρθρώσεις στις κορυφές των στύλων του μεσοβάθρου. Αντίστοιχα, η στροφή περί τον εγκάρσιο άξονα της γέφυρας προκαλεί σημαντικές καμπτικές ροπές στη βάση των στύλων, καθιστώντας κρίσιμη τη διαρροή των διατομών στις θέσεις εκείνες. Ωστόσο, δεν παρατηρείται αστοχία στα μεταλλικά στοιχεία της γέφυρας, παρά μόνο κάποια φαινόμενα λυγισμού στους διαγώνιους συνδέσμους δυσκαμψίας, οι οποίοι είναι εύκολα αντικαταστάσιμοι και δεν μπορούν να προκαλέσουν κατάρρευση της γέφυρας. Επίσης δεν παρατηρείται καμία βλάβη στα εφέδρανα. Η μικρότερη ανεκτή καθίζηση ρ που μπορεί να υποστεί η γέφυρα χωρίς να προκληθούν ανεπανόρθωτες βλάβες που μπορεί να οδηγήσουν σε κατάρρευση είναι της τάξεως των $\rho_{\max}=24\text{cm}$, ενώ η συνδυασμένη στροφή ως προς τυχαίο άξονα ανέρχεται σε $\theta_{\max}=0.05\rho_{\max}= 1.2^\circ$.



NATIONAL TECHNICAL UNIVERSITY OF ATHENS
SCHOOL OF CIVIL ENGINEERING – GEOTECHNICAL DEPARTMENT
9 Iroon Polytechniou str., 15780, Zografou Campus, Greece
Tel: 210 772 3780, Fax: 210 772 3428,
e-mail: gbouck@central.ntua.gr www.georgebouckovalas.com

PROJECT:

«**THALIS-NTUA: INNOVATIVE DESIGN OF BRIDGE PIERS
ON LIQUEFIABLE SOILS WITH THE USE OF NATURAL
SEISMIC ISOLATION**»

MIS 380043

Coordinator: Prof. G. BOUCKOVALAS

WORK PACKAGE 8

Application to Steel Cable Bridge

DELIVERABLES:

Performance Criteria for Steel Cable Bridge (D8a)

January 2015



TABLE OF CONTENTS

1.	INTRODUCTION	8
2.	BRIDGE DESCRIPTION	10
2.1	Geometry and cross sections	10
2.2	Materials	14
3.	DEFORMATION LIMITS FOR BRIDGES.....	15
3.1	Bridge deformations	15
3.2	Movement Criteria	17
3.2.1	Literature survey	17
3.2.2	Provisions of Codes	19
3.2.3	Other approaches	21
3.3	Performance criteria for the case study	22
4.	APPLIED CODES.....	25
5.	MODELING ISSUES	26
5.1	Model of the bridge	26
5.2	Constitutive laws of materials	29
5.2.1	Structural Steel S355	29
5.2.2	Reinforced Concrete C35/45 of deck's slab.....	30
5.2.3	Reinforced Concrete C30/37 of pier's beam.....	30
5.2.4	Reinforced Concrete C30/37 of the pier	30
5.2.5	Reinforcing steel B500C.....	31
5.3	Nonlinear behavior of the bridge's components.....	32
5.3.1	Pier's columns.....	32
5.3.2	Bearings	34
5.4	Load Cases	36
5.5	Load Combinations at Ultimate Limit State (ULS)	39
6.	LINEAR BUCKLING ANALYSIS	41
6.1	Buckling modes	41
6.2	Initial imperfections	43

7.	IMPOSED ROTATIONS AND SETTLEMENTS	47
7.1	Loading sequence.....	47
7.2	Case 1 ($\theta_x + \rho$)	48
7.2.1	Imposed settlement ρ and rotation θ_x	48
7.2.2	Response of the bridge for Combination 1	49
7.2.3	Permissible rotation and settlement for Combination 1	56
7.2.4	Inclination angle of the pier for Combination 1.....	57
7.2.5	Response of the bridge for Combination 2	58
7.2.6	Permissible rotation and settlement for Combination 2	61
7.2.7	Inclination angle of the pier for Combination 2.....	62
7.3	Case 2 ($\theta_y + \rho$)	63
7.3.1	Imposed settlement ρ and rotation θ_y	63
7.3.2	Response of the bridge for Combination 1	63
7.3.3	Permissible rotation and settlement for Combination 1	67
7.3.4	Inclination angle of the pier for Combination 1.....	68
7.3.5	Response of the bridge for Combination 2	69
7.3.6	Permissible rotation and settlement for Combination 2	72
7.3.7	Inclination angle of the pier for Combination 2.....	73
7.4	Case 3 ($\theta_x + 0.3\theta_y + \rho$).....	74
7.4.1	Imposed settlement ρ and rotations θ_x and θ_y	74
7.4.2	Response of the bridge for Combination 1	74
7.4.3	Permissible rotation and settlement for Combination 1	78
7.4.4	Inclination angle of the pier for Combination 1.....	79
7.4.5	Response of the bridge for Combination 2	80
7.4.6	Permissible rotation and settlement for Combination 2	84
7.4.7	Inclination angle of the pier for Combination 2.....	85
7.5	Case 4 ($0.3\theta_x + \theta_y + \rho$).....	85
7.5.1	Imposed settlement ρ and rotations θ_x and θ_y	85
7.5.2	Response of the bridge for Combination 1	86
7.5.3	Permissible rotation and settlement for Combination 1	90
7.5.4	Inclination angle of the pier for Combination 1.....	91
7.5.5	Response of the bridge for Combination 2	92
7.5.6	Permissible rotation and settlement for Combination 2	95
7.5.7	Inclination angle of the pier for Combination 2.....	97
8.	SUMMARY AND CONCLUSIONS	98
9.	REFERENCES	100

Chapter 1

INTRODUCTION

This Technical Report constitutes part of Deliverable 8 of the Research Project entitled:

THALIS-NTUA (MIS 380043)

Innovative Design of Bridge Piers on Liquefiable Soils with the use of Natural Seismic Isolation

performed under the general coordination of Professor George Bouckovalas (Principal Investigator) and Professor Charis Gantes (Scientific Responsible for WP8).

Namely, it presents the actions taken and the associated results of Work Package WP8, entitled:

"Application to large span, cable-stayed bridges"

The Scope of **Work Package WP8**, has been described in the approved Research Proposal as follows:

"The aim of this WP is to explore the feasibility of the proposed new design methodology, and the resulting advantages over conventional design methods, in the case of a cable-stayed bridge, with steel piers and composite deck system. This bridge type, although less common in Greece, may provide a technically and economically optimum solution for cases of medium-large spans between the piers (e.g. larger than 80 m). In parallel, it presents specific peculiarities as compared to the RC bridges of WP 6 and WP 7, due to the different construction materials, as well as due to the more flexible response which may lead to: (a) less strict performance criteria with regard to the allowable foundation movements, but also (b) increased risk of structure-to-excitation resonance when part of the liquefied ground will act as a "natural" base isolation system.

The main work tasks required to achieve the aim of this WP are the following:

(a) *Initially, the allowable foundation movements (settlements and rotations) will have to be established for different types of cable-stayed bridges, namely "harp" and "fan" types, with one or two pylons, as well as cable suspended bridges with a main suspension cable between the pylon tops and vertical hangers. The relevant criteria will take into account the permissible damage and serviceability levels (e.g. driving discomfort, repairable damage, non-repairable damage), as well as the anticipated seismicity level (e.g. seismic excitation with 90, 450 or 900 years return period), and will be established after a joint evaluation of:*

- *an extensive literature survey of relevant codes and guidelines (e.g. Eurocode 2-Part 2, Eurocode 8-Part 2, Eurocode 7, MCEER & FHA-chapter 11.4),*

- *examples of actual bridge performance during recent earthquakes, and*
- *parametric analyses of various bridge components (e.g. pylons, cables, deck) under static and cyclic dynamic loading.*

(b) *Next, the pylons of a typical "harp" or "fan" type cable-stayed bridge, with a midspan of 80-120m, will be designed using the conventional foundation approach, i.e. pile groups with ground improvement between and around the piles. It is our intention to select an actual (existing or in the design stage) river bridge site, where the subsoil conditions are well established by geotechnical surveys, while extensive liquefaction is expected underneath one or more of the bridge piers.*

(c) *Finally, the static and seismic design of this bridge will be repeated with the new methodology of "natural" seismic isolation (i.e. shallow foundation and partial improvement, of the top part only of the liquefiable soil), in connection with the allowable foundation movements which were established in work task (1) above. The comparative advantages and limitations of the new design methodology, relative to the conventional ones, will be consequently evaluated on the basis of technical, as well as cost criteria."*

The present Research Report -Deliverable (D8a) refers to work task (a) above, while the remaining work tasks (b) and (c) are currently in progress and will be described in a separate Research Report - Deliverable (D8b).

It should be clarified in advance that, during the initial phases of this investigation it was established that the soil stresses due to permanent loads developing under the piers of common cable-stayed and cable suspended bridges exceeded the values which are considered as acceptable for the proposed innovative solution of piers seated on liquefiable soil. It was therefore decided to address in this WP the case of an arch steel bridge with suspended deck, which is a solution adopted for smaller spans and therefore leads to smaller soil stresses under permanent loads. Furthermore, this bridge type maintains a number of basic characteristics of cable suspended bridges (i.e. the capacity to sustain relatively large foundation displacements) and consequently satisfies all relevant project requirements.

Chapter 2

BRIDGE DESCRIPTION

2.1 Geometry and cross sections

The bridge under investigation is situated over a riverbank and it is a steel arch road bridge with two simply supported spans, with total length 87.60m. The total width of the deck is equal to 15.00m, while at the supports it becomes 15.55m. The steel members of each span include two (2) main beams, seventeen (17) transverse beams, two (2) arches connected with transverse and diagonal bracing members. Each main beam is suspended by each arch with seven (7) hangers. The distance of the transverse steel beams is 2.625m. A composite deck is formed using trapezoidal profiles of type SYMDECK 150 and a concrete slab. The total thickness of the composite slab is 35cm. The concrete slab is connected with the transverse and main beams through steel shear connectors in order to ensure composite action.

The characteristics of the bridge's steel members are listed in Table 2.1. The elevation view of a single span is illustrated in Figure 2.1, the arrangement in plan view of the main and transverse beams is shown in Figure 2.2, the plane view of the bridge in Figure 2.3 and the section of the bridge at mid span in Figure 2.4.

Table 2.1: Characteristics of the bridge's steel members

Πίνακας 2.1: Χαρακτηριστικά των μεταλλικών στοιχείων της γέφυρας

Type	Total number	Cross section	Length of each member	Theoretical span/rise
Main beams	4	HEB900	43.30m	42.00m
Transverse beams	34	HEB900	14.30m	14.70m
Arches	4	CHS750/20	47.70m	42.00m / 10.00m
Transverse bracing members	10	CHS244.5/8	13.95m	14.70m
Diagonal bracing members	16	CHS139.7/8	8.45m	9.13m
Hangers	28	CHS168.3/8	3.90m – 9.625m	4.375m – 10.00m

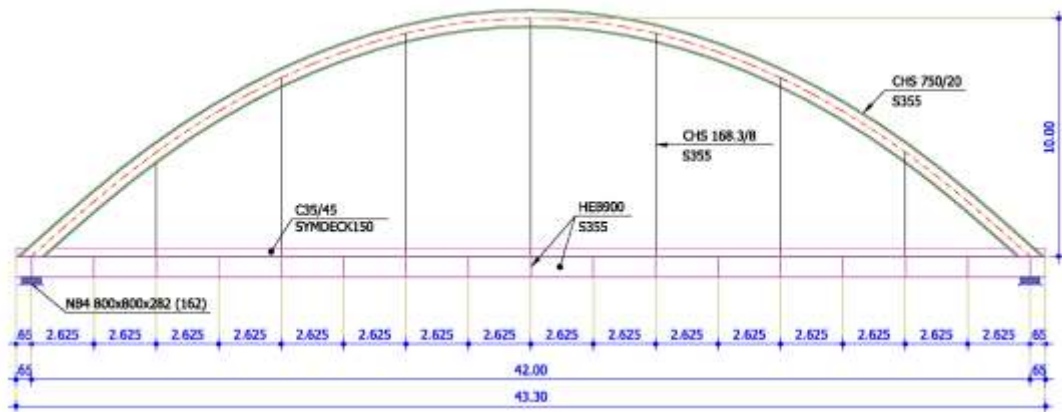


Figure 2.1: Elevation view of a single span

Σχήμα 2.1: Όψη εντός ανοίγματος γέφυρας

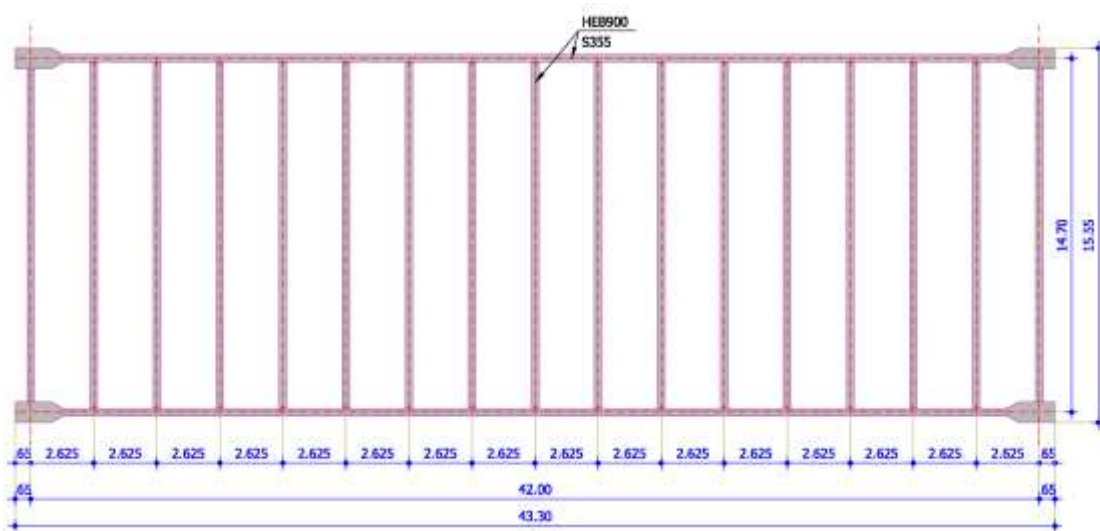


Figure 2.2: Arrangement in plan view of the deck's beams of a single span

Σχήμα 2.2: Διάταξη δοκών καταστρώματος εντός ανοίγματος γέφυρας

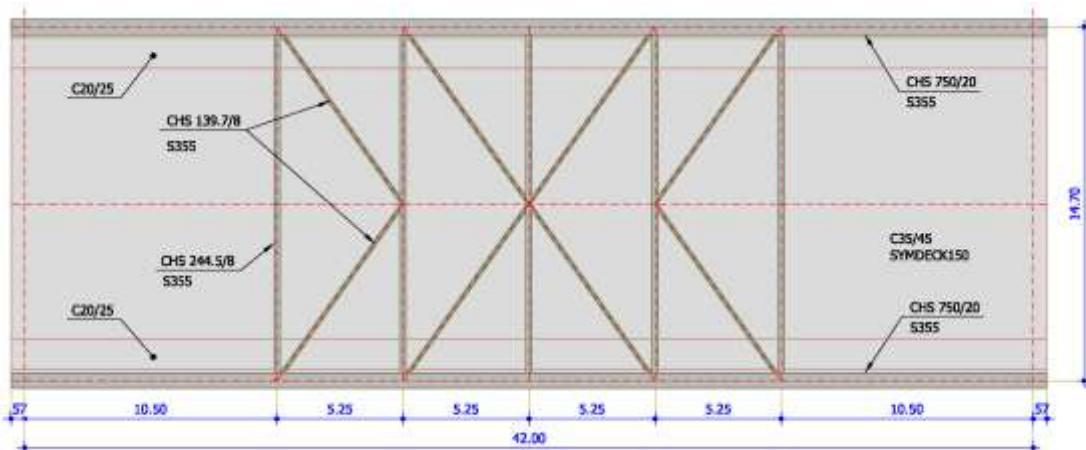


Figure 2.3: Plan view of a single span

Σχήμα 2.3: Κάτοψη εντός ανοίγματος γέφυρας

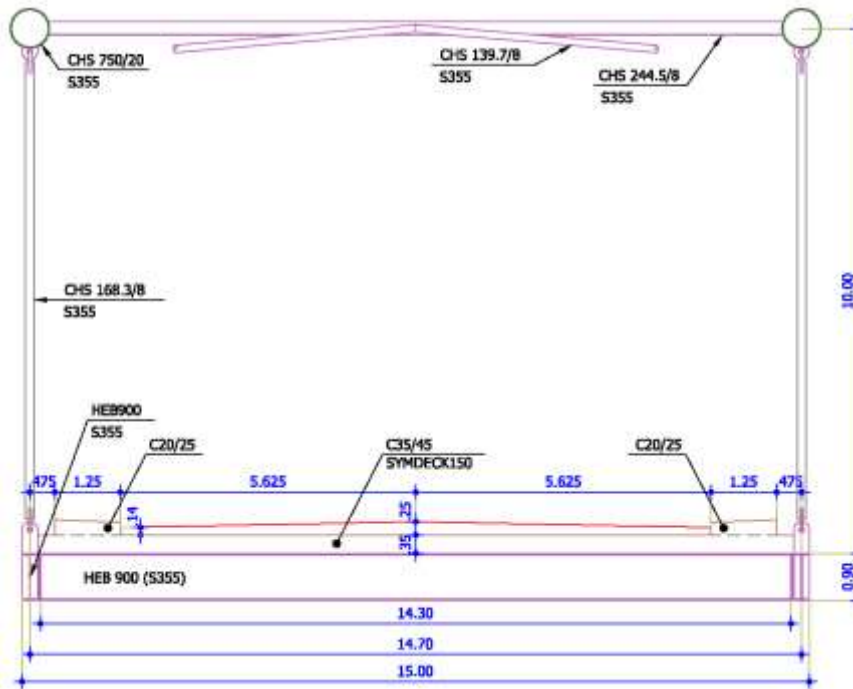


Figure 2.4: Section of the bridge at midspan

Σχήμα 2.4: Εγκάρσια τομή γέφυρας στο μέσον του ανοίγματος

The pier consists of three circular reinforced concrete columns, 8.00m tall, having a circular cross section of 1.50m diameter. The distance between the three columns is equal to 7.35m. They are connected at the top with a 17.00m long concrete beam, having the rectangular cross-section of dimensions 4.50m x 2.00m. Fixed supports are considered at the base of the columns. The geometry of the pier in the longitudinal direction of the bridge is shown in Figure 2.5. The section of the bridge at the pier is given in Figure 2.6. The elevation view of the bridge is illustrated in Figure 2.7.

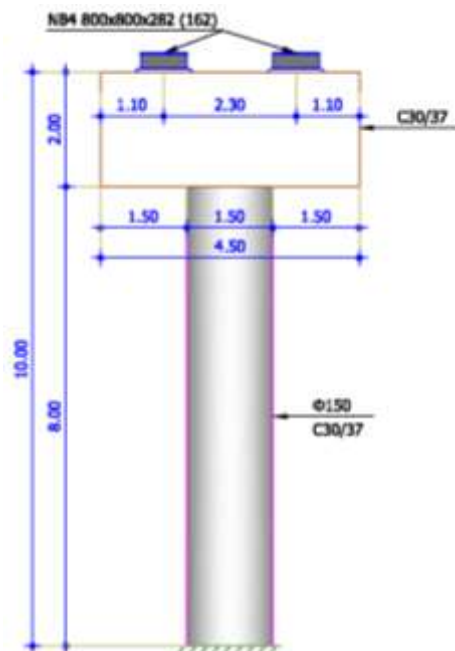


Figure 2.5: Geometry of the pier in longitudinal section

Σχήμα 2.5: Γεωμετρία μεσοβάθρου στη διαμήκη έννοια

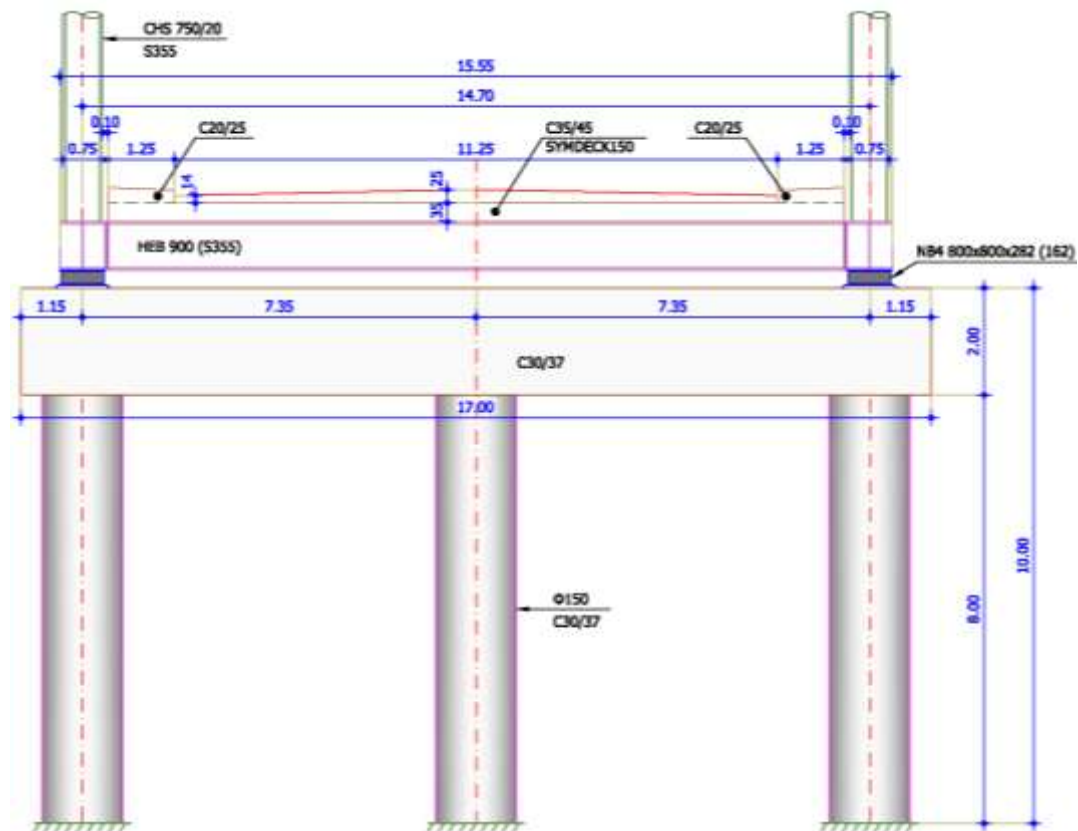


Figure 2.6: Section of the bridge at the pier
Σχήμα 2.6: Εγκάρσια τομή γέφυρας στη θέση μεσοβάθρου

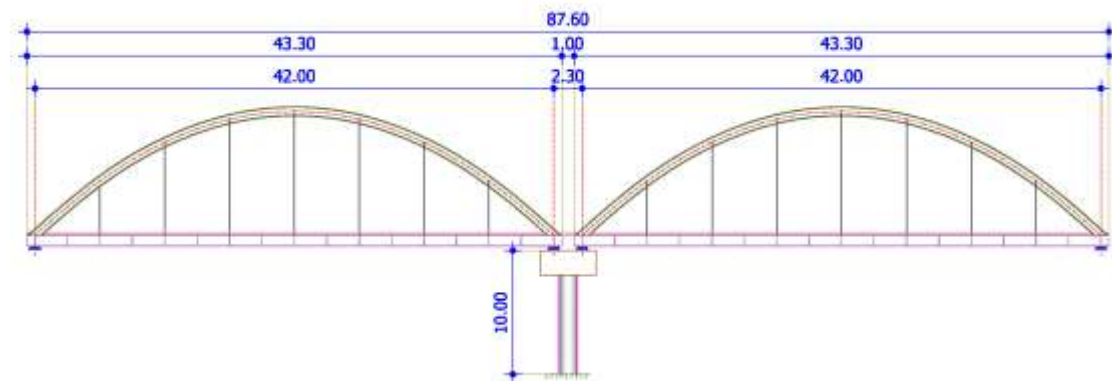


Figure 2.7: Elevation view of the bridge
Σχήμα 2.7: Όψη γέφυρας

The connection of the deck and the pier and the abutments is realized with anchored elastomeric bearings type NB4 800x800x282 (162). The bearings consist of nine (9) layers of elastomer, with thickness $t_e=0.018\text{m}$. The total thickness of the elastomer is $t=0.162\text{m}$. Details of the bearings are shown in Figure 2.8.

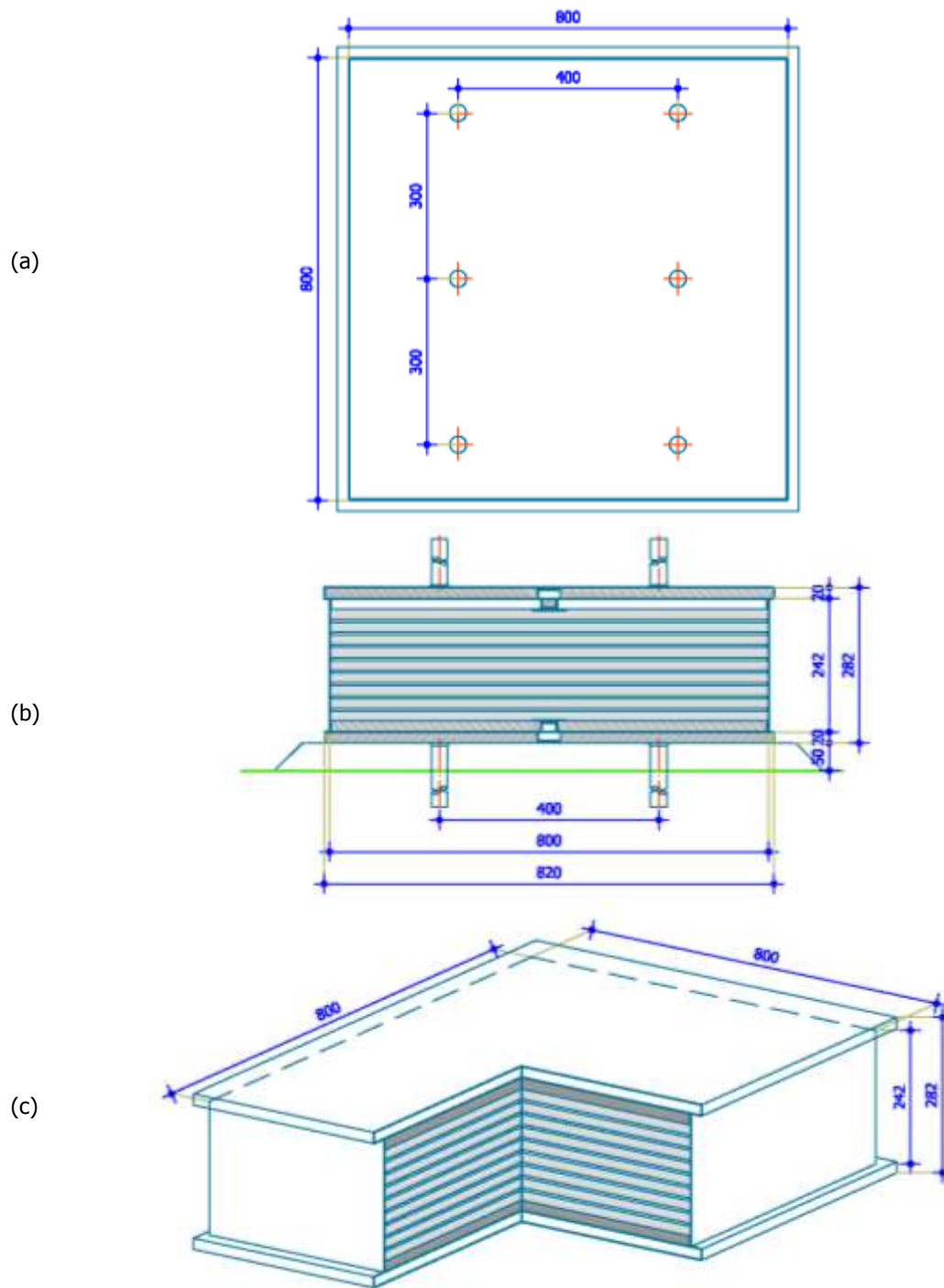


Figure 2.8: Details of the elastomeric bearings: (a) plan view, (b) vertical section, (c) perspective view

Σχήμα 2.8: Λεπτομέρειες ελαστομερικών εφεδράνων: (α) κάτοψη (β) κατακόρυφη τομή (γ) προοπτικό

2.2 Materials

All steel members are made of S355 structural steel. For the composite deck reinforced concrete C35/45 is used, for the sidewalks C20/25, for the columns and the beam of the pier C30/37. The reinforcement steel is B500C.

Chapter 3

DEFORMATION LIMITS FOR BRIDGES

3.1 Bridge deformations

Barker et al. [1] provide the definitions illustrated in Figure 3.1, concerning possible types of deformations (settlements) that may occur in bridges. According to their investigation, bridge deformations may appear in the form of uniform settlement (ρ), uniform tilt (ω) or rotation (θ) and differential settlement (δ).

- Uniform settlement (ρ) is described as the rather theoretical situation in which each of the bridge foundations settles by the same amount. Even though no distortion of the superstructure occurs, excessive uniform settlement can lead to issues such as insufficient clearance at underpasses, as well as discontinuities at the juncture between approach slabs and the bridge deck, also referred to as “the bump at the end of the bridge” [2] and inadequate drainage at the end of the bridge.
- Uniform tilt (ω) or rotation (θ) relates to settlements that vary linearly along the length of the bridge. Such type of deformation is most likely to occur in very stiff superstructures and single-span bridges. Usually, no distortion occurs in the superstructure, except in the case of non-monolithic connection between bridge components. In terms of traffic disturbance the same problems (bumps, drainage and clearance height) as mentioned above may occur.
- Non-uniform settlements correspond to the case when the settlement at each support of a multi span bridge is different. It may be either regular or irregular. A regular pattern in deformation (Figure 3.1c) is characterized by a symmetrical distribution of settlement, from both ends of the bridge towards the center. In the irregular pattern (Figure 3.1d), deformation is randomly distributed along the length of the bridge.
- The non-uniform settlement of bridge foundations is also responsible for the onset of angular distortion (β), which affects the structural integrity of the superstructure. It is schematically described in Figure 3.1c and Figure 3.1d, and defined as:

$$\beta = \frac{\delta}{S} \quad (3-1)$$

where,

β is the angular distortion (dimensionless)

δ is the differential settlement between two consecutive foundations; in units of length

S is span length expressed in the same length units as the differential settlement.

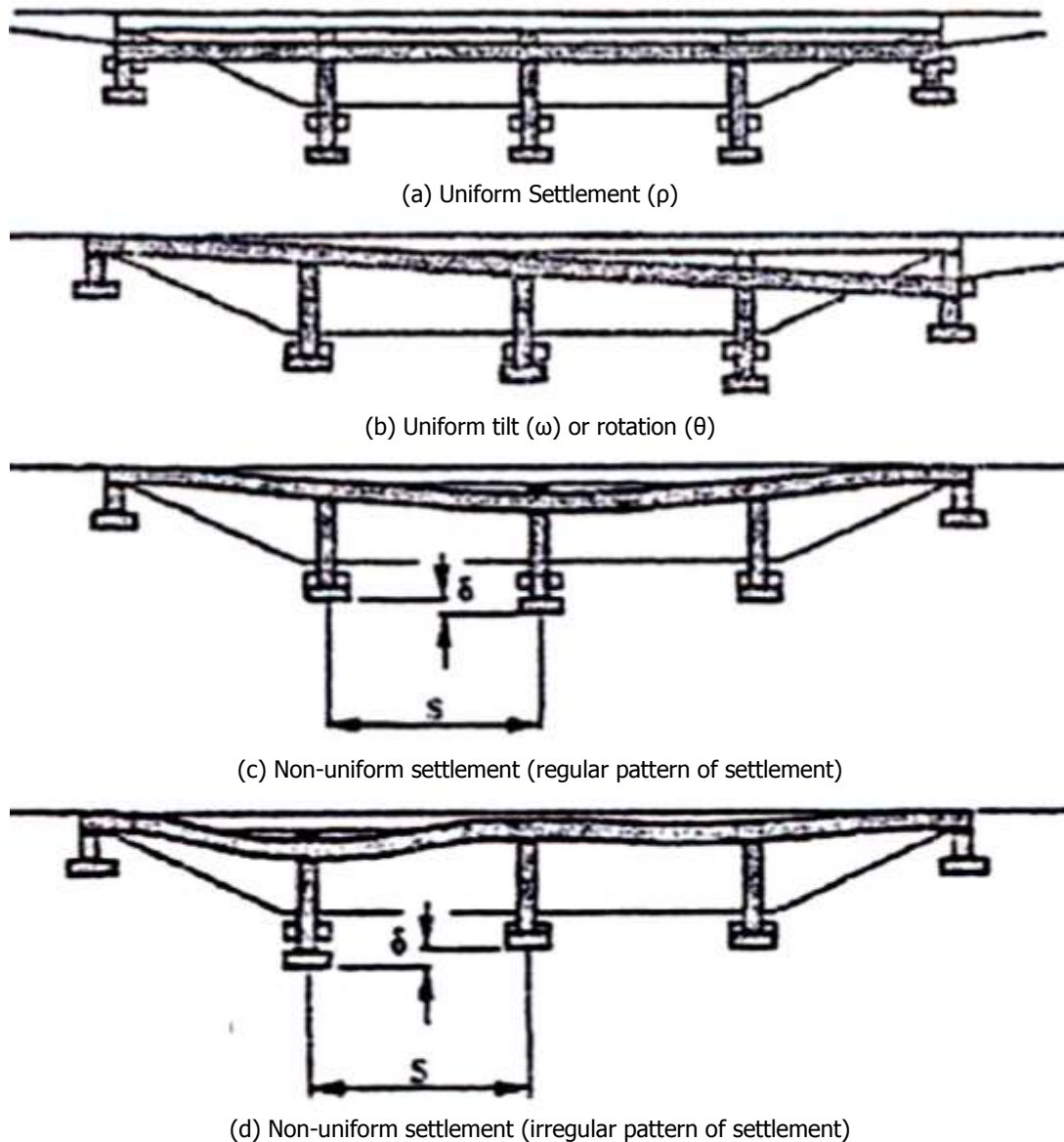


Figure 3.1: Components of settlement and angular distortion in bridges (Barker et al., [1])

Σχήμα 3.1: Συνιστώσες καθίζησης και γωνιακής παραμόρφωσης σε γέφυρες (Barker et al., [1])

Differential settlements induce bending moments and shear in the bridge superstructure when the spans are continuous over supports. These moments and shears can potentially cause structural damage. Distress in the superstructure consists of cracks or other evidence of excessive stress in beams, girders, struts and diaphragms as well as cracking and spalling of the deck. To a lesser extent, differential settlements can also cause damage to a bridge consisting of simple spans. However, the major concern with simple spanned bridges is the operational problems, i.e. inadequate drainage and insufficient clearance height at underpasses and mainly quality surface and aesthetics. Due to a lack of continuity over the supports, the changes in slope of the riding surface near the supports of a simple spanned bridge induced by differential settlements may be more severe than those in a continuous span bridge [3].

In addition to the various types of settlements previously illustrated by Barker et al. [1], horizontal displacement may also be induced in the foundation of bridges founded on spread footings. Excessive horizontal displacements may cause damage to the bearings and to the expansion joints of the bridge. Damage to bearings includes tilting or jamming of rockers, as well as cases where rockers have pulled off the bearings, or where movement resulted in an improper fit between bearing shoes and rockers requiring repositioning. Neoprene bearing

pads are deformed, anchor bolts in the bearing shoes are sheared and cracking of concrete at the bearings is apparent. Other problems due to horizontally imposed displacement may involve horizontal movements occurring to the floor system, causing loss of the support of the deck or deck extending beyond the abutment and beams, jammed against the abutment, requiring to be cut. Sometimes, cutting of relief joints may also be necessary [4].

3.2 Movement Criteria

The selection of limiting values of imposed displacements constitutes a difficult issue to handle, due to a great number of factors affecting them, namely the type of structure (type of spans, length and stiffness of spans), the type of construction material, the type of soil, the proposed use of the structure, the confidence with which the acceptable value of the movement can be specified, the occurrence and rate of ground movements, etc.

On the other hand, the limit between tolerable and non-tolerable movement is often difficult to discern, and may depend on factors other than the physical condition of the bridge, such as the cost and practical problems involved in repair and maintenance. Generally, the definition for non-tolerable damage proposed by the Transportation Research Board's Committee A2K03 on "Foundations of bridges and other structures" is adopted: "*Movement is not tolerable if damage requires costly maintenance and/or repairs and a more expensive construction to avoid this would have been preferable*".

3.2.1 Literature survey

In the following, a literature overview is attempted of the existing allowable values of deformation under static loading. The results are mainly based on field studies of numerous existing bridges founded on spread footings. This outline provides useful insight as to the order of magnitude and the type of such deformations as well as, to their effect on the serviceability and on the structural integrity of bridges.

Bozozuk [5] attempted to distinguish tolerable from non-tolerable displacements for abutments and piers founded on spread footings. His survey involved 120 cases of spread footings, without specific distinction in terms of type or size. He classified displacements as tolerable, when the maintenance needs of the bridge are moderate, despite the magnitude of the displacements and as non-tolerable when considerable maintenance and repair works are required. The work of Bozozuk was parallel to that of Walkinshaw [6] and Grover [7] and was documented via an extensive research on allowable displacements undertaken in the U.S.A. and Canada and published by the Transportations Research Board (TRB). Therefore Bozozuk's definition of tolerable and non-tolerable displacements also applies to the limiting values proposed by Walkinshaw and Grover.

DiMillio [8] attempted to evaluate the behavior of 148 highway bridges supported by spread footings on engineered fills, in conjunction with detailed survey investigations of the foundation movement of 28 selected bridges. It was found that bridges easily tolerated differential settlements of 1 to 3 inches (25 to 75 mm) without significant distress, especially when high embankments of good quality borrow materials are constructed over satisfactory foundation soils.

Moulton et al. [4] carried out a survey that was based on a nationwide study of 314 concrete and steel bridges on spread footings in USA and Canada. In this study, an effort was made to provide information regarding the possible structural damage induced by excessive vertical and horizontal displacement. The definition for non-tolerable damage proposed by the Transportation Research Board's Committee A2K03 was adopted. The results were classified according to the type of spans, to the length and stiffness of spans and to the type of construction material. It was shown that many highway bridges can tolerate significant magnitudes of total and differential vertical settlement without becoming seriously overstressed, sustaining serious structural damage, or suffering impaired riding quality. In

particular, it was found that a longitudinal angular distortion (differential settlement to span length) of 0.004rad would most likely be tolerable for continuous bridges of both steel and concrete, while a value of angular distortion of 0.005rad would be a more suitable limit for simply supported bridges. In this project, it was also pointed out that, in the case of coexistence of vertical and horizontal movements, the tolerable horizontal movement should be limited to 25mm, while in the case where the vertical displacement is small, the tolerable horizontal movement can be increased by 50%.

According to their surveys, Wahls [2] and [9] and Stark et al. [10] arrived to the conclusion that angular distortions of 1/250 of the span length for continuous spans and 1/200 for simply supported spans were considered acceptable. Additionally, differential movements not greater than 2 inches (50 mm) laterally and less than 4 inches (100 mm) vertically, appear to be tolerable, assuming that approach slabs or other provisions are made to minimize the effects of any differential movements between abutments and approach embankments.

Engineering performance of bridges examined in the aforementioned studies, in terms of vertical and horizontal displacements of abutments and piers are illustrated in Table 3.1, classified in increasing order of magnitude. In Table 3.2, proposed serviceability criteria for bridges by the aforementioned researchers are summarized.

Table 3.1: Damage levels on bridges due to displacement of spread footings

Πίνακας 3.1: Επίπεδα βράβης σε γέφυρες λόγω μετακινήσεων των θεμελίων

Type of deformation	Magnitude	Damage Level	Reference
Settlement ρ_v (mm)	<50	Tolerable	Bozozuk [5]
	63	Harmful but tolerable (Ride quality)	Walkinshaw [6]
	25.4 – 76.2	Harmful but tolerable	DiMillio [8]
	50 – 100	Harmful but tolerable	Bozozuk [5]
	> 63	Structural damage	Walkinshaw [6]
	> 100	Intolerable	Bozozuk [5]
	102	Intolerable (Ride quality and structural damage)	Grover [7]
	>102	Intolerable (for abutments)	Wahls [2]
Horizontal displacement ρ_H (mm)	< 25	Tolerable	Bozozuk [5]
	25.4 – 50.8	Harmful but tolerable	Moulton et al. [4]
	25 – 50	Harmful but tolerable	Bozozuk [5]
	50	Structural damage	Walkinshaw [6]
	> 50	Not tolerable (Ride quality and structural damage)	Bozozuk [5]
	> 51	Intolerable (for abutments)	Wahls [2]

Table 3.2: Serviceability Criteria for bridges proposed by various researchers

Πίνακας 3.2: Κριτήρια λειτουργικότητας για γέφυρες σύμφωνα με διάφορους ερευνητές

Type of deformation	Magnitude	Bridge type	Reference
Angular Distortion β [rad]	0.004 (1/250)	Continuous steel / concrete bridges with $L \geq 15.24\text{m}$ (50ft) steel	Moulton et al. [4]
	0.005 (1/200)	Simply supported steel / concrete bridges with $L \geq 15.24\text{m}$ (50ft)	Moulton et al. [4]
	1/250	Continuous bridges (Bridge abutment)	Wahls [2], Stark et al. [10]
	1/200	Simply supported bridges (Bridge abutment)	Wahls [2], Stark et al. [10]
Differential Settlement $\Delta\rho$	<76.2	Bridge abutment for bridge lifetime (steel / concrete bridges)	Moulton et al. [4]

(mm)	<50.8	Bridge pier for bridge lifetime (steel & concrete bridges)	Moulton et al. [4]
	< 50.8	Bridge abutment following bridge completion (steel & concrete bridges)	Moulton et al. [4]
	< 31.75	Bridge pier following bridge completion (steel bridges)	Moulton et al. [4]
	<38.1	Bridge pier following bridge completion (concrete bridges)	Moulton et al. [4]
Horizontal displacements (mm)	<38	Acceptable	Moulton et al. [4]
Horizontal along with vertical displacements (mm)	<25	Acceptable	Moulton et al. [4]

3.2.2 Provisions of Codes

Codes, currently in effect in Europe and other areas (Eurocodes, AASHTO, etc.), do not directly correlate the desired performance of a bridge to limiting values of measurable deformations either of the structure or the foundation (performance levels). However, the main attitude of the Codes is that the desired behavior of a structure (in terms of service and damage level) becomes more demanding, as the importance of the structure and the probability of an earthquake increase. The requirement for a specific behavior of a bridge under static and dynamic actions is today indirectly fulfilled, when the structure satisfies two limit states, the Ultimate Limit State (ULS) and the Serviceability Limit State (SLS).

- Ultimate Limit State (ULS) is associated with the safety of the people and / or the loss of the bearing capacity of the structure. This limit condition can occur either due to structural failure or a failure of the soil.
- Serviceability Limit State (SLS), deals with the functionality and service requirements of a structure to ensure adequate performance under expected conditions. Conditions of total collapse are not involved here. Nevertheless, conditions are examined, which prevent the intended use of the structure and criteria are set concerning deformations affecting the appearance and the comfort of the users, vibrations that cause discomfort to people or restrict the operational efficiency of the structure and finally damage that affect the appearance, durability or the function of the project.

According to AASHTO [11] and [12], for bridges on spread footings, movement of foundations in both vertical and lateral directions shall be investigated in the frame of Serviceability Limit State, i.e. settlements and / or horizontal displacements, as well as the angular distortion caused by differential settlements of adjacent footings. Design shall be based on rideability and cost criteria. Immediate settlement shall be determined using the service load combinations while for time dependent settlements only the permanent loads shall be taken into account. Concerning proposed limiting values for movement of footings, appropriate criteria should be developed, consistent with the function and type of structure, anticipated service life and consequences of unacceptable movements on structure performance and should be established by empirical procedures or structural analyses.

Due to the complexity of the phenomenon, only in the comments of the Code, limiting values are suggested for angular distortion (δ/S) between adjacent foundations, as a function of the structural system of the bridge, namely 0.008rad for simple span bridges and 0.004rad for continuous span bridges. For rigid frames special analyses are required. These limits lead to relatively high values of acceptable differential settlements, for example for a span of 30m a differential settlement of 120mm for a continuous span and 240mm of a simple span are acceptable. It should be noted that such high values of differential settlements create concern

for structural designers who often arbitrarily limit the criteria to one-half or to one-quarter of the suggested values, not so much for reasons related to the structural integrity of the bridge but mainly for practical reasons based on the tolerable limits of deformation of other structures associated with a bridge e.g. approach slabs, wingwalls, pavement structures, drainage grades, utilities of the bridge, deformations that adversely affect quality of ride, etc. [3]. That is why, the suggested criteria should be considered in conjunction with functional or performance criteria not only for the bridge structure itself but for all the associated facilities as well.

Finally, according to AASHTO, when designing against seismic actions in the frame of the ultimate limit state, foundation movements are not taken into account. In Division I-A of the Code, referring to the design of foundations in seismically active areas, it is pointed out that special consideration should be given to the potential settlement of footings on sand, resulting from ground motions induced by earthquake loadings.

A similar approach is also followed in Eurocodes. According to EN1992-2:2005 [13], the effects of uneven settlements of the structure due to soil subsidence should be considered for the verification for serviceability limit states. Concerning ultimate limit states, they should be considered only where they are significant, for example where second order effects are of importance. In other cases for ultimate limit states they need not be considered, provided that the ductility and rotation capacity of the elements are sufficient.

Moreover, according to EC1997-1:2004 [14], the assessment of the behavior of bridges on shallow foundations involves both, displacement of the entire foundation and differential displacements of parts of the foundation. Specifically, as suggested in Appendix H of the Code, the following components of foundation movement should be considered: settlement, relative (or differential) settlement, rotation, tilt, relative deflection, relative rotation, horizontal displacement and vibration amplitude. According to the code, any differential movements of foundations leading to deformation in the supported structure should be limited to ensure that they do not lead to a limit state in the supported structure and this is achieved when design values remain lower of certain limiting values. As limiting value for a particular deformation is defined the value of the deformation at which a serviceability limit state, such as unacceptable cracking etc., is deemed to occur in the supported structure. As noted in the Code, selection of design values for limiting movements and deformations is not an easy task and should take into account various factors, such as the type of structure, the type of construction material, the type of foundation, the services entering the structure, etc. Thus, certain limiting values are not given and it is suggested that they should be agreed during the design of the supported structure. However, in the absence of specified limiting values of structural deformations of the supported structure, it is proposed that for normal, routine structures the values of structural deformation and foundation movement given in Annex H of the Code may be used. More specifically, to prevent the occurrence of a serviceability limit state in the structure, permissible values of relative rotations of various types of structures could range from 1/2000 to about 1/300, while a maximum relative rotation of 1/500 is judged as acceptable for many structures. The relative rotation likely to cause an ultimate limit state is proposed to be 1/150. For normal structures with isolated foundations, total settlements up to 50mm are often acceptable. Larger settlements may be acceptable provided the relative rotations remain within acceptable limits and provided the total settlements do not cause problems with the services entering the structure, or cause tilting etc. On the other hand, an ultimate limit state due to differential vertical and horizontal foundation displacements could be avoided by adopting appropriate prescriptive measures. The above criteria are summarized in Table 3.3.

Table 3.3: Tolerable movement criteria for bridges proposed by various Codes**Πίνακας 3.3:** Κριτήρια ανεκτών μετακινήσεων για γέφυρες σύμφωνα με διάφορους Κανονισμούς

Code	Type of deformation	Magnitude	Bridge type	Limit State
AASHTO 2002, 2007 with 2009 Interims	Angular Distortion β [rad]	0.004 (1/250)	Continuous	SLS
		0.008 (1/125)	Simply supported	
EN1997-1 (Annex H)	Angular Distortion β [rad]	0.002 (1/500)	all normal, routine structures	SLS
		1/150	all normal, routine structures	ULS
	Total settlement	50 mm	normal structures with isolated foundations	SLS

According to EN 1998-2:2005 [15], the desired behavior of a bridge against seismic actions is qualitatively defined in terms of service and damage level after the seismic event, as a function of the importance of the bridge and the probability of the earthquake. For Ultimate Limit State (ULS), the bridge is implicitly anticipated to preserve its structural integrity and hold adequate residual resistance in order to avoid total collapse. Considerable damage is expected to occur, mainly in the form of flexural yielding of specific sections (i.e. the formation of plastic hinges) in the piers, which in the absence of seismic isolation is a desirable situation. The bridge deck should in general be designed to avoid damage, except for breakage of secondary components, such as expansion joints and continuity slabs. Also, the bridge deck must be able to accommodate loads from piers experiencing plastic hinging and must not become unseated under extreme seismic displacement. In the case of rare seismic actions, the parts of the bridge contributing to energy dissipation should be designed to enable emergency traffic and inspections in the post-earthquake period and to be easily repairable. For Serviceability Limit State (SLS), a high probability of occurrence seismic scenario may cause only minor damage to secondary components and to contributing to energy dissipation parts of the bridge. All other components of the bridge are expected to remain untouched; traffic should not be disturbed and repairs should not be urgent. Although the design seismic criteria proposed in the Code aim explicitly at satisfying the no-collapse requirement, they implicitly cover the damage minimization requirement as well.

Further, as noted in EN1998-2, the aforementioned requirements are satisfied for ULS (and consequently for SLS as well), by verifying the structure against seismic combinations that do not include action effects due to imposed deformations caused by settlements of supports or residual ground movements due to seismic faulting. An exception to this rule is the case of bridges in which the seismic action is resisted by elastomeric laminated bearings, where elastic behavior of the system shall be assumed and the action effects due to imposed deformations shall be accounted for. In the code, no limiting values for foundation movements under seismic conditions are proposed.

3.2.3 Other approaches

On the other hand, other approaches may be adopted to specify limiting values for foundation movements of bridges. According to the Japanese method JBDPA '90-91, which applies to the post-earthquake inspection and rapid damage assessment of buildings, a damage classification is attempted according to the maximum inclination of the building after a certain event [16]. The classification according to the inclination angle θ is illustrated in Table 3.4. Although the method refers to the damage assessment of buildings, the magnitude of the inclination angle of the piers may also be considered as a criterion for the damage assessment of bridges.

Table 3.4: Damage classification according to JBDPA 90-91 [16]**Πίνακας 3.4:** Κατάταξη βλαβών σύμφωνα με JBDPA 90-91 [16]

Type of deformation	Magnitude	Damage level
Inclination angle θ (rad)	< 0.01	Small
	0.01 - 0.03	Moderate
	0.03 - 0.06	Severe
	> 0.06	Collapse

Finally, according to FEMA-356 [17], four discrete Structural Performance Levels related to certain post-earthquake damage states, are defined for buildings:

- Immediate Occupancy (S-1), defined as the post-earthquake damage state that remains safe to occupy, essentially retains the pre-earthquake design strength and stiffness of the structure
- Life Safety (S-3), defined as the post-earthquake damage state that includes damage to structural components but retains a margin against onset of partial or total collapse
- Collapse Prevention (S-5), defined as the post-earthquake damage state that includes damage to structural components such that the structure continues to support gravity loads but retains no margin against collapse
- Not Considered (S-6), defined as the post-earthquake damage state where a building rehabilitation does not address the performance of the structure.

Appropriate acceptance criteria relate these Structural Performance Levels to limiting damage states for vertical elements of lateral-force-resisting systems, in terms of drift values. The drift values proposed by FEMA are presented in Table 3.5 and are discerned into transient and permanent. They are typical values provided to illustrate the overall structural response associated with various Structural Performance Levels. In this sense, these values may also be adopted as limiting drift values for piers of bridges.

Table 3.5: Structural Performance Levels and damage for common vertical elements of lateral-force-resisting systems of buildings according to FEMA-356 [17]**Πίνακας 3.5:** Επίπεδα επιτελεστικότητας και βλαβών για συνηθισμένα κατακόρυφα στοιχεία κτιρίων σύμφωνα με FEMA-356 [17]

Type of deformation	Magnitude	Structural Performance Level
Drift ϕ (rad) Concrete Frames	4% transient or permanent	Collapse Prevention
	2% transient and 1% permanent	(S-5) Life Safety
	1% transient and negligible permanent	(S-3) Immediate Occupancy
Drift ϕ (rad) Concrete Walls	2% transient or permanent	Collapse Prevention
	1% transient and 0.5% permanent	(S-5) Life Safety
	0.5% transient and negligible permanent	(S-3) Immediate Occupancy

3.3 Performance criteria for the case study

As previously presented, limiting values of various types of displacements are generally not directly associated with certain limit states of the structure. Thus, only simplified approaches are possible. Most researchers (see Table 3.1) have the opinion that settlements less than 5cm are tolerable or acceptable; which could constitute a performance criterion for the Serviceability Limit State. The same value is also suggested by EN1997-1 in Annex H (see Table 3.2). Furthermore, in Table 3.1, vertical displacements from 5cm up to 10cm are considered harmful but tolerable. This could correspond to an Ultimate Limit State condition.

Assuming that the settlement of the abutment is practically zero, limiting values of differential settlements will correspond to the allowable vertical displacement of the pier. For simply supported steel bridges, which is our case, Moulton et al. [4] set a limit in the allowable angular distortion equal to 0.005rad (see Table 3.2), corresponding to a differential settlement of 21cm considering the 42m span of the bridge. Moreover, Moulton et al. [4] specify a differential settlement of less than 3.2cm to be acceptable for a bridge pier of a steel bridge following completion, which is a rather conservative value and should not be taken into consideration. In addition, AASHTO [11] and [12] sets a limit of 0.008rad in the allowable angular distortion of simply supported bridges (see Table 3.3), which corresponds to 33.6cm of differential settlement. Finally, according to EN1997-1 [14] (see Table 3.3), a limiting value of 0.002rad is set in the allowable angular distortion of normal structures for Serviceability Limit State corresponding to 8.4cm of differential settlement. Further, for Ultimate Limit State, a limiting value of 1/150 is proposed, corresponding to 28.0cm of differential settlement.

Conclusively, maximum allowable settlements for the Serviceability Limit State should not exceed 8.5cm, while for the Ultimate Limit State the limit arises at 28cm.

For statically determinate bridges the most critical structural member is the pier, which essentially dictates the tolerance of the entire system to liquefaction-induced deformations. In such systems, where the piers are simple cantilevers, when rotations in the transverse direction of the bridge prevail, the formation of plastic hinges at their base is not allowed, since the structural system becomes a mechanism, unable to carry even the vertical loads (Figure 3.2). Moreover, when rotations about the longitudinal axis are dominant, the pier of the bridge under investigation acts as a statically indeterminate frame, thus, the formation of plastic hinges is allowed at the top of its columns (Figure 3.3). Hence, the maximum permissible ground settlement and rotations correspond to the first yield at the pier's base, or the plastic hinge at the top of the pier, or the plastic resistance of the steel members, whichever occurs first. Regarding the inclination angle of the pier a limit of 0.04rad is considered for ULS, accounting for "Severe" damage level and 0.02rad for SLS referring to a "Moderate" damage level.

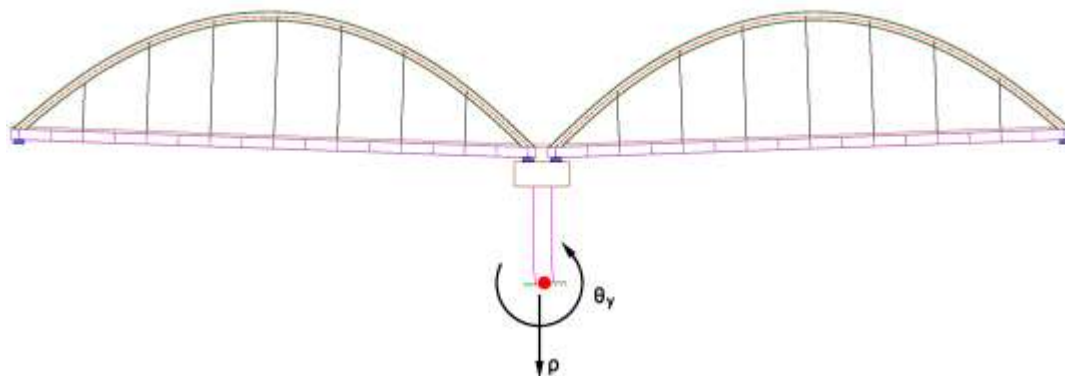


Figure 3.2: A statically determinate bridge becomes a mechanism after the formation of a plastic hinge at the base of the pier

Σχήμα 3.2: Οι ισοστατικές γέφυρες μετατρέπονται σε μηχανισμό μετά τη δημιουργία πλαστικής άρθρωσης στη βάση του μεσοβάθρου

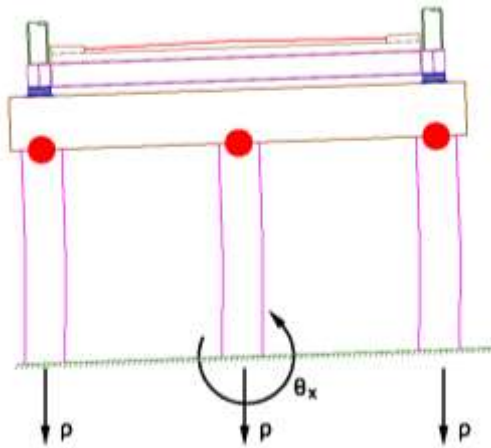


Figure 3.3: For rotation about the longitudinal axis of the bridge, the pier acts as a frame and plastic hinges are allowed at the top of its columns

Σχήμα 3.3: Για στροφές περί τον διαμήκη άξονα της γέφυρας, το μεσόβαθρο λειτουργεί ως πλαίσιο και επιτρέπεται ο σχηματισμός πλαστικής άρθρωσης την κορυφή των στύλων του

Chapter 4

APPLIED CODES

The codes that are used for the design of the bridge are the following:

- Eurocode 0: Basis of structural design;
- Eurocode 1-1.4: Actions on structures – General actions, Wind actions;
- Eurocode 1-1.5: Actions on structures – General actions, Thermal actions;
- Eurocode 1-2: Actions on structures – Traffic loads on bridges;
- Eurocode 2-1.1: Design of concrete structures – General rules and rules for buildings;
- Eurocode 2-2: Design of concrete structures – Concrete Bridges – Design and detailing rules;
- Eurocode 3-1: Design of steel structures – General rules and rules for buildings;
- Eurocode 3-1.8: Design of steel structures – Design of joints;
- Eurocode 3-2: Design of steel structures – Steel Bridges;
- Eurocode 4-1.1: Design of composite steel and concrete structures – General rules and rules for buildings;
- Eurocode 4-2: Design of composite steel and concrete structures – General rules and rules for bridges;
- Eurocode 8-1: Design of structures for earthquake resistance – General rules, seismic actions and rules for buildings;
- Eurocode 8-2: Design of structures for earthquake resistance – Bridges;
- DIN 4141-14: Structural bearings, laminated elastomeric bearings – design and construction;
- EN1337-1: Structural bearings – General design rules;
- EN1337-3: Structural bearings – Elastomeric bearings;
- DIN 4014: Bored Cast-in-place Piles - Formation, Design and Bearing Capacity.

Chapter 5

MODELING ISSUES

5.1 Model of the bridge

All members are modeled with beam elements. Moment releases are applied at the ends of the transverse beams, the diagonal bracing members and the hangers. The concrete slab is simulated by shell elements with a thickness of 25cm, accounting for the mean value of the slab's thickness. The numerical model of the bridge is shown in Figure 5.1.

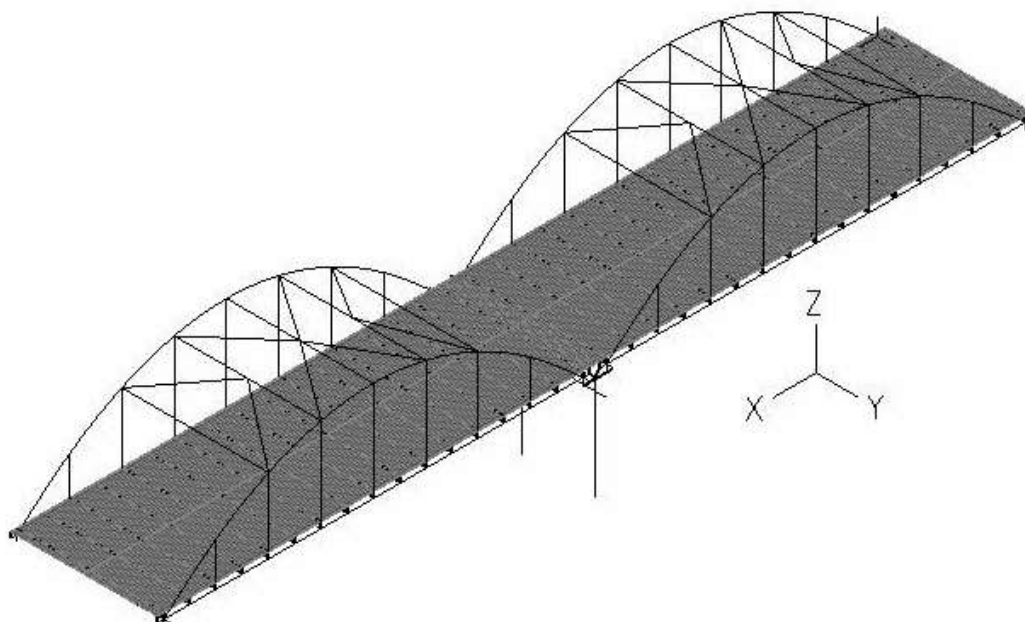


Figure 5.1: Model of the bridge

Σχήμα 5.1: Προσομοίωμα γέφυρας

The connection between the nodes of the slab, simulated with shell elements, with the ones of the main and secondary beams is realized by rigid links, taking into account the eccentricity between them, as shown in Figure 5.2. Hinges are considered at the ends of the continuous slab after the application of the vertical loads, accounting for damages after the earthquake. To this end, double nodes are taken into account, (Figure 5.3) connected with rotational springs about the y global axis, which is the transverse axis of the bridge, having large value of stiffness constant, equal to 10^9kNm/rad . These springs act when the permanent and live loads are applied on the bridge. They cease to exist when the ground displacement and rotations begin to evolve. Rigid links connect these double nodes referring to the other degrees of freedom (x, y and z translational and x and z rotational).

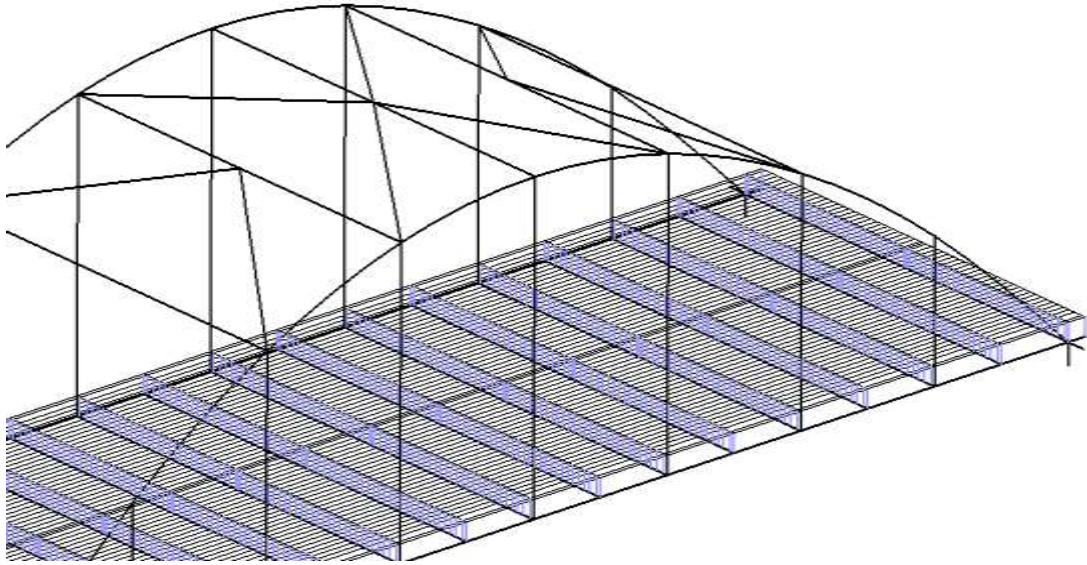


Figure 5.2: Connection of the deck's slab with beams with rigid links

Σχήμα 5.2: Σύνδεση της πλάκας καταστρώματος με τις δοκούς, μέσω άκαμπτων στοιχείων

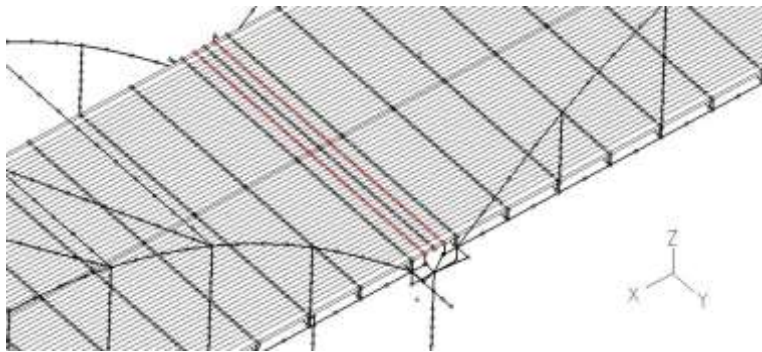


Figure 5.3: Double nodes for the modeling of the plastic hinges of the continuous slab

Σχήμα 5.3: Διπλοί κόμβοι για την προσομοίωση των πλαστικών αρθρώσεων της πλάκας συνέχειας

The bearings at the abutments and the pier, of type NB4 800×800×282 (162), are modeled with equivalent elastic springs. For the horizontal springs the stiffness of the bearings is:

$$K_h = \frac{G \times A}{t} = \frac{900 \text{ kN/m}^2 \times 0.8 \text{ m} \times 0.8 \text{ m}}{0.162 \text{ m}} = 3556 \text{ kN/m} \quad (5-1)$$

where $G=900\text{kN/m}^2$ is the conventional shear modulus, A the overall plan area of the bearing and t the total thickness of the elastomer layers. The vertical springs have a stiffness constant equal to:

$$K_p = \frac{A}{\sum t_i \times \left(\frac{1}{5 \times G \times S^2} + \frac{1}{E_b} \right)} \Rightarrow$$

$$K_p = \frac{0.80 \text{ m} \times 0.80 \text{ m}}{0.162 \text{ m} \times \left(\frac{1}{5 \times 900 \text{ kN/m}^2 \times 11.11^2} + \frac{1}{2000000 \text{ kN/m}^2} \right)} \approx 2 \times 10^6 \text{ kN/m} \quad (5-2)$$

where S is the shape factor of the elastomeric bearing equal to:

$$S = \frac{A}{L \times t_e} = \frac{0.80\text{m} \times 0.80\text{m}}{2 \times (0.80\text{m} + 0.80\text{m}) \times 0.018\text{m}} = 11.11 \quad (5-3)$$

with A the overall plan area of the bearing, L the perimeter of the bearing, $t_e=0.018\text{m}$ the effective thickness of an individual elastomer layer and the bulk modulus is taken equal to $E_b=2000\text{MPa}$.

Figure 5.4 shows with red lines the three translational springs, simulating the bearings at the abutments. The ends of these springs are fixed. Similarly, Figure 5.5 illustrates the corresponding springs at the pier. In this case, the ends of the springs are connected with the top of the pier's columns via rigid links.

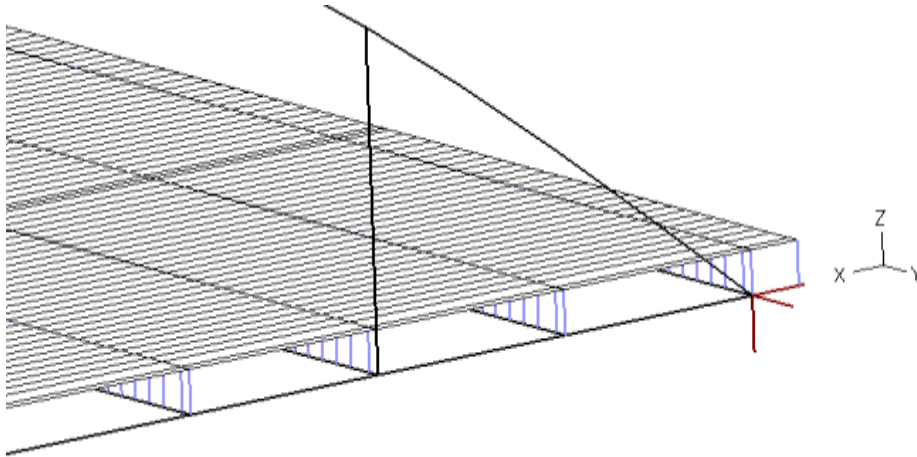


Figure 5.4: Springs simulating the bearings at the abutments

Σχήμα 5.4: Ελατήρια που προσομοιώνουν τα εφεδρανα στα ακρόβαθρα

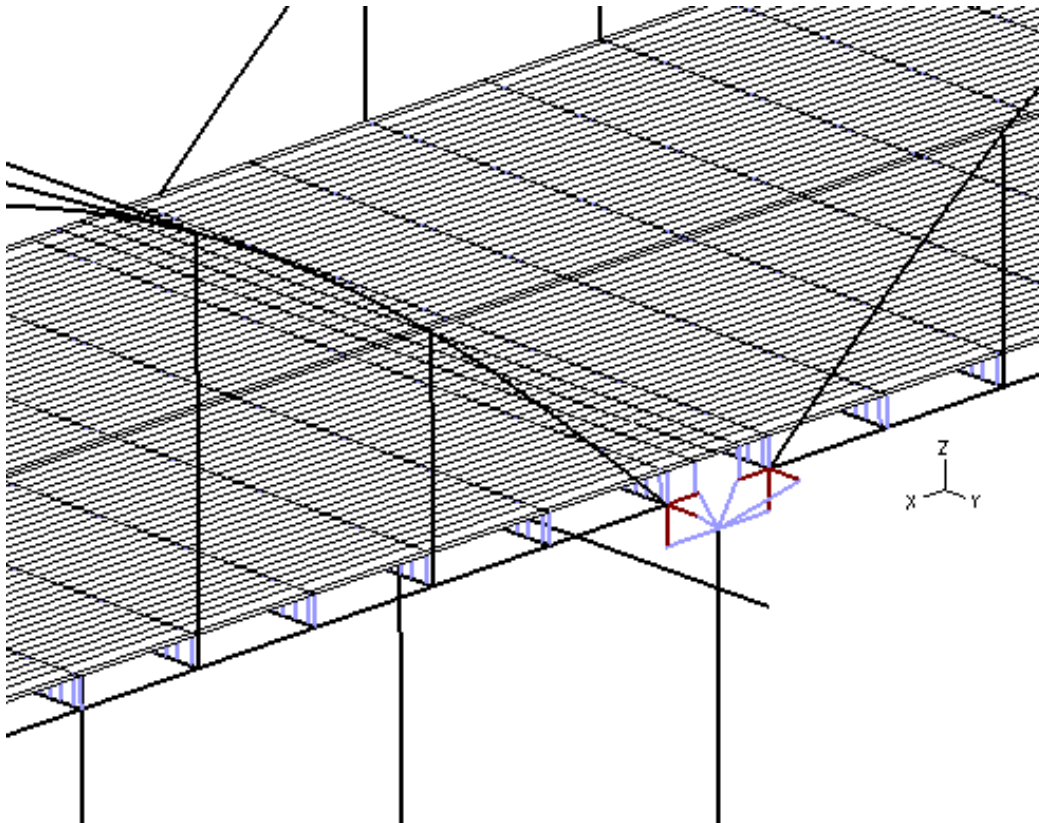


Figure 5.5: Springs simulating the bearings at the pier

Σχήμα 5.5: Ελατήρια που προσομοιώνουν τα εφεδρανα στο μεσόβαθρο

The horizontal translational degree of freedom and the rotational one about z-axis are fixed at the base of the columns. The other three degrees of freedom (z-displacement, x-rotation, y-rotation) are released, while the fixed supports referring to these degrees of freedom are simulated by springs with large values of stiffness constant ($k_z=10^{11}$ kN/m, $k_{rx}=10^{11}$ kNm/rad and $k_{ry}=10^{11}$ kNm/rad) connecting the base of the columns with ground. These springs are shown in Figure 5.6.

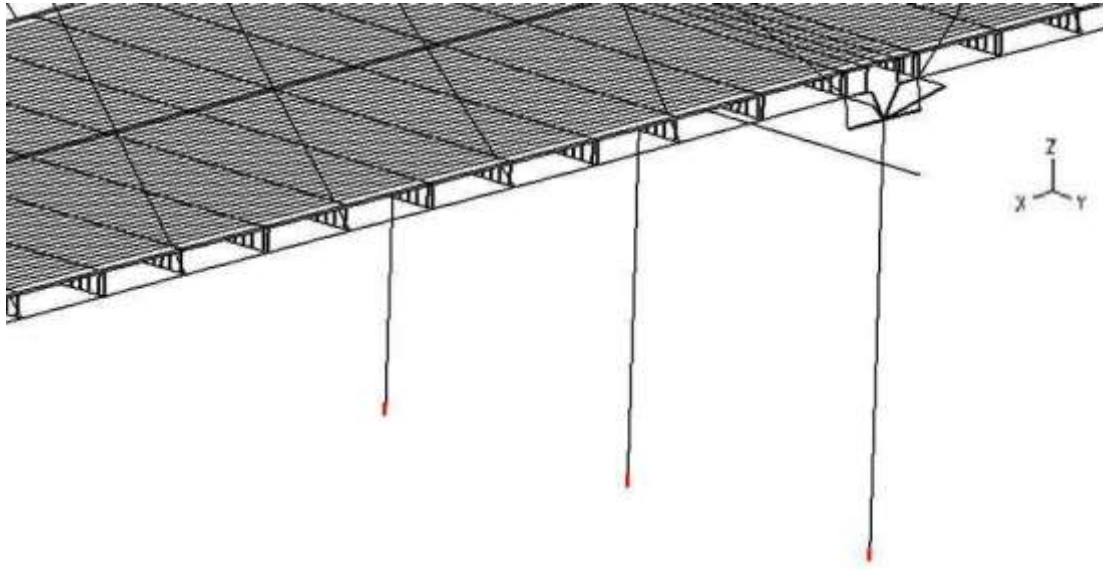


Figure 5.6: Springs simulating the fixed support at the pier's base

Σχήμα 5.6: Ελατήρια που προσομοιώνουν τις στηρίξεις στη βάση του μεσοβάθρου

The finite element analysis software that is used is ADINA v.8.5.0 [18]. The model has been compared with the corresponding one using SOFiSTiK [19] and the results showed a satisfactory agreement.

5.2 Constitutive laws of materials

5.2.1 Structural Steel S355

For the material of the structural steel S355, the design yield strength is:

$$f_{yd} = 355\text{MPa} \quad (5-4)$$

with yield strain:

$$\epsilon_{yd} = \frac{f_{yd}}{E_s} = \frac{355\text{MPa}}{210000\text{MPa}} = 0.00169 = 0.17\% \quad (5-5)$$

where $E_s=210\text{GPa}$ is the elastic modulus. The stress-strain relation is described as:

$$\sigma_s = E_s \cdot \epsilon_s \text{ when } 0 \leq \epsilon_s \leq \epsilon_{yd} \quad (5-6)$$

$$\sigma_s = f_{yd} \text{ when } \epsilon_{yd} \leq \epsilon_s \leq \epsilon_u \quad (5-7)$$

where the ultimate strain is $\epsilon_u=22\%$. The diagram of Figure 5.7 describes the stress-strain material law.

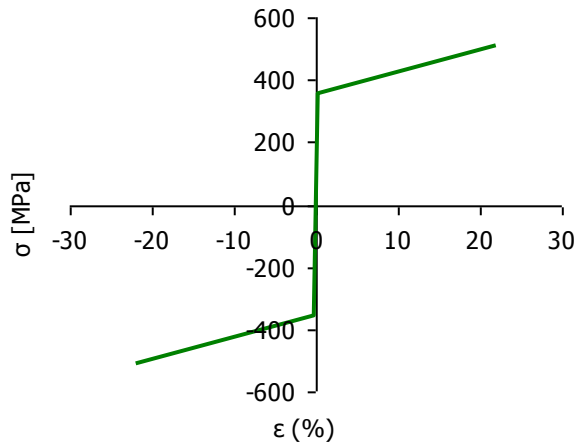


Figure 5.7: Material law of structural steel S355

Σχήμα 5.7: Νόμος υλικού χάλυβα S355

5.2.2 Reinforced Concrete C35/45 of deck's slab

The material of the deck's slab is assumed to be infinitely linearly elastic with elastic modulus $E=33282\text{MPa}$.

5.2.3 Reinforced Concrete C30/37 of pier's beam

The material of the pier's beam is assumed to be infinitely linearly elastic with elastic modulus $E=31939\text{MPa}$.

5.2.4 Reinforced Concrete C30/37 of the pier

According to EC2 the value of the design compressive strength of the concrete C30/37 is:

$$f_{cd} = \alpha_{cc} \frac{f_{ck}}{\gamma_c} = 0.85 \frac{30\text{MPa}}{1.50} = 17\text{MPa} \quad (5-8)$$

where $f_{ck}=30\text{MPa}$ is the characteristic strength, $\gamma_c=1.50$ is the partial safety factor and $\alpha_{cc}=0.85$ is a coefficient which takes account of long term effects on the compressive strength and of unfavorable effects resulting from the way the load is applied. The tensile strength of the concrete is assumed to be equal to zero. The stress-strain relation is expressed as:

$$\sigma_c = f_{cd} \left[1 - \left(1 - \frac{\epsilon_c}{\epsilon_{c2}} \right)^n \right] \quad \text{when } 0 \leq \epsilon_c \leq \epsilon_{c2} \quad (5-9)$$

$$\sigma_c = f_{cd} \quad \text{when } \epsilon_{c2} \leq \epsilon_c \leq \epsilon_{cu2}$$

where,

$n=2$ for concrete with characteristic strength $f_{ck} \leq 50\text{MPa}$

ϵ_{c2} is the strain at reaching the maximum strength ($\epsilon_{c2}=2\text{‰}$ for C30/37)

ϵ_{cu2} is the ultimate strain ($\epsilon_{cu2}=3.5\text{‰}$ for C30/37)

Figure 5.8 illustrates the stress-strain relation of the concrete C30/37.

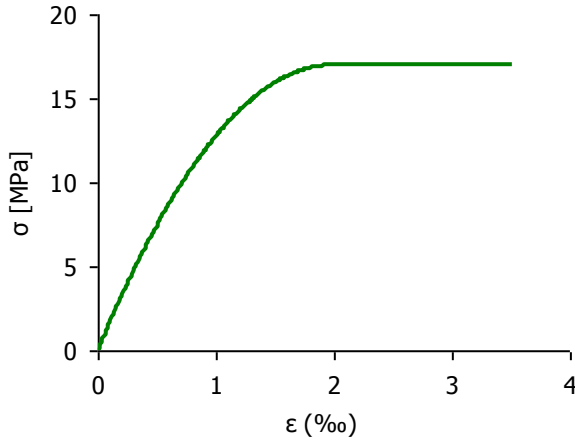


Figure 5.8: Material law of reinforced concrete C30/37

Σχήμα 5.8: Νόμος υλικού οπλισμένου σκυροδέματος C30/37

5.2.5 Reinforcing steel B500C

The design yield strength of reinforcing steel B500C is:

$$f_{ryd} = \frac{f_{ryk}}{\gamma_s} = \frac{500\text{MPa}}{1.15} = 434.78\text{MPa} \quad (5-10)$$

with partial safety factor $\gamma_s=1.15$ and yield strain:

$$\epsilon_{ryd} = \frac{f_{ryd}}{E_{rs}} = \frac{434.78\text{MPa}}{200000\text{MPa}} = 0.00217 = 0.217\% \quad (5-11)$$

where $E_{rs}=200\text{GPa}$ is the elastic modulus. The stress-strain relation, shown in Figure 5.9, is described as:

$$\begin{aligned} \sigma_{rs} &= E_{rs} \cdot \epsilon_{sr} \text{ when } 0 \leq \epsilon_{rs} \leq \epsilon_{ryd} \\ \sigma_{rs} &= f_{ryd} \text{ when } \epsilon_{ryd} \leq \epsilon_{rs} \leq \epsilon_{ru} \end{aligned} \quad (5-12)$$

where the ultimate strain is $\epsilon_{ru}=15\%$.

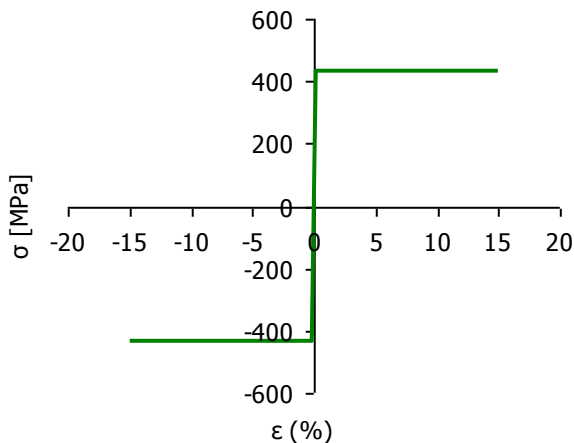


Figure 5.9: Material law of reinforcing steel B500C

Σχήμα 5.9: Νόμος υλικού χάλυβα οπλισμού B500C

5.3 Nonlinear behavior of the bridge's components

5.3.1 Pier's columns

The reinforcement of the pier's columns is $45\Phi 25$ (220.95cm^2) arranged radially, as shown in Figure 5.10, satisfying the minimum percentage of 1%. The cover of the longitudinal reinforcement is assumed to be equal to 8cm. The design of the pier is obtained by the analysis of the conventional solution.

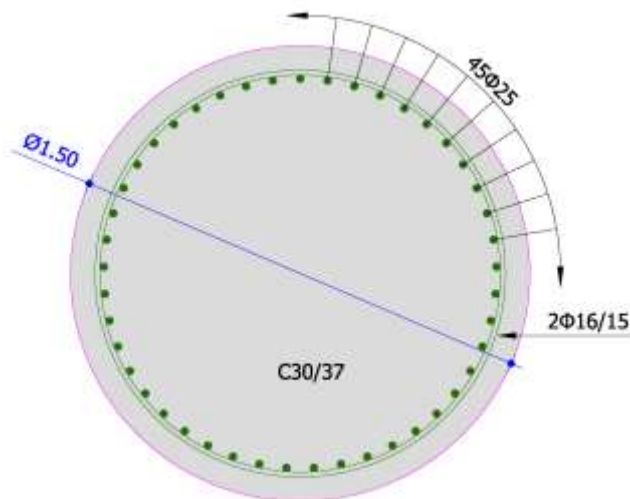


Figure 5.10: Reinforcement of the pier's columns

Σχήμα 5.10: Οπλισμός στύλων μεσοβάθρου

The interaction diagram M-N of this cross-section of the pier's columns is calculated by the free software Response-2000 [20] and it is shown in Figure 5.11. According to this diagram the maximum absolute value of the bending moment is equal to $\max M = 8045\text{kNm}$ for axial force $N = -13870\text{kN}$, while the maximum (tensile) axial force is $\max N = 9606\text{kN}$ and the minimum (compressive) force is $\min N = -38880\text{kN}$.

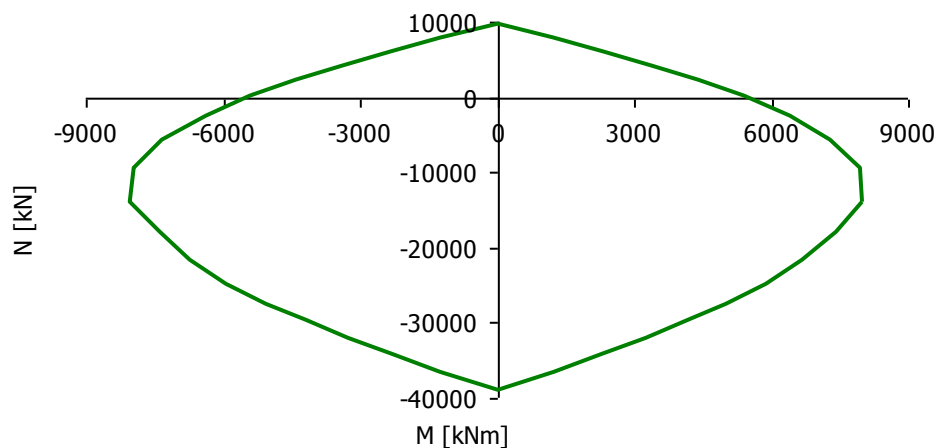


Figure 5.11: Interaction diagram M-N for the cross section of the pier's columns

Σχήμα 5.11: Διάγραμμα αλληλεπίδρασης M-N για τη διατομή στύλων μεσοβάθρου

According to the interaction diagram M-N, twelve (12) curves of bending moment-curvatures are calculated for characteristic values of the axial force N , using the program MyBiAxial [21]-[22]. The maximum and minimum values of N are taken equal to $N = 8000\text{kN}$ and $N = -30000\text{kN}$, respectively, which are almost equal to the strength of the cross section to uniaxial tension and compression, respectively. The curves that are taken into account in the analysis

are drawn in Figure 5.12. Due to the symmetry of the cross section and the reinforcement, these curves are used for both bending moments, M_y and M_z .

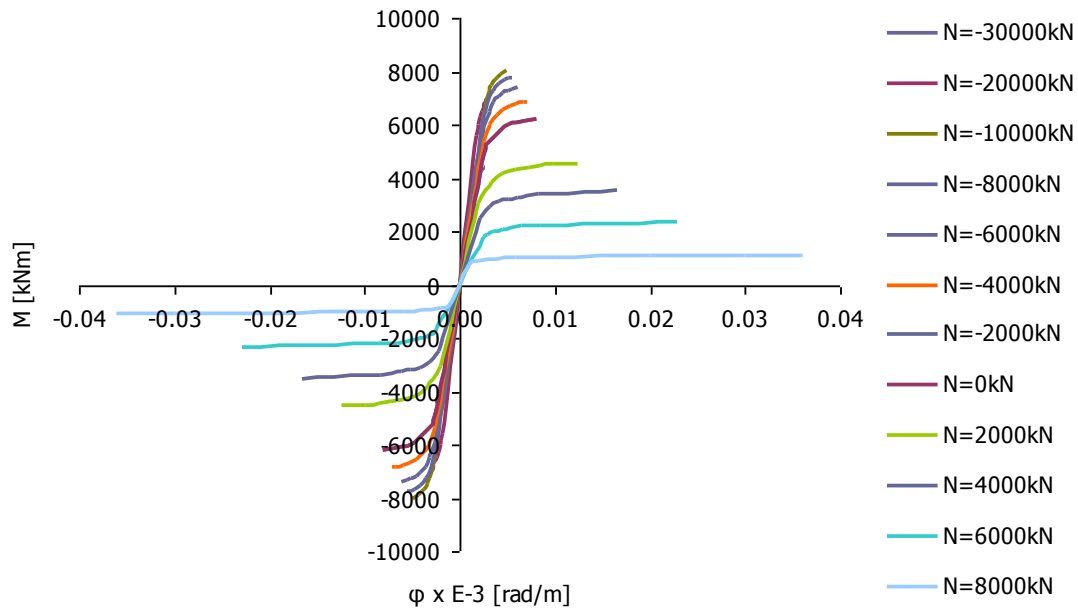


Figure 5.12: Curves of moment – curvature ($M-\phi$) for the cross section of the pier's columns

Σχήμα 5.12: Καμπύλες ροπών – καμπυλοτήτων ($M-\phi$) για τη διατομή στύλων μεσοβάθρου

Taking into account the diagram of the reinforced concrete of the pier's columns, shown in Figure 5.8, and the stress-strain diagram of the reinforcing steel B500C, plotted in Figure 5.9, as well as their corresponding expressions of Eqs. (5-9) and (5-12), respectively, the compressive force is calculated as:

$$N_c = \sigma_c A_c + \sigma_s A_s \quad (5-13)$$

where A_c is the cross sectional area of the columns and A_s is the total area of the reinforcement 45 Φ 25, thus:

$$A_c = \pi d^2 / 4 = \pi (1.50\text{m})^2 / 4 = 1.767\text{m}^2 \quad (5-14)$$

$$A_s = 45 * 4.91\text{cm}^2 = 220.95\text{cm}^2 = 0.022095\text{m}^2 \quad (5-15)$$

For the tensile branch only the reinforcement is considered:

$$N_t = \sigma_s A_s \quad (5-16)$$

The yield values of the diagram $N-\epsilon$ are given in Table 5.1, which are in accordance with the maximum and minimum values of N of Figure 5.11. The diagram $N-\epsilon$ for the pier's columns is illustrated in Figure 5.13.

Table 5.1: Yield values of parameters in uniaxial tension and compression for the cross section of the pier's columns of structural steel S355

Πίνακας 5.1: Τιμές παραμέτρων στη διαρροή σε μονοαξονικό εφελκυσμό και μονοαξονική θλίψη για τη διατομή στύλων μεσοβάθρου

TENSILE BRANCH		COMPRESSIVE BRANCH	
Maximum Force:	Ultimate strain:	Minimum Force:	Ultimate strain:
$N_{\max} = 9606\text{kN}$	$\epsilon = 2.17\text{‰}$	$N_{\min} = -38880\text{kN}$	$\epsilon = 2.0\text{‰}$

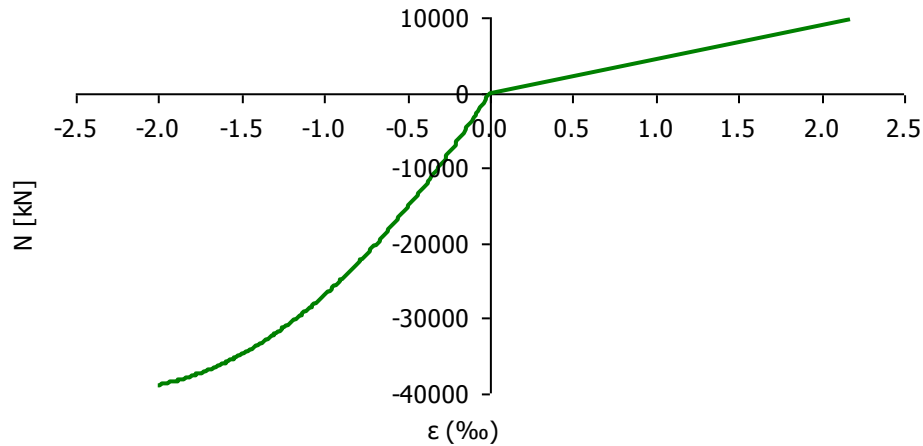


Figure 5.13: Diagram of axial force – axial strain (N-ε) for the cross section of the pier's columns

Σχήμα 5.13: Διάγραμμα αξονικής δύναμης – ανηγμένης αξονικής παραμόρφωσης (N-ε) για τη διατομή στύλων μεσοβάθρου

5.3.2 Bearings

According to EC8, the shear strain $\epsilon_{q,d}$ of the elastomer due to translational movement shall not exceed 2.00. The shear strain is given by the expression:

$$\epsilon_{q,d} = \frac{\delta_{q,d}}{t} \leq 2 \quad (5-17)$$

where

$\delta_{q,d}$: is the maximum resultant horizontal relative displacement of parts of the bearing obtained by vectorial addition of $\delta_{x,d}$ and $\delta_{y,d}$

$\delta_{x,d}$: is the maximum horizontal relative displacement of parts of the bearing in the direction of dimension a of the bearing due to all design load effects

$\delta_{y,d}$: is the maximum horizontal relative displacement of parts of the bearing in the direction of dimension b of the bearing due to all design load effects

t : is the total thickness of the elastomer in shear including the top and bottom cover, unless relative movement between the outer plates of the bearing and the structure is restrained by dowelling or other means

The design strain due to compressive loads, $\epsilon_{c,d}$ is given by the expression:

$$\epsilon_{c,d} = \frac{1.5 \cdot N_{sd}}{S \cdot G \cdot A_r} \quad (5-18)$$

where $S=11.11$ is the shape factor of the elastomeric bearing calculated by Eq. (5-3), $G=900\text{kN/m}^2$ is the conventional shear modulus, N_{sd} is the compressive design load at the bearing and A_r is the reduced effective plan area due to the loading effects, where A_r is given by the expression:

$$A_r = A \left(1 - \frac{\delta_{x,d}}{a} - \frac{\delta_{y,d}}{b} \right) \quad (5-19)$$

with A the overall plan area of the bearing, with a and b are the width and the length of the bearing.

The nominal strain due to angular rotation is given by the expression:

$$\varepsilon_{a,d} = \frac{a^2 \times \alpha_{a,d} + b^2 \times \alpha_{b,d}}{2 \times t_e \times t} \quad (5-20)$$

where $\alpha_{a,d}$ is the angle of rotation across the width, a , of the bearing and $\alpha_{b,d}$ the angle of rotation (if any) across the length, b , of the bearing.

According to EN1337-3, at any point in the bearing the sum of the strains ($\varepsilon_{t,d}$) due to the design load effects is given by the expression:

$$\varepsilon_{t,d} = K_L (\varepsilon_{q,d} + \varepsilon_{c,d} + \varepsilon_{a,d}) \leq \varepsilon_{u,d}=7 \quad (5-21)$$

where:

$\varepsilon_{q,d}$ is the design shear strain due to design translational movements (Eq. (5-17))

$\varepsilon_{c,d}$ is the design strain due to compressive design loads (Eq. (5-18))

$\varepsilon_{a,d}$ is the design strain due to the design angular rotation (Eq. (5-20))

K_L is a type-loading factor equal to 1.

The maximum design strain $\varepsilon_{t,d}$ shall not exceed the maximum value $\varepsilon_{u,d}$ given by the expression:

$$\varepsilon_{u,d} = \frac{\varepsilon_{u,k}}{\gamma_m} = 7 \quad (5-22)$$

where $\varepsilon_{u,k}$ is the maximum permissible value of 7 for ULS and $\gamma_m=1.00$ is a partial safety factor.

The horizontal springs that simulate the stiffness of the bearings to horizontal displacements are assumed to have a nonlinear behavior. As mentioned in section 5.1, Eq. (5-1) gives the initial stiffness of the horizontal springs equal to $k_h=3556\text{kN/m}$. According to EC8, the shear strain of the elastomer due to translational movement shall not exceed the value of 2.00, as defined in Eq. (5-17), thus:

$$\max \varepsilon_{q,d} = \frac{\max \delta_{q,d}}{t} = 2 \Leftrightarrow \max \delta_{q,d} = 2 \times 0.162\text{m} = 0.324\text{m} \quad (5-23)$$

Hence, the springs are considered to act linearly up to that limit.

Additionally, the sum of the strains ($\varepsilon_{t,d}$) due to the design load effects, including the design strains due to compressive design loads and the design angular rotation, as well as the design shear strain due to design translational movements, as defined in Eq. (5-21), shall not exceed the value of 7. Thus:

$$\max \varepsilon_{t,d} = \frac{\max \delta_{t,d}}{t} = 7 \Leftrightarrow \max \delta_{t,d} = 7 \times 0.162\text{m} = 1.13\text{m} \quad (5-24)$$

The maximum permissible horizontal displacement $\max\delta_{t,d}=1.13\text{m}$ is almost equal to the distance of the bearings from the edges of the pier's beam, as shown in Figure 2.5 regarding the longitudinal direction and in Figure 2.6 for the transverse direction of the bridge. Bearing's displacements larger than these overlap lengths would result in the unseating of the deck causing the failure of the bridge. Hence, it is assumed that the springs lose their stiffness if the limit of Eq. (5-23) is exceeded, but the analysis continues until the bearings' displacement reaches the value of $\max\delta_{t,d}$. The load-displacement diagram that the horizontal springs follow is shown in Figure 5.14. The vertical springs are assumed to be infinitely linear.

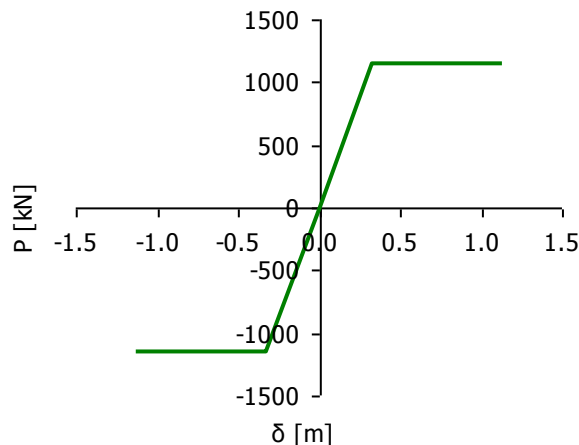


Figure 5.14: Constitutive law of horizontal springs simulating the bearings

Σχήμα 5.14: Καταστατικός νόμος οριζοντίων ελατηρίων που προσομοιώνουν τα εφεδρανα

5.4 Load Cases

The load cases considered are the following:

LC 1: Self weight

The self weight is applied on all components of the bridges. The shell elements simulating the deck's slab are not activated. Their weight is applied on the secondary beams as linear load (Figure 5.15).

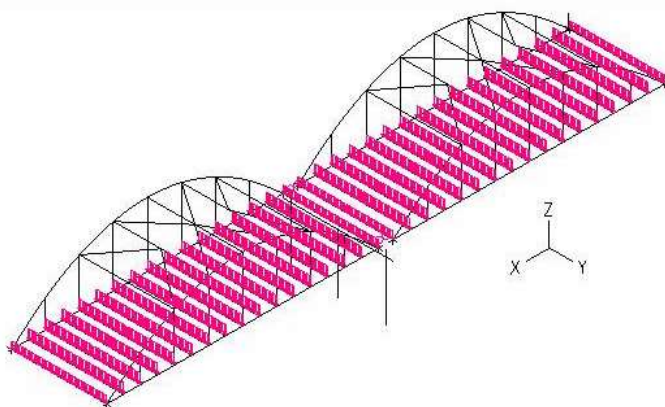


Figure 5.15: Self weight of the slab applied on the secondary beams

Σχήμα 5.15: Εφαρμογή ίδιου βάρους έγχυτης πλάκας στις διαδοκίδες

LC 2: Superimposed

Pavement and future layer: $g_p=0.20\text{m}\times 24\text{kN/m}^3+0.50\text{kN/m}^2=5.30\text{kN/m}^2$

Sidewalks: $g_s=(0.33\text{m}^2\times 25\text{kN/m}^3) / 1.25\text{m} = 6.60\text{kN/m}^2$

Barriers: $g_b=0.95\text{kN/m}$

The loads are applied on the bridge as shown in Figure 5.16, while Figure 5.17 illustrates the loads on the model.

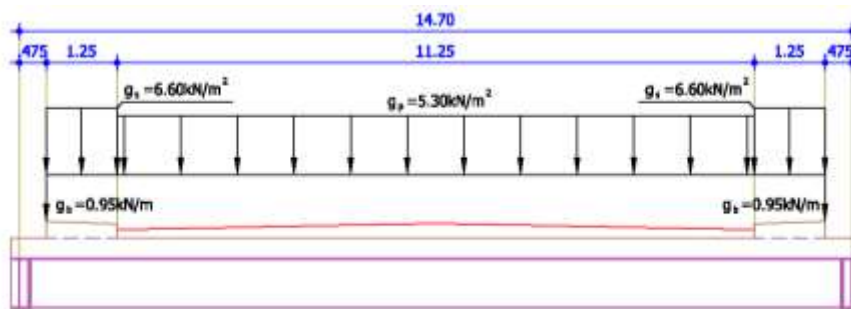


Figure 5.16: Superimposed permanent loads on the bridge

Σχήμα 5.16: Πρόσθετα μόνιμα φορτία στη γέφυρα

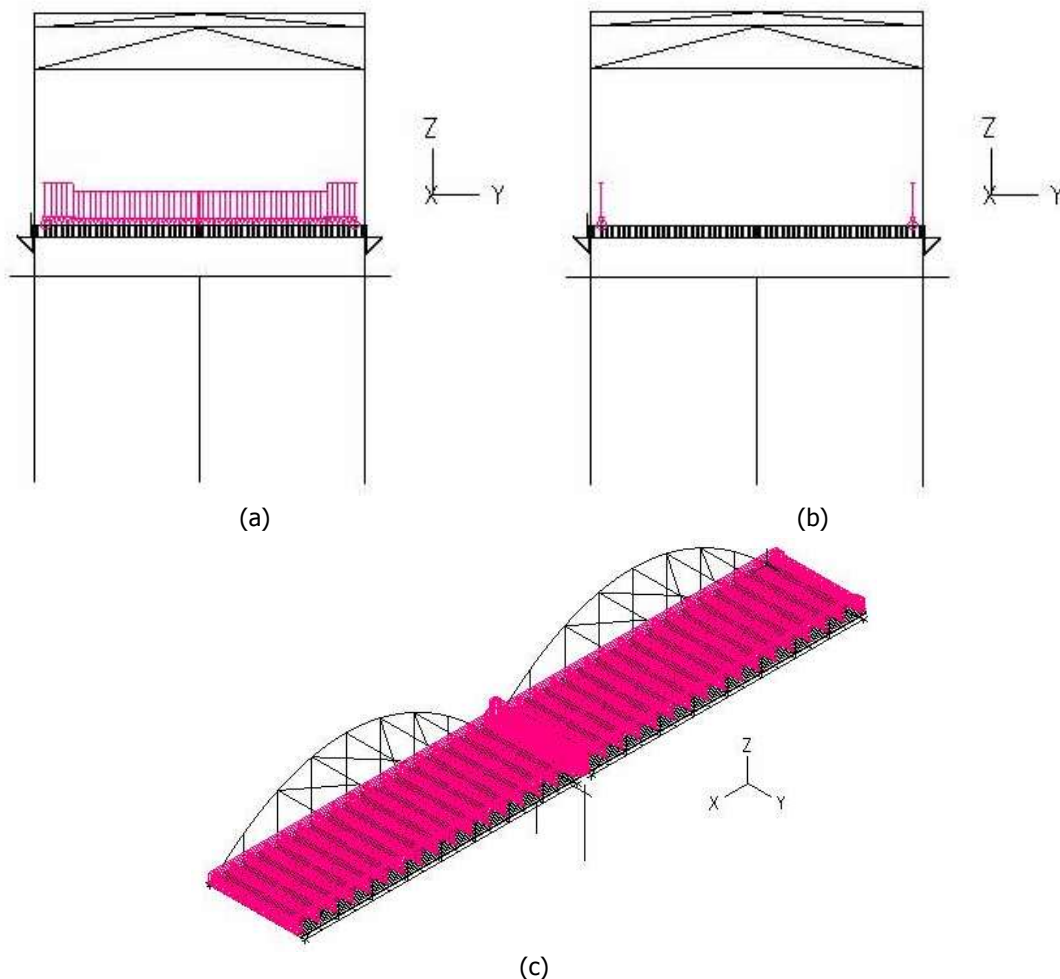


Figure 5.17: Superimposed permanent loads on the model: (a) g_p+g_s , (b) g_b , (c) perspective view

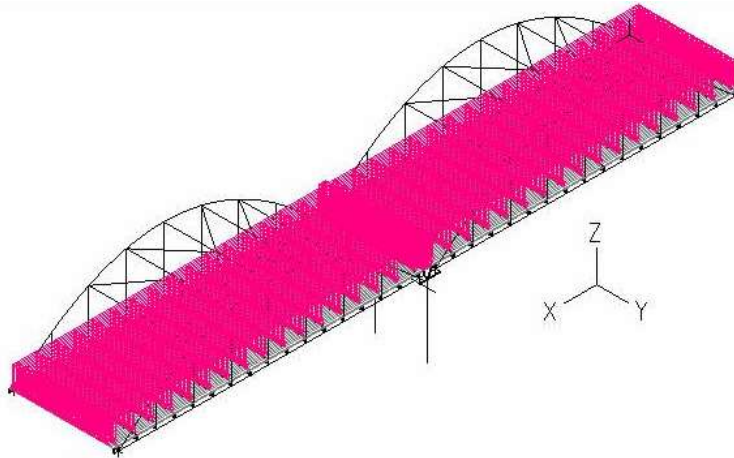
Σχήμα 5.17: Πρόσθετα μόνιμα φορτία στο προσομοίωμα: (a) g_p+g_s , (b) g_b , (c) προοπτικό

LC3: Uniform road traffic loads

The Traffic Load Model 1 consists of three lanes with width 3.00m. The loads considered for this LC are listed in Table 5.2. A uniform load is applied to the shell elements equal to 4.67kN/m^2 , as illustrated in Figure 5.18.

Table 5.2: Live Load of the road bridge**Πίνακας 5.2:** Κινητό φορτίο οδογέφυρας

	Load	Width	Length	Sum of Loads
TS	Lane 1: $0.9 \cdot 600 \text{kN} = 540 \text{kN}$ Lane 2: $0.9 \cdot 400 \text{kN} = 360 \text{kN}$ Lane 3: $0.9 \cdot 200 \text{kN} = 180 \text{kN}$			1080.00kN
UDL	9.00kN/m^2	3.00m	87.60m	2365.20kN
UDL	2.50kN/m^2	14.70m-3.00m	87.60m	2562.30kN
Total Load				6007.50kN
Distributed Load		14.70m	87.60m	4.67kN/m^2

**Figure 5.18:** Live loads on the model**Σχήμα 5.18:** Κινητά φορτία στο προσομοίωμα**LC4:** Ground settlement and rotations at the pier's footing

It is assumed that the footing rotation is always combined with a uniform settlement according to Eq. (5-25).

$$\theta = 0.05\rho \quad (5-25)$$

where θ is the rotation of the pier's footing in degrees and ρ is the uniform settlement in cm. Four cases are studied, listed in Table 5.3. The longitudinal rotation θ_x is taken into account as differential settlement on the two outside columns (Figure 5.19), while, for the transverse one, denoted as θ_y , imposed rotation is considered applied at the base of the three columns (Figure 5.20).

Table 5.3: Combination between rotations and settlements at the pier's footing**Πίνακας 5.3:** Συνδυασμός μεταξύ στροφών και καθιζήσεων στο πέδιλο μεσοβάθρου

Case	θ_x (degrees)	θ_y (degrees)	ρ (cm)
1	0.05	0	1
2	0	0.05	1
3	0.05	0.3×0.05	1
4	0.3×0.05	0.05	1

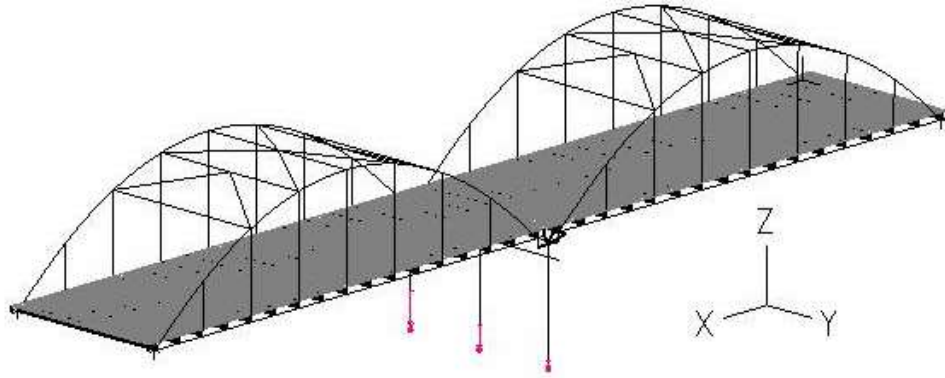


Figure 5.19: Imposed longitudinal rotation θ_x with combined settlement

Σχήμα 5.19: Επιβαλλόμενη διαμήκης στροφή θ_x και συζευγμένη καθίζηση

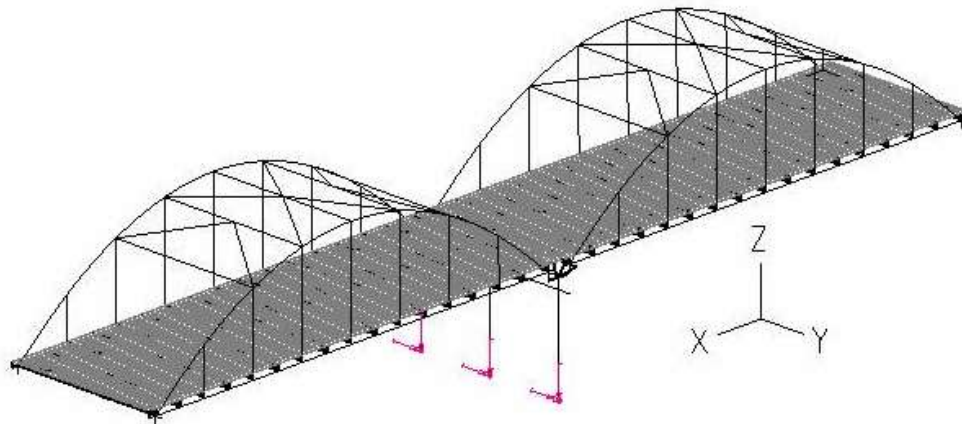


Figure 5.20: Imposed transverse rotation θ_y with combined settlement

Σχήμα 5.20: Επιβαλλόμενη εγκάρσια στροφή θ_y και συζευγμένη καθίζηση

5.5 Load Combinations at Ultimate Limit State (ULS)

The load combinations at ULS are described as:

$$\sum_{j \geq 1} \xi \gamma_{Gj} \cdot G_{kj} + \gamma_{Q1} \cdot Q_{k1} + \sum_{i \geq 1} \gamma_{Qi} \cdot \psi_{0i} \cdot Q_{ki} \quad (5-26)$$

and

$$\sum_{j \geq 1} \gamma_{Gj} \cdot G_{kj} + \gamma_{Q1} \cdot Q_{k1} + \sum_{i \geq 1} \gamma_{Qi} \cdot \psi_{0i} \cdot Q_{ki} \quad (5-27)$$

where ξ is a reduction factor for unfavorable permanent actions G and it is equal to $\xi=0.85$, while the partial factors γ_G and γ_Q are listed in Table 5.4 and the factors ψ_0 in Table 5.5. In this investigation the ground settlements are considered as permanent actions.

Table 5.4: Partial factors for actions in ULS

Πίνακας 5.4: Επιμέρους συντελεστές για δράσεις σε OKA

Action	Contribution	Factor	
Permanent actions	unfavourable	γ_{Gsup}	1.35
	favourable	γ_{Ginf}	1.00
Traffic loads	unfavourable	γ_Q	1.35
	favourable	γ_Q	0.00

Table 5.5: Factors ψ for road bridges**Πίνακας 5.5:** Συντελεστές ψ για οδογέφυρες

Actions	Symbol	ψ_0	
Traffic load	Gr1 (LM1)	TS	0.75
		UDL	0.40
Thermal actions		0.60	
Horizontal forces		0.00	
Wind forces		1.00	

The following ULS load combinations are considered:

Combination 1:

LC1×0.85×1.35	Self weight
+LC2×0.85×1.35	Superimposed
+LC3×1.35	Traffic load
+LC4×0.85×1.35	Ground displacements and rotations

This combination is considered crucial for the superstructure.

Combination 2:

LC1	Self weight
+LC2	Superimposed
+LC4×0.85×1.35	Ground settlement and rotations

This combination is considered crucial for the columns of the pier.

Chapter 6

LINEAR BUCKLING ANALYSIS

6.1 Buckling modes

For the design of the steel members, first a linear buckling analysis (LBA) is conducted, taking into account the permanent loads, i.e. the self weight (LC1) and the superimposed (LC2), as described in section 5.4. The initial imperfections are calculated according to the buckling modes for the in-plane (Figure 6.1) and out-of-plane (Figure 6.2) buckling of the middle diagonal bracing members, the modes of Figure 6.3 for the out-of-plane buckling of the arch and those of Figure 6.4 for the in-plane buckling of the outer diagonal bracing members.

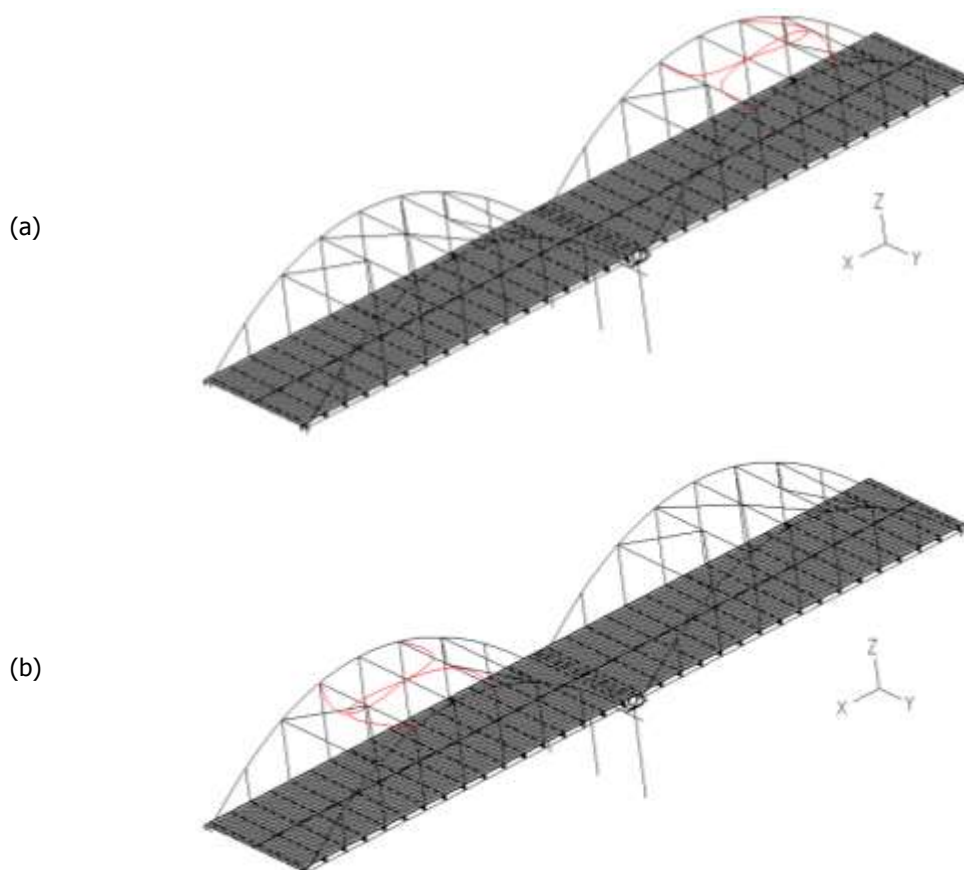


Figure 6.1: In-plane buckling modes of the middle diagonal bracing members: (a) 5th mode, (b) 6th mode

Σχήμα 6.1: Εντός επιπέδου ιδιομορφές λυγισμού των μεσαίων διαγώνιων συνδέσμων δυσκαμψίας; (a) 5^η ιδιομορφή, (b) 6^η ιδιομορφή

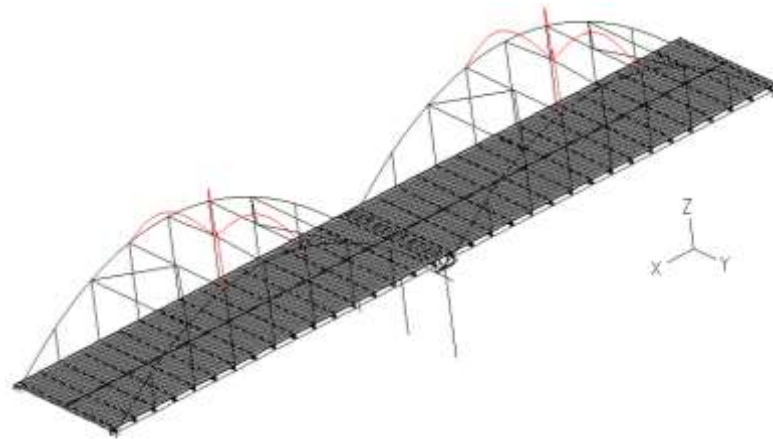


Figure 6.2: Out-of-plane buckling mode of the middle diagonal bracing members: 13th mode
Σχήμα 6.2: Εκτός επιπέδου ιδιομορφή λυγισμού των μεσίων διαγώνιων συνδέσμων δυσκαμψίας: 13^η ιδιομορφή

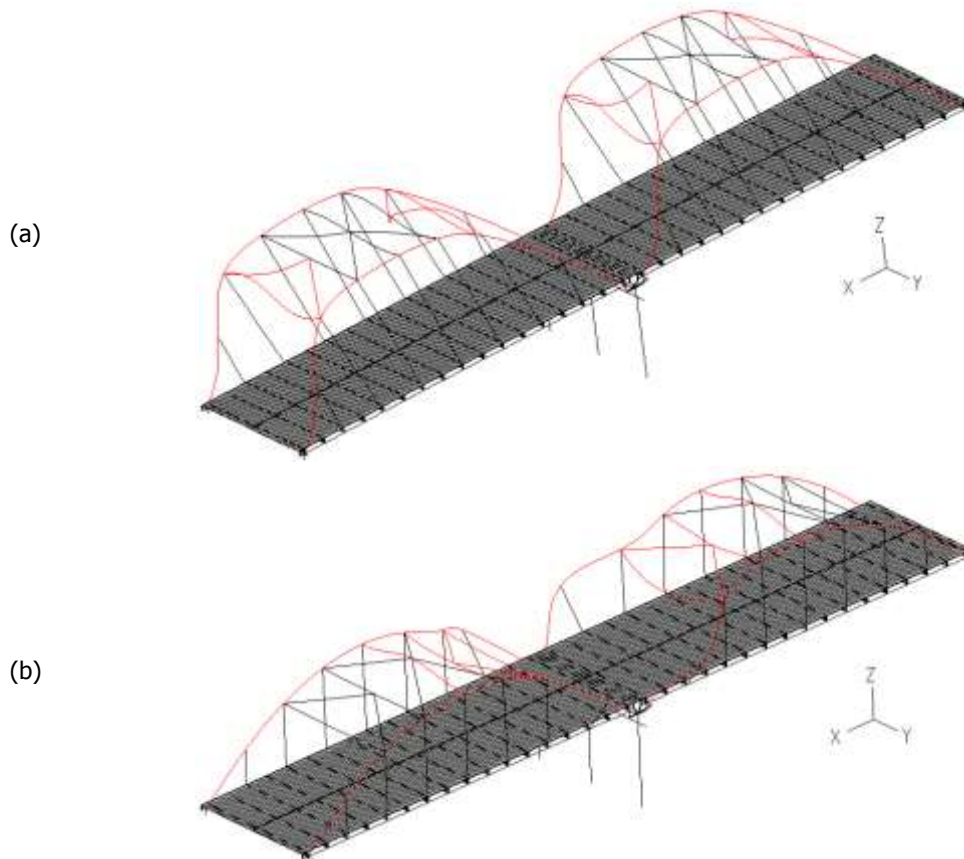


Figure 6.3: Out-of-plane buckling modes of the arch: (a) 34th mode, (b) 40th mode
Σχήμα 6.3: Εκτός επιπέδου ιδιομορφές λυγισμού τόξων: (a) 34^η ιδιομορφή, (b) 40^η ιδιομορφή

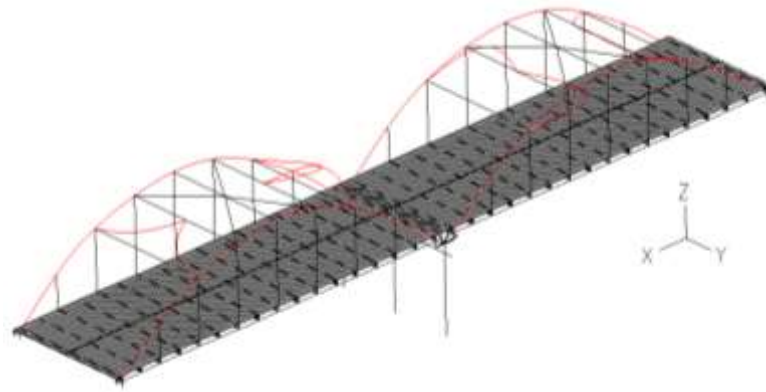


Figure 6.4: In-plane buckling mode of the outer diagonal bracing members: 70th mode

Σχήμα 6.4: Εντός επιπέδου ιδιομορφή λυγισμού των ακραίων διαγώνιων συνδέσμων δυσκαμψίας: 70^η ιδιομορφή

6.2 Initial imperfections

In order to verify the stability of the steel members automatically by means of nonlinear analyses, rather than performing code-based buckling checks, initial imperfections are considered, the amplitudes of which are calculated according EC3-1. For the diagonal bracing members and a buckling curve c (cold formed hollow sections) a maximum initial imperfection is considered equal to:

$$L/150=0.06\text{m, where } L=9.13\text{m} \quad (6-1)$$

For the horizontal bracing members the maximum initial imperfection is:

$$L/150=0.098\text{m, where } L=14.70\text{m} \quad (6-2)$$

According to EC3-2, for the out-of-plane buckling of the arches the maximum imperfection is assumed equal to:

$$\frac{\ell_1}{200} = 0.15\text{m where } \ell_1 = \sqrt{20L} = \sqrt{20 \times 42} = 28.98\text{m} \quad (6-3)$$

where $L=42\text{m}$ is the span of the arch. The total imperfection at each member, resulting from the combination of all buckling modes that are taken into account, should not exceed these limits. The initial imperfections considered in this study are given in Table 6.1.

Table 6.1: Initial imperfections

Πίνακας 6.1: Αρχικές ατέλειες

Buckling mode	Initial imperfection	Direction	Member	Position
5	3.60cm	X-tranlation	Middle diagonal bracing	Figure 6.5
6	5.00cm	X-tranlation	Middle diagonal bracing	Figure 6.6
13	2.20cm	Z-tranlation	Middle diagonal bracing	Figure 6.5
34	13.50cm	Y-tranlation	Arch	Figure 6.7
40	10.40cm	Y-tranlation	Arch	Figure 6.8
70	-4.60cm	X-tranlation	Outer diagonal bracing	Figure 6.9

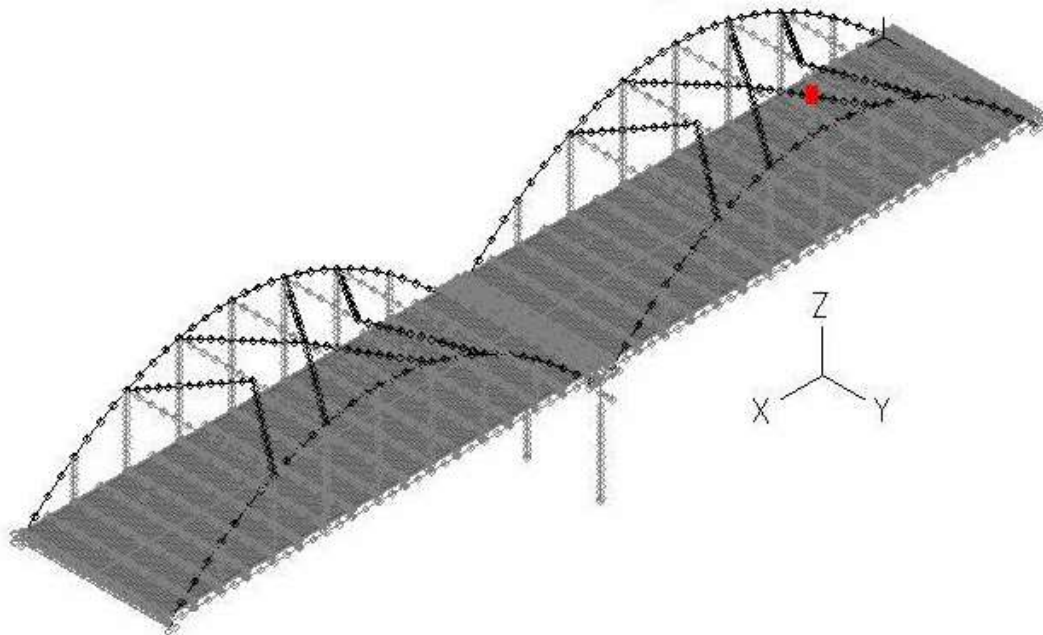


Figure 6.5: Position of imperfection according to the 5th and 13th buckling modes

Σχήμα 6.5: Θέση εφαρμογής της ατέλειας σύμφωνα με την 5^η και 13^η ιδιομορφές λυγισμού

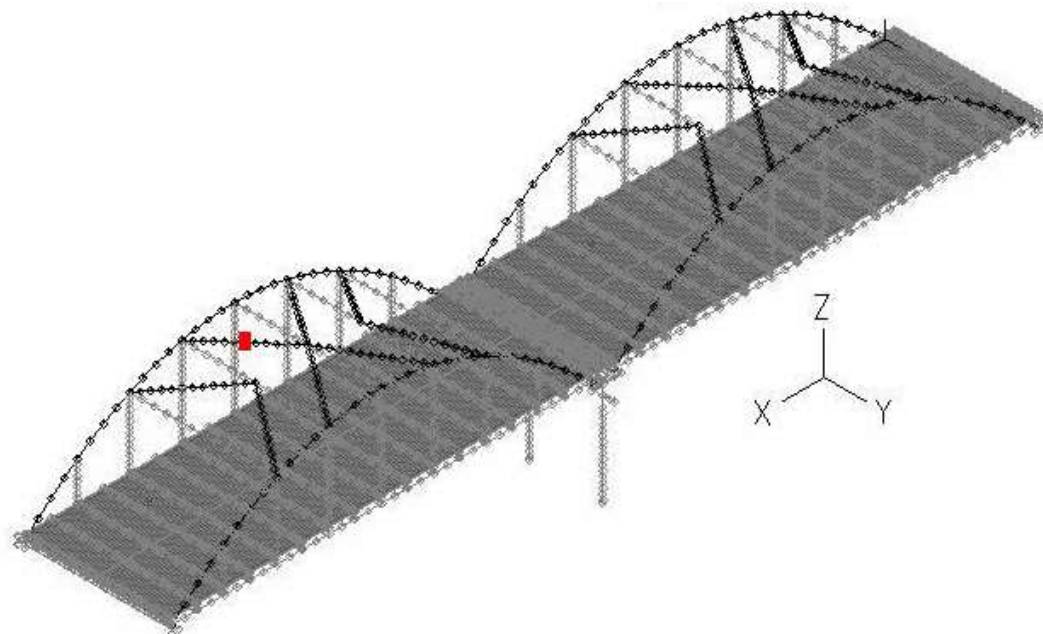


Figure 6.6: Position of imperfection according to the 6th buckling mode

Σχήμα 6.6: Θέση εφαρμογής της ατέλειας σύμφωνα με την 6^η ιδιομορφή λυγισμού

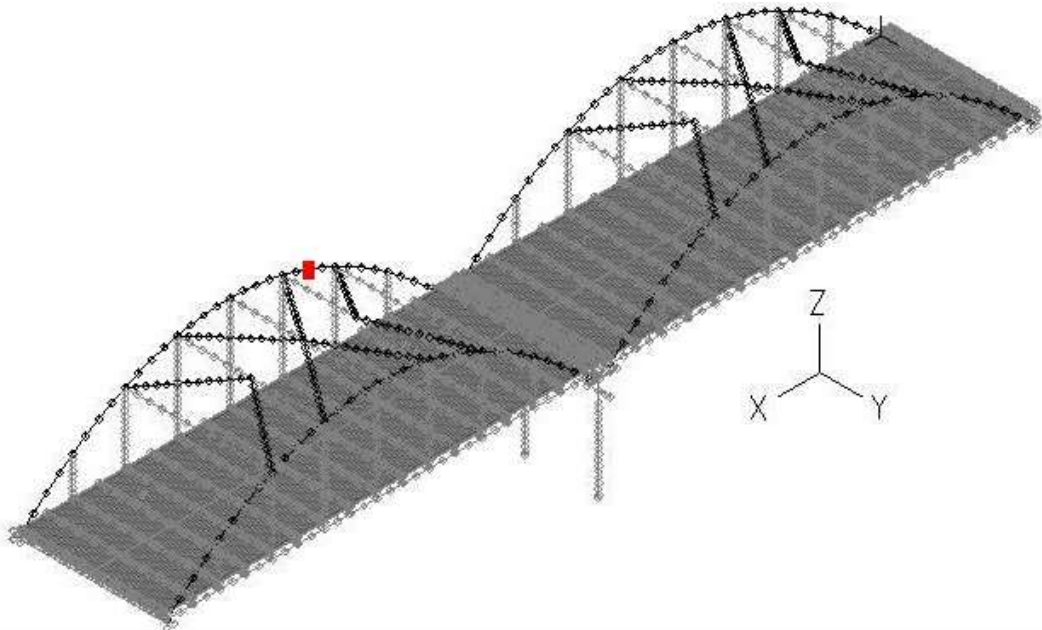


Figure 6.7: Position of imperfection according to the 34th buckling mode
Σχήμα 6.7: Θέση εφαρμογής της ατέλειας σύμφωνα με την 34^η ιδιομορφή λυγισμού

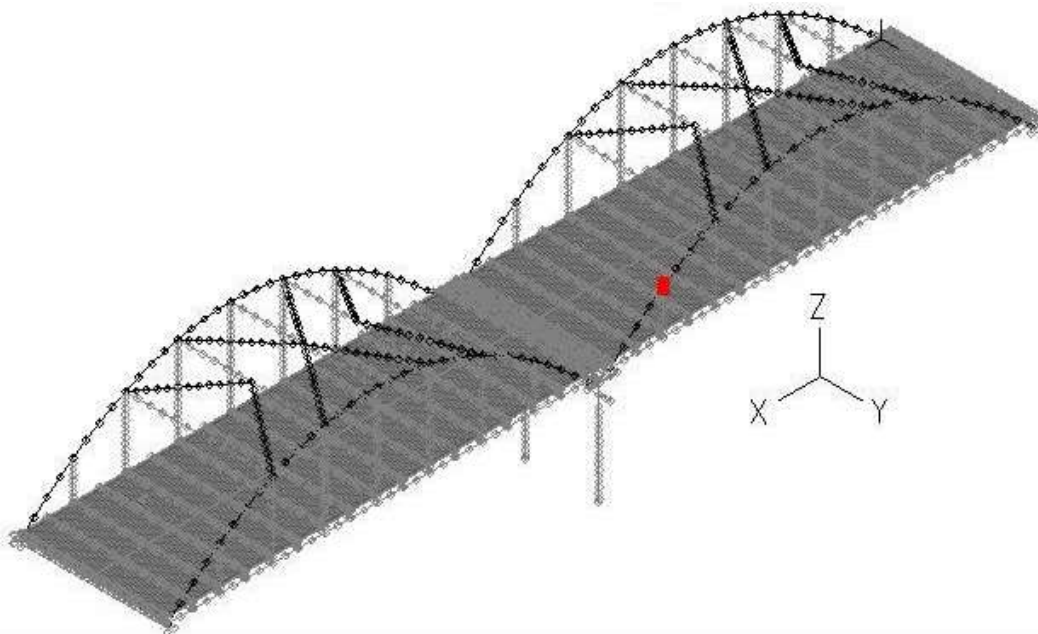


Figure 6.8: Position of imperfection according to the 40th buckling mode
Σχήμα 6.8: Θέση εφαρμογής της ατέλειας σύμφωνα με την 40^η ιδιομορφή λυγισμού

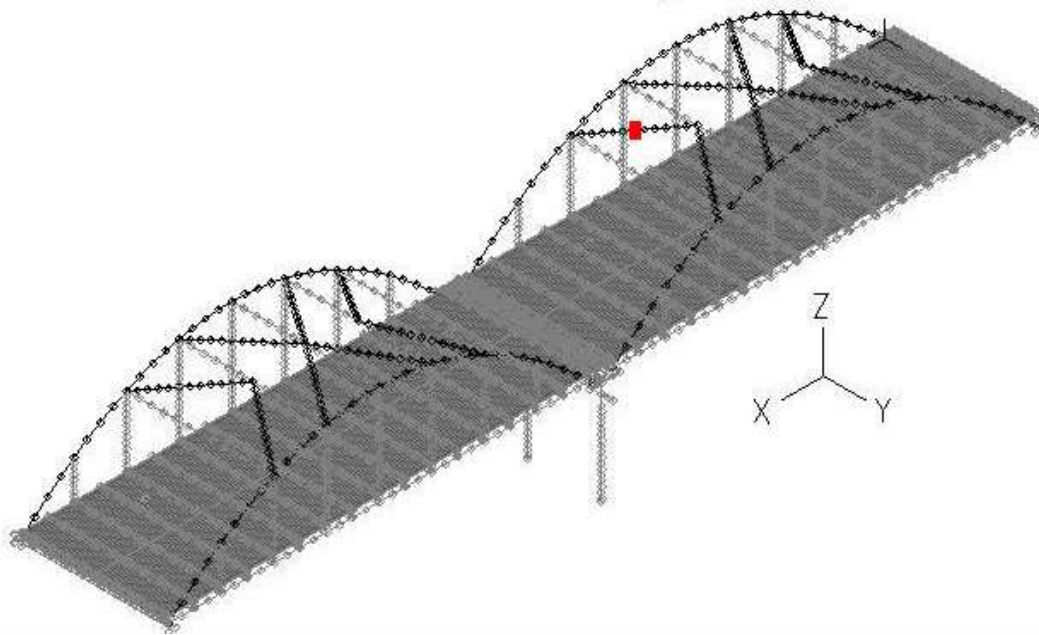


Figure 6.9: Position of imperfection according to the 70th buckling mode

Σχήμα 6.9: Θέση εφαρμογής της ατέλειας σύμφωνα με την 70^η ιδιομορφή λυγισμού

Chapter 7

IMPOSED ROTATIONS AND SETTLEMENTS

7.1 Loading sequence

First, at $t=0$ until $t=0.995$, the self weight of the structure (LC1) is imposed, neglecting the stiffness of the deck's slab. Then, the shell elements are activated at $t=0.995$ and the permanent loads (LC2) begin to evolve. When LC2 is completed, at $t=2$, the live loads (LC3) are applied until $t=2.99$. Then, the rotational springs of the continuous slab die at $t=2.995$ and LC4 begins to evolve at $t=3.00$ until the first failure occurs and the analysis stops, close to $t=4$. Table 7.1 gives the described sequence of the load imposition for the first load combination, in which the live loads are taken into account, while Table 7.2 accounts for the second load combination, in which the live loads are not included.

Table 7.1: Sequence of loads for Combination 1 (see §5.5)

Πίνακας 7.1: Σειρά εφαρμογής φορτίων για τον Συνδυασμό 1 (βλ. §5.5)

t	LC1	LC2	LC3	LC4	Shell elements	Slab's springs
0	0%	0%	0%	0%	–	√
0.995	100%	0%	0%	0%	–	√
1	100%	0%	0%	0%	√	√
2	100%	100%	0%	0%	√	√
2.99	100%	100%	100%	0%	√	√
2.995	100%	100%	100%	0%	√	–
3	100%	100%	100%	0%	√	–
4	100%	100%	100%	100%	√	–

Table 7.2: Sequence of loads for Combination 2 (see §5.5)

Πίνακας 7.2: Σειρά εφαρμογής φορτίων για τον Συνδυασμό 2 (βλ. §5.5)

t	LC1	LC2	LC4	Shell elements	Slab's springs
0	0%	0%	0%	–	√
0.995	100%	0%	0%	–	√
1	100%	0%	0%	√	√
2.99	100%	100%	0%	√	√
2.995	100%	100%	0%	√	–
3	100%	100%	0%	√	–
4	100%	100%	100%	√	–

7.2 Case 1 ($\theta_x + \rho$)

7.2.1 Imposed settlement ρ and rotation θ_x

A rotation at the footing of the pier along the longitudinal axis x (θ_x) is applied as a differential settlement at the outer columns (Figure 7.1a,b), equal to:

$$\rho^{\theta} = \pm L_y \theta_x = \pm 7.35 \theta_x \text{ [m]} \quad (7-1)$$

where $L_y = 7.35\text{m}$ the distance of the columns and θ_x is measured in [rad], while ρ in [m]. Moreover, Eq. (5-25) gives the combined uniform settlement, which, keeping the same units [rad] and [m] for the rotation and settlement, respectively, becomes (Figure 7.1c):

$$\frac{180}{\pi} \theta_x = 0.05 \cdot 100 \cdot \rho \Rightarrow \rho = \frac{180}{0.05 \cdot 100 \cdot \pi} \theta_x = 11.459 \theta_x \text{ [m]} \quad (7-2)$$

The sum of settlements at the pier's columns is shown in Figure 7.1d.

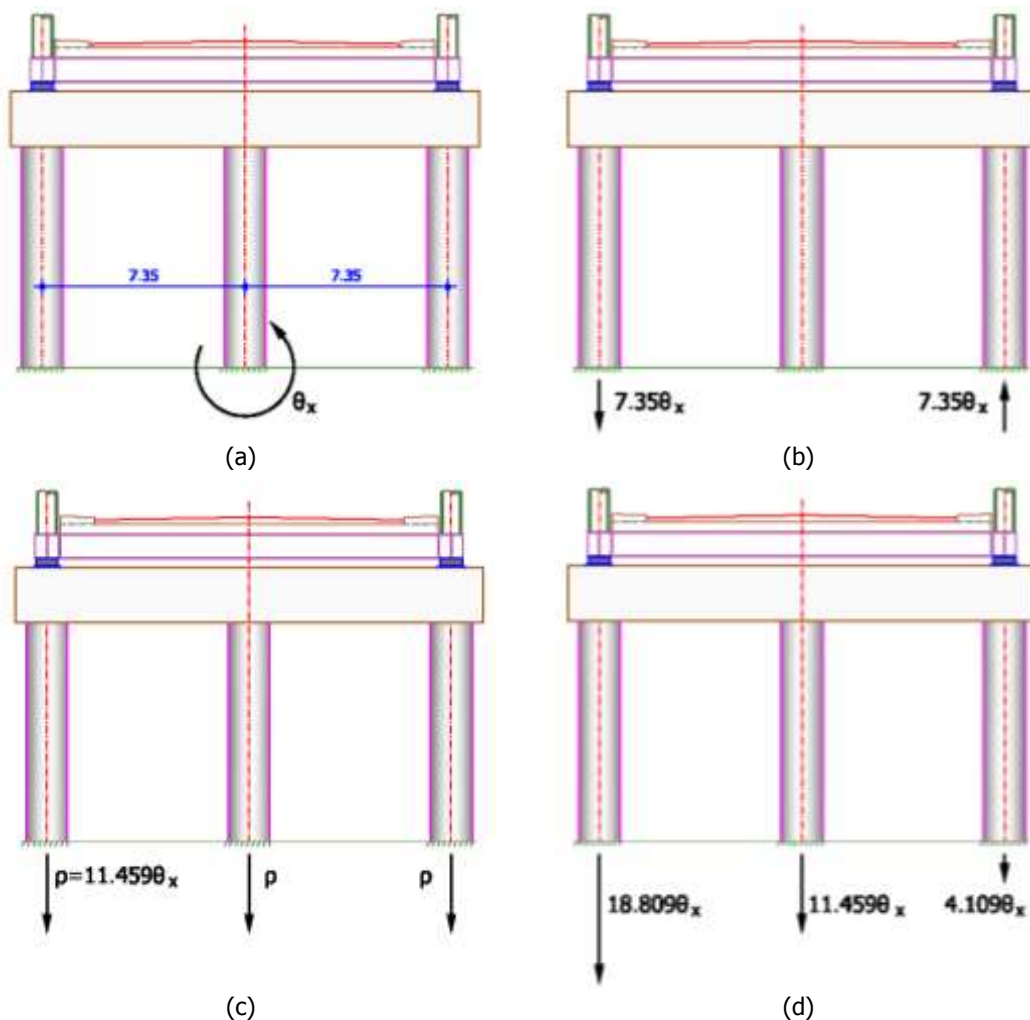


Figure 7.1: Imposed longitudinal rotation θ_x and settlement ρ : (a) imposed rotation, (b) differential settlement ρ^{θ} , (c) uniform settlement ρ , (d) sum of settlements at the pier's columns

Σχήμα 7.1: Επιβαλλόμενη διαμήκης στροφή θ_x και καθίζηση ρ : (a) επιβαλλόμενη στροφή, (b) διαφορική καθίζηση ρ^{θ} , (c) ομοιόμορφη καθίζηση ρ , (d) συνολική καθίζηση στους στύλους μεσοβάθρου

7.2.2 Response of the bridge for Combination 1

The initial imperfections are assumed as described in section 6.2. The permanent loads are applied with a loading factor $\xi_{\gamma G}=0.85 \times 1.35=1.15$, and the live loads with a factor equal to 1.35, as defined in section 5.5. A maximum rotation θ_x is assumed equal to $\max \theta_x=0.026 \text{ rad}$. The analysis stops when $\theta_x=0.0245 \text{ rad}=1.40^\circ$, at $t=3.94$, because of the bending failure at the top of the middle column (column 2), which is defined in Figure 7.2. The deformed state at the moment of failure is illustrated in Figure 7.3.

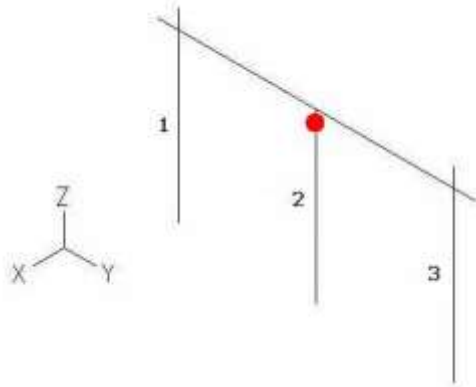


Figure 7.2: Failure at the top of column 2

Σχήμα 7.2: Αστοχία στην κορυφή του σύλου 2

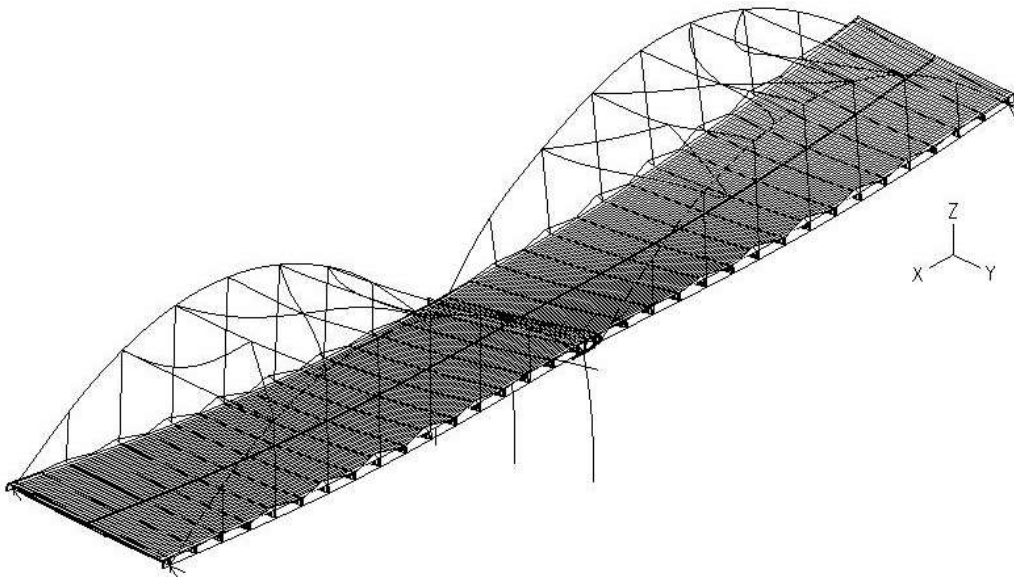


Figure 7.3: Deformed state at failure

Σχήμα 7.3: Παραμορφωμένη κατάσταση στην αστοχία

The diagram $M-\varphi$ is depicted in Figure 7.4 (a) for the top and (b) for the base of all three columns, where it is noted that the sections at the base of the pier remain in the elastic zone, while significant bending moments are evolved at the top of them, leading to the failure of the pier. The corresponding magnitudes are also listed in Table 7.3. The $M-t$ diagrams are plotted in Figure 7.5, in which the first yield is detected, for $t=3.643$, occurring simultaneously at the top of columns 1 and 2. In these diagrams, the bending moments that correspond to yield are denoted with the dotted lines for the top section of each column.

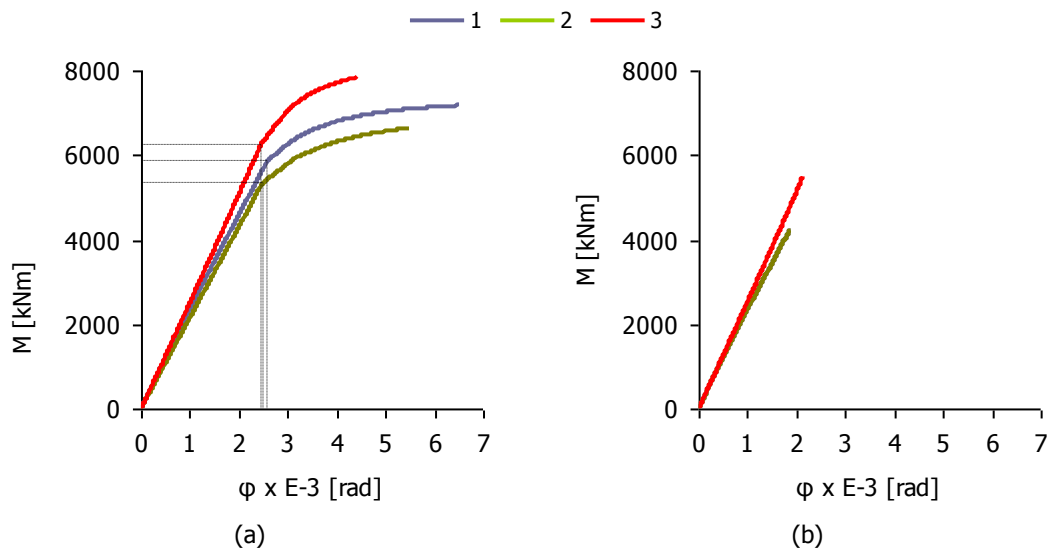


Figure 7.4: M- ϕ diagrams for (a) the top and (b) the base of the three columns

Σχήμα 7.4: Διαγράμματα M- ϕ για (a) τις κορυφές και (b) τις βάσεις των τριών στύλων

Table 7.3: Yield at the top of the pier's columns

Πίνακας 7.3: Διαρροή στην κορυφή των στύλων μεσοβάθρου

Columns	t	M [kNm]	ϕ E-3 [rad]
1	3.643	5848.61	2.58
2	3.643	5331.41	2.48
3	3.711	6254.65	2.46

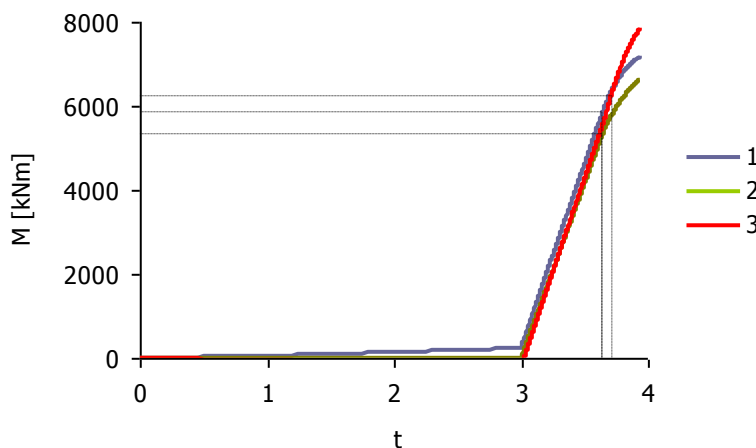


Figure 7.5: M-t diagrams for the top of the three columns

Σχήμα 7.5: Διαγράμματα M-t για τις κορυφές των τριών στύλων

Regarding the steel members, at the time of failure, they all remain in the elastic zone, except of the diagonal bracing members, which slightly exceed the yield stress due to buckling. The response of the steel members at the end of the analysis, as well as at the time of the first yield at the top of the pier's column, is summarized in Table 7.4. At the time of the first yield, but also when the pier's failure occurs, the steel members' stresses are smaller than the ultimate stress $f_u=510\text{MPa}$. The diagonal bracing members are considered replaceable, thus, their buckling does not indicate an overall bridge failure. More specifically, the maximum stress of the arches (Figure 7.6) at the time of the pier's failure reaches the value of 254.78MPa (Figure 7.7), the one of the main beams (Figure 7.8) is 190.00MPa (Figure 7.9) and the secondary ones (Figure 7.10) 111.10MPa (Figure 7.11), for the horizontal bracing members (Figure 7.12) it is 256.23MPa (Figure 7.13), for the diagonal bracing members

(Figure 7.14) it is 363.06MPa (Figure 7.15) and for the hangers (Figure 7.16) it reaches the value of 272.26MPa (Figure 7.17).

Table 7.4: Maximum stresses in the steel members at the time of the first yield ($t=3.643$) and the time of failure ($t=3.94$)

Πίνακας 7.4: Μέγιστες τάσεις στα μεταλλικά στοιχεία τη στιγμή της πρώτης διαρροής ($t=3.643$) και τη στιγμή της αστοχίας ($t=3.94$)

Members	t=3.643		t=3.94	
	σ [MPa]	ϵ %	σ [MPa]	ϵ %
Arches	233.96	0.11	254.78	0.12
Main beams	176.19	0.08	190.00	0.09
Secondary beams	111.02	0.05	111.10	0.05
Horizontal bracing	161.24	0.08	256.23	0.12
Diagonal bracing	359.21	0.76	363.06	1.30
Hangers	269.55	0.13	272.26	0.13

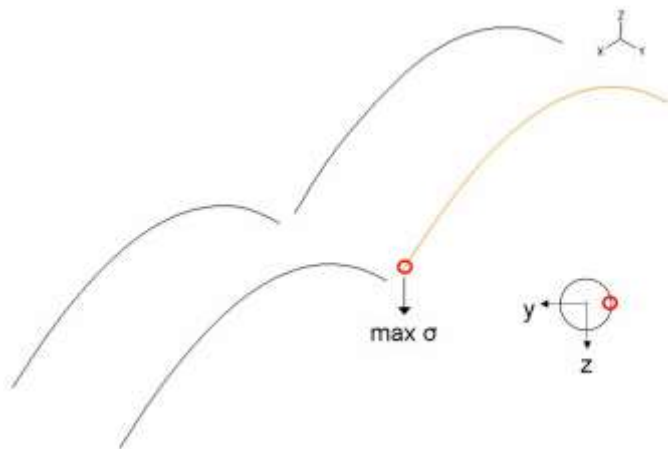


Figure 7.6: Point of maximum stress in the arches

Σχήμα 7.6: Σημείο μέγιστης τάσης στα τόξα

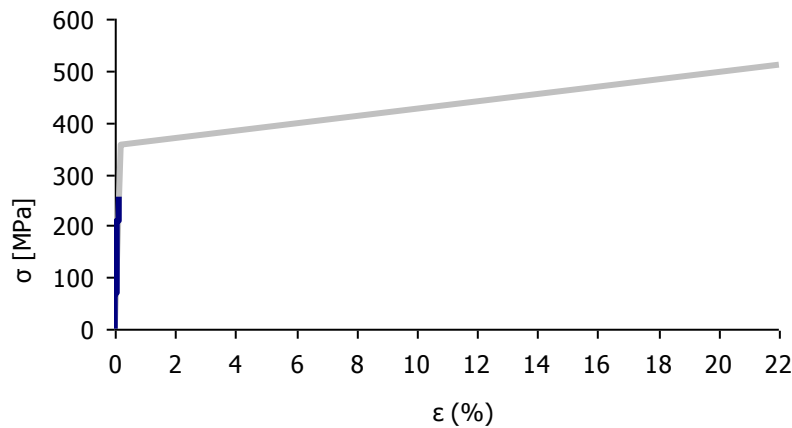


Figure 7.7: Maximum stress – strain diagram for the arches

Σχήμα 7.7: Διάγραμμα μέγιστων τάσεων – παραμορφώσεων για τα τόξα

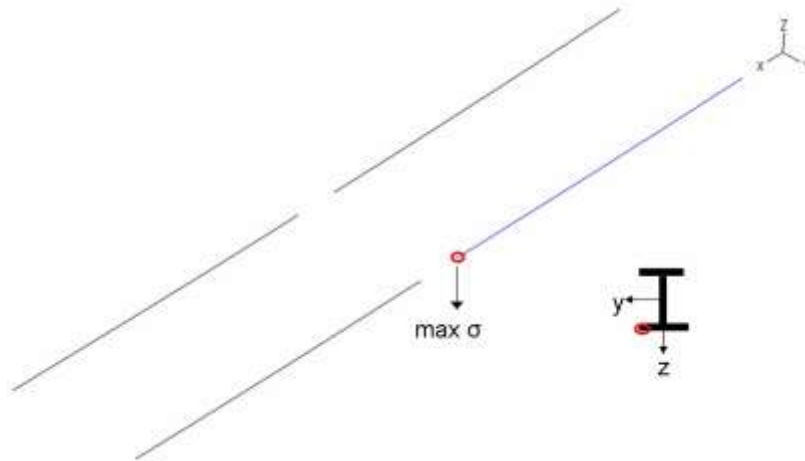


Figure 7.8: Point of maximum stress in the main beams

Σχήμα 7.8: Σημείο μέγιστης τάσης στις κύριες δοκούς

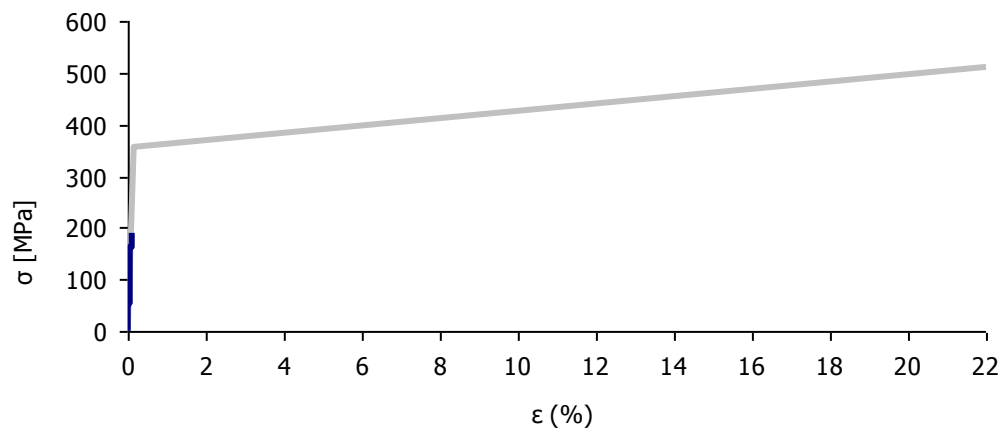


Figure 7.9: Maximum stress – strain diagram for the main beams

Σχήμα 7.9: Διάγραμμα μέγιστων τάσεων – παραμορφώσεων για τις κύριες δοκούς

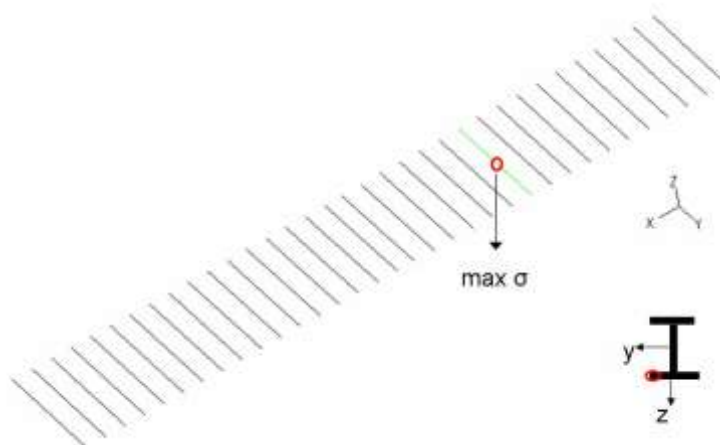


Figure 7.10: Point of maximum stress in the secondary beams

Σχήμα 7.10: Σημείο μέγιστης τάσης στις διαδοκίδες

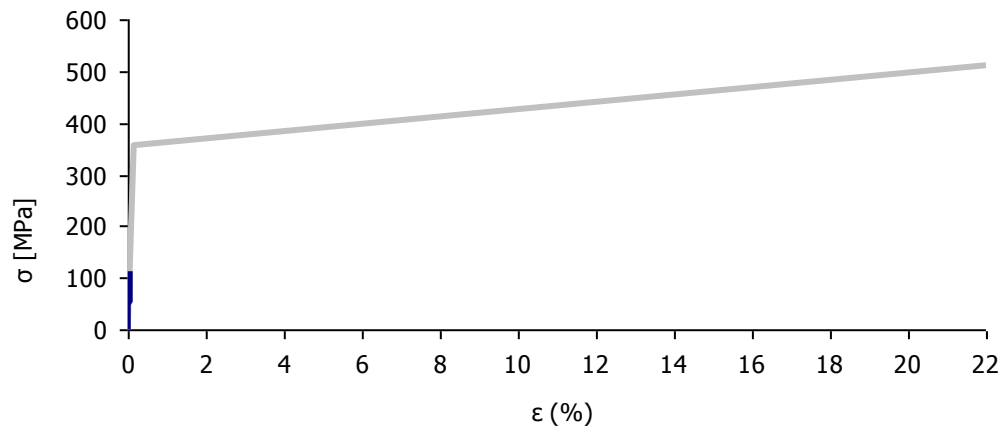


Figure 7.11: Maximum stress – strain diagram for the secondary beams

Σχήμα 7.11: Διάγραμμα μέγιστων τάσεων – παραμορφώσεων για τις διαδοκίδες

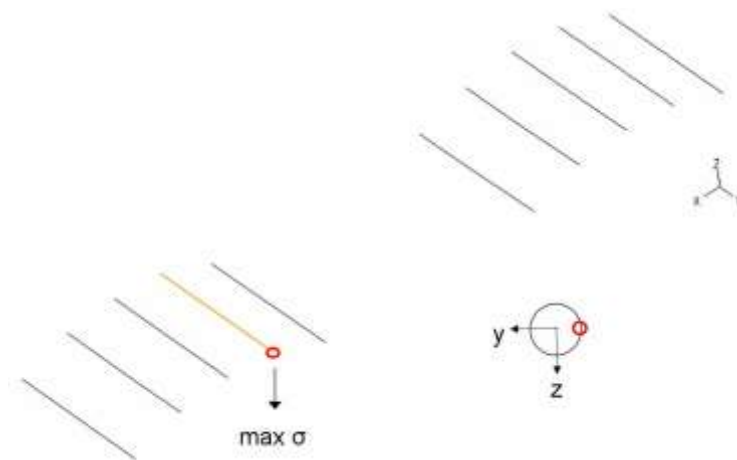


Figure 7.12: Point of maximum stress in the horizontal bracing members

Σχήμα 7.12: Σημείο μέγιστης τάσης στους εγκάρσιους συνδέσμους δυσκαμψίας

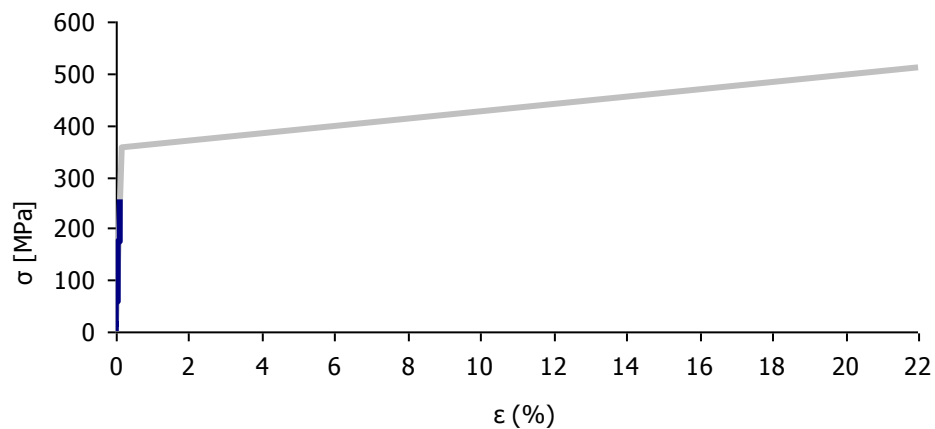


Figure 7.13: Maximum stress – strain diagram for the horizontal bracing members

Σχήμα 7.13: Διάγραμμα μέγιστων τάσεων – παραμορφώσεων για τους εγκάρσιους συνδέσμους δυσκαμψίας

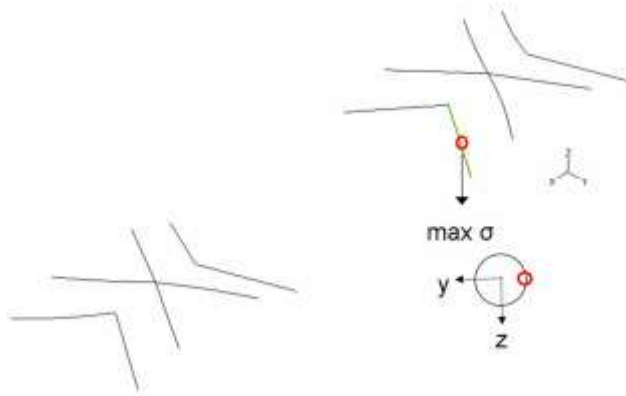


Figure 7.14: Point of maximum stress in the diagonal bracing members

Σχήμα 7.14: Σημείο μέγιστης τάσης στους διαγώνιους συνδέσμους δισκαμψίας

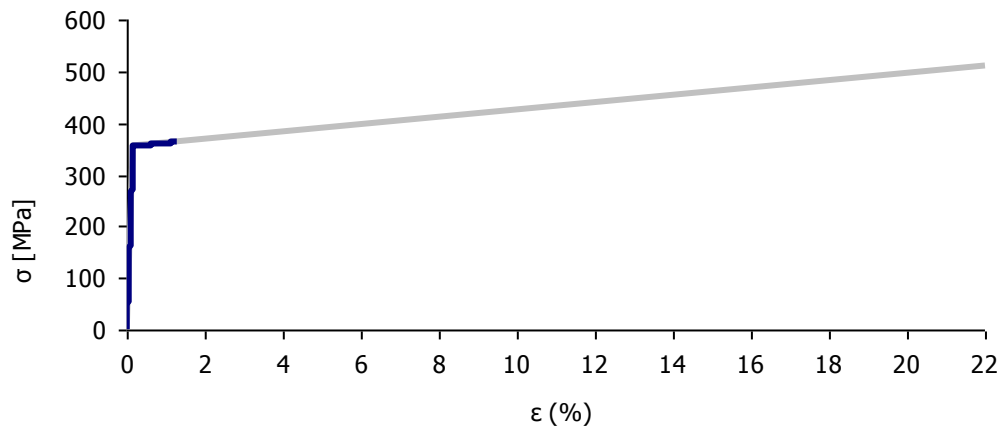


Figure 7.15: Maximum stress – strain diagram for the diagonal bracing members

Σχήμα 7.15: Διάγραμμα μέγιστων τάσεων – παραμορφώσεων για τους διαγώνιους συνδέσμους δισκαμψίας

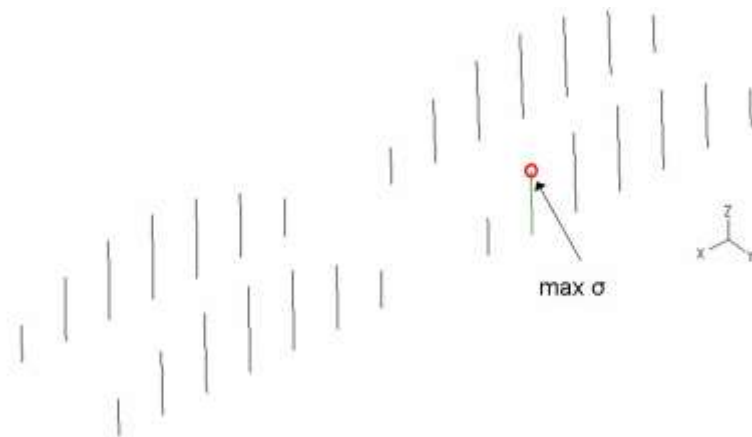


Figure 7.16: Point of maximum stress in the hangers

Σχήμα 7.16: Σημείο μέγιστης τάσης στους αναρτήρες

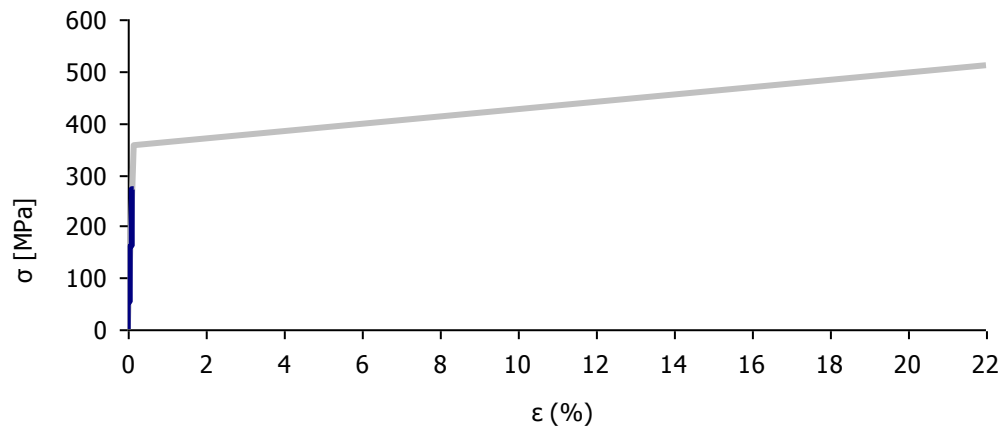


Figure 7.17: Maximum stress – strain diagram for the hangers

Σχήμα 7.17: Διάγραμμα μέγιστων τάσεων – παραμορφώσεων για τους αναρτήρες

The load – displacement diagrams of the horizontal springs in the transverse direction of the bridge are illustrated in Figure 7.18 for the abutment and in Figure 7.19 for the pier, where it is noted that the springs behave elastically, until the end of the analysis. The maximum force and the horizontal displacement of the springs arise at 288kN and 0.08m, respectively, for the bearings of both abutment and pier.

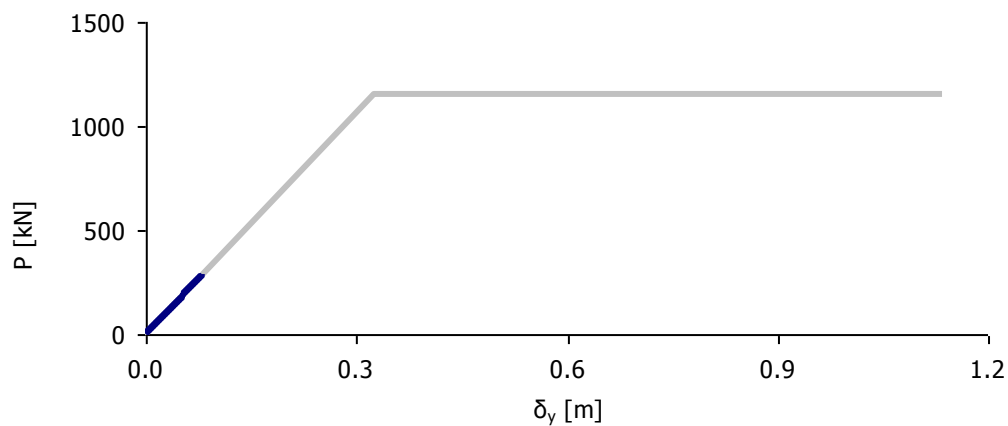


Figure 7.18: Diagram of load – displacement for the abutment's bearings

Σχήμα 7.18: Διάγραμμα φορτίου – παραμόρφωσης εφεδρώνων ακροβάθρου

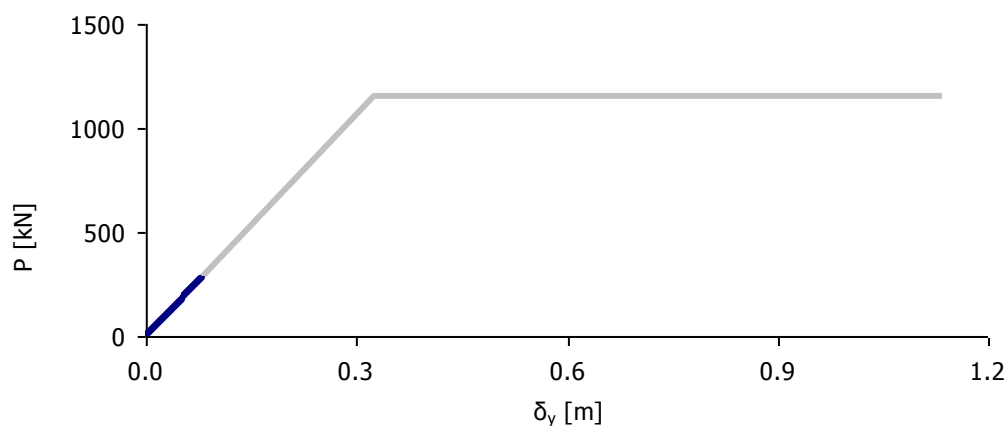


Figure 7.19: Diagram of load – displacement for the pier's bearings

Σχήμα 7.19: Διάγραμμα φορτίου – παραμόρφωσης εφεδρώνων μεσοβάθρου

In Figure 7.20 the evolution of the shear strains of the abutment's bearings is plotted, while Figure 7.21 refers to the pier's bearings. The shear strain due to translational movements $\varepsilon_{q,d}$ remains at low levels for the vertical loads, and it increases when the rotation and settlement at the base of the pier are imposed, but it never exceeds the limit of 2 (see Eq. (5-17)), while the maximum design strain $\varepsilon_{t,d}$ remains smaller than the limit of 7 (see Eq. (5-21)), until the end of the analysis.

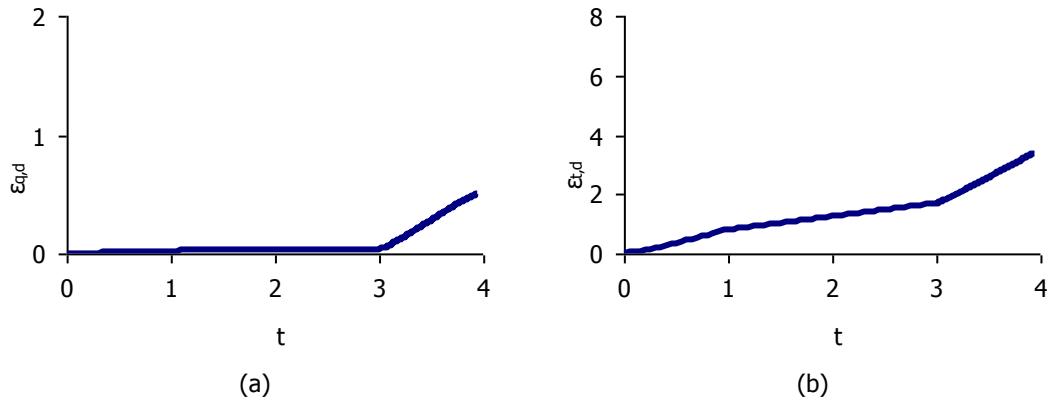


Figure 7.20: Strains of the abutment's bearings: (a) shear strain due to translational movements $\varepsilon_{q,d}$, (b) maximum design strain $\varepsilon_{t,d}$

Σχήμα 7.20: Παραμορφώσεις εφεδράνων ακροβάθρου: (α) διατμητική παραμόρφωση λόγω μετακίνησης $\varepsilon_{q,d}$, (β) συνολική διατμητική παραμόρφωση $\varepsilon_{t,d}$

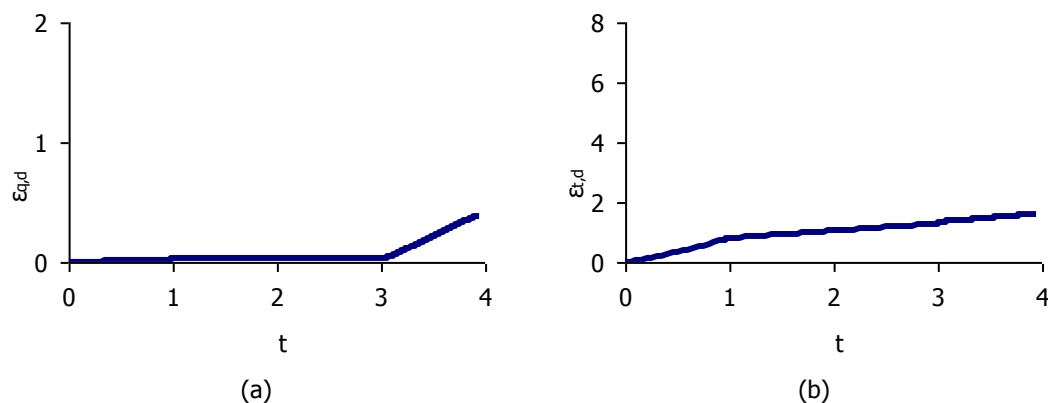


Figure 7.21: Strains of the pier's bearings: (a) shear strain due to translational movements $\varepsilon_{q,d}$, (b) maximum design strain $\varepsilon_{t,d}$

Σχήμα 7.21: Παραμορφώσεις εφεδράνων μεσοβάθρου: (α) διατμητική παραμόρφωση λόγω μετακίνησης $\varepsilon_{q,d}$, (β) συνολική διατμητική παραμόρφωση $\varepsilon_{t,d}$

7.2.3 Permissible rotation and settlement for Combination 1

Plotting the diagrams of the longitudinal rotation θ_x (Figure 7.22) and the uniform settlement ρ vs t (Figure 7.23), the settlement occurring at the first yield of the pier's columns, $t=3.643$, is equal to $\rho_Y=19.16\text{cm}$, corresponding to a rotation $\theta_{x,Y}=0.0167\text{rad}=0.96^\circ$. Nevertheless, as explained in section 3.3, the exceedance of the yield stress at the column tops is permitted for rotation about the longitudinal axis of the bridge, because the pier acts as a frame (Figure 3.3). Hence, in this case, the admissible settlement for the simply supported bridge under investigation corresponds to the time of the failure, arising at $\rho_F=28\text{cm}$ and a corresponding rotation equal to $\theta_{x,F}=0.0244\text{rad}=1.40^\circ$. Moreover, in order to take into account the combination loading factor for LC4, as described in section 5.5, which is equal to $\xi_{\gamma G}=0.85 \cdot 1.35=1.15$, the maximum permissible values of the settlement and rotation should be equal to the F-values corresponding to failure, divided by the loading factor 1.15, leading to $\rho_P=24.4\text{cm}$ and $\theta_{x,P}=0.0212\text{rad}=1.22^\circ$. In these diagrams the dotted lines correspond to the

imposed rotation and settlement at the time of the first yield of the pier’s columns. All values of the calculated settlement and rotation are given in Table 7.5.

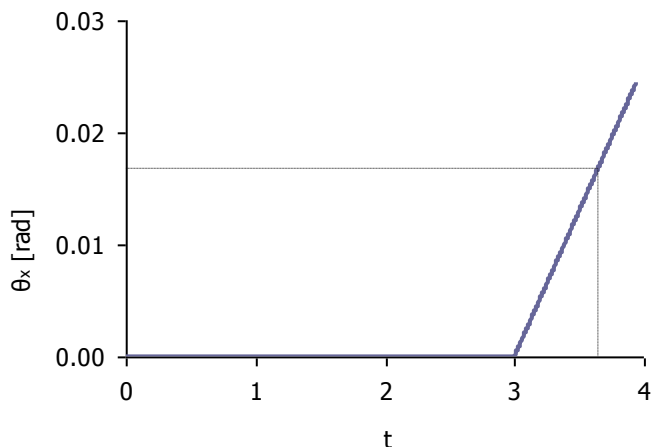


Figure 7.22: Longitudinal rotation θ_x vs t
Σχήμα 7.22: Διαμήκης στροφή θ_x συναρτήσει t

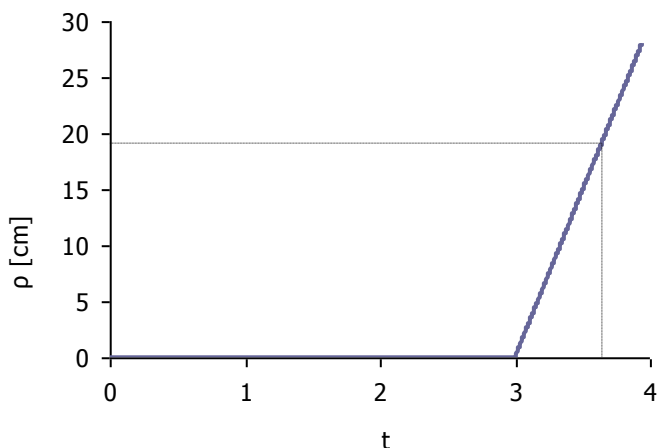


Figure 7.23: Uniform settlement ρ vs t
Σχήμα 7.23: Ομοιόμορφη καθίζηση ρ συναρτήσει t

Table 7.5: Maximum, yield and permissible values of rotation θ_x and uniform settlement ρ
Πίνακας 7.5: Μέγιστη τιμή, τιμή στην πρώτη διαρροή και επιτρεπόμενη τιμή διαμήκουσ στροφής θ_x και ομοιόμορφης καθίζησής ρ

	t	ρ [cm]	θ_x [rad]	θ_x [degrees]
Yield (Y)	3.643	19.2	0.0167	0.96
Failure (F)	3.940	28.0	0.0244	1.40
Permissible (P=F/1.15)	–	24.4	0.0212	1.22

7.2.4 Inclination angle of the pier for Combination 1

The diagram of Figure 7.24 gives the evolution of the inclination angle θ_i of the pier’s columns during the analysis. At the time of failure, the inclination angle is $\theta_{i,F}=0.0104\text{rad}=0.60^\circ$, and at the time of the first yield, it is $\theta_{i,Y}=0.0078\text{rad}=0.44^\circ$. Dividing with the loading factor $\xi_{G}=0.85 \times 1.35=1.15$ the inclination angle at failure corresponds to the permissible settlement, thus $\theta_{i,P}=0.0090\text{rad}=0.52^\circ$, which is smaller than $\text{max}\theta_i=0.04\text{rad}$, as specified in section 3.3.

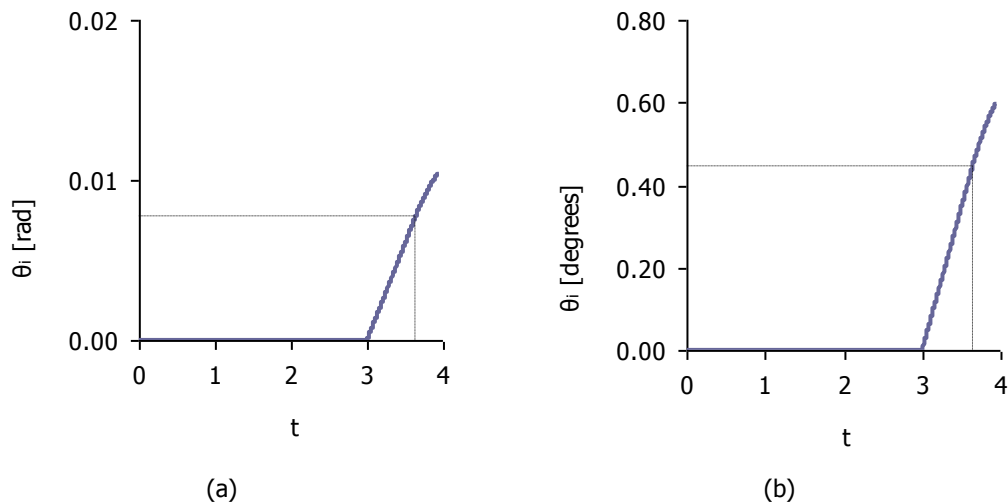


Figure 7.24: Inclination angle of the pier's columns θ_i vs t in (a) [rad] and (b) [degrees]

Σχήμα 7.24: Γωνία κλίσης στύλων μεσοβάθρου θ_i σε σχέση με το χρόνο σε (a) [rad] και (b) [μοίρες]

7.2.5 Response of the bridge for Combination 2

Similarly, considering only the permanent loads with a loading factor equal to $\gamma_G=1.00$ and the initial imperfections as described in section 6.2, a maximum rotation θ_x is assumed equal to $\max\theta_x=0.0255\text{rad}$. The analysis stops when $\theta_x=0.0249\text{rad}=1.43^\circ$, at $t=3.975$, because of the bending failure at the top of the middle column again (column 2). The diagram $M-\phi$ is depicted in Figure 7.25 for the top and the base of the three columns. Even in this combination, the bending moments at the pier's base remain at low levels, while large bending moments at the top of them cause the failure of the pier.

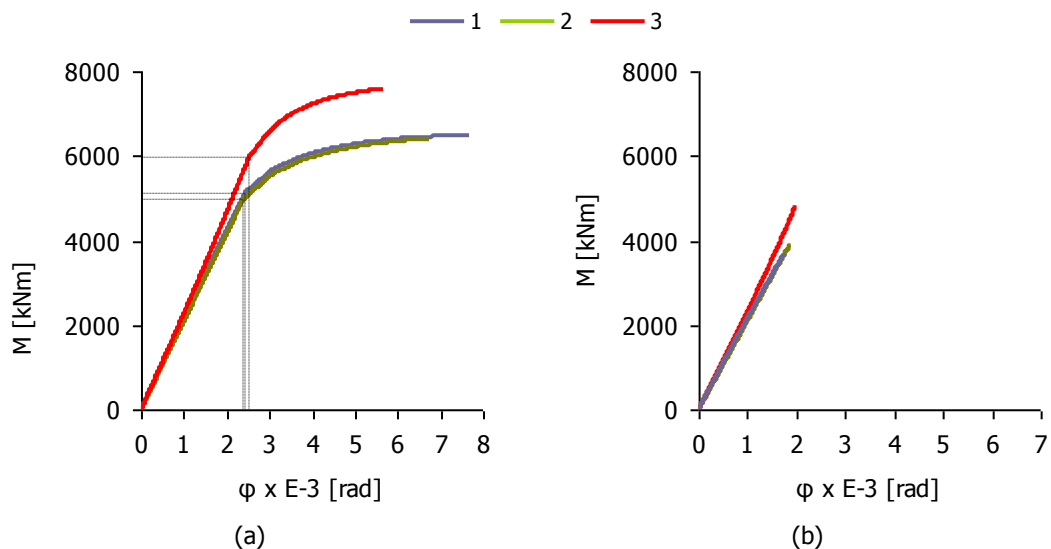


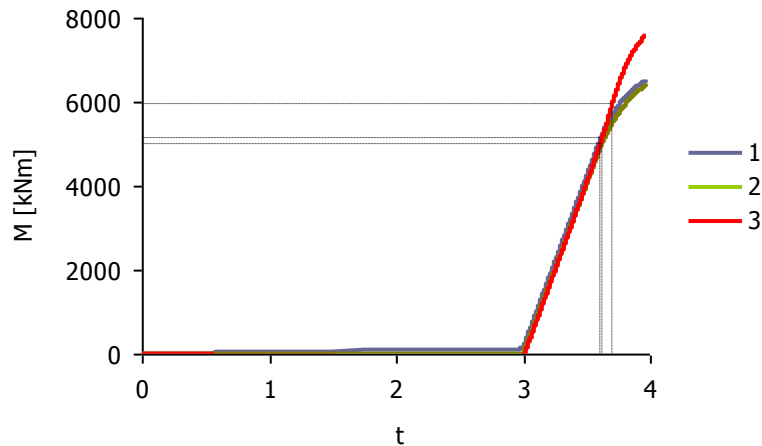
Figure 7.25: $M-\phi$ diagrams for (a) the top and (b) the base of the three columns

Σχήμα 7.25: Διαγράμματα $M-\phi$ για (a) τις κορυφές και (b) τις βάσεις των τριών στύλων

The bending moments that correspond to yield are given in Table 7.6 and the $M-t$ diagrams are plotted in Figure 7.26, in which the first yield is detected for the outer column 1, for $t=3.613$. In these diagrams, the dotted lines denote the bending moments that correspond to the first yield of each column.

Table 7.6: Yield at the top of the pier's columns**Πίνακας 7.6:** Διαρροή στην κορυφή των στύλων μεσοβάθρου

Columns	t	M [kNm]	φ E-3 [rad]
1	3.613	5130.65	2.43
2	3.622	4981.69	2.41
3	3.704	5953.96	2.52

**Figure 7.26:** M-t diagrams for the top of the three columns**Σχήμα 7.26:** Διαγράμματα M-t για τις κορυφές των τριών στύλων

As noted in section 7.2.2 all steel members remain in the elastic zone, except of the diagonal bracing members, which buckle. The response of the steel members at the end of the analysis, as well as at the time of the first yield, is summarized in Table 7.7. Until the end of the analysis, corresponding to the bridge's failure, the steel members' stresses remain smaller than the ultimate stress $f_u=510\text{MPa}$. As mentioned in section 7.2.2, the buckling of the diagonal bracing members, that are considered replaceable, does not indicate a bridge failure. Comparing with the stresses of Table 7.4 it is pointed out that Combination 1 is more crucial for the superstructure.

Table 7.7: Maximum stresses in the steel members at the time of the first yield ($t=3.613$) and the time of failure ($t=3.975$)**Πίνακας 7.7:** Μέγιστες τάσεις στα μεταλλικά στοιχεία τη στιγμή της πρώτης διαρροής ($t=3.613$) και τη στιγμή της αστοχίας ($t=3.975$)

Members	t=3.613		t=3.975	
	σ [MPa]	ϵ %	σ [MPa]	ϵ %
Arches	162.34	0.08	185.16	0.09
Main beams	134.62	0.06	158.05	0.08
Secondary beams	59.22	0.03	78.37	0.04
Horizontal bracing	142.34	0.07	222.30	0.11
Diagonal bracing	356.83	0.43	361.84	1.13
Hangers	171.44	0.08	174.58	0.08

Regarding the bearings, the load – displacement diagrams of the horizontal springs in the transverse direction of the bridge are illustrated in Figure 7.27 for the abutment and in Figure 7.28 for the pier, where it is noted that the springs behave elastically, until the end of the analysis. The maximum force and the horizontal displacement of the springs at the abutment arise at 288kN and 0.08m, respectively, for the bearings of both abutment and pier, showing a similar behavior with the one of Combination 1.

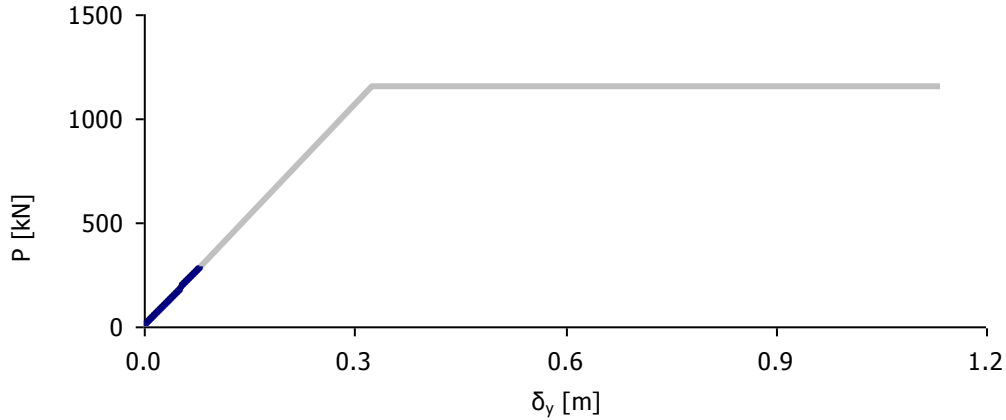


Figure 7.27: Diagram of load – displacement for the abutment's bearings

Σχήμα 7.27: Διάγραμμα φορτίου – παραμόρφωσης εφεδράνων ακροβάθρου

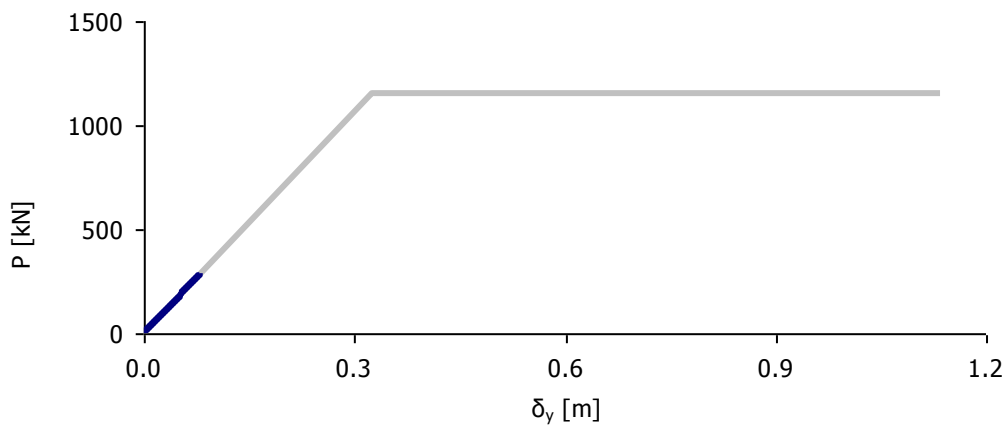


Figure 7.28: Diagram of load – displacement for the pier's bearings

Σχήμα 7.28: Διάγραμμα φορτίου – παραμόρφωσης εφεδράνων μεσοβάθρου

The shear strains of the abutment's bearings are plotted in Figure 7.29, while the ones of the pier's bearings are shown in Figure 7.30. The shear strain due to translational movements $\epsilon_{q,d}$ does not exceed the limit of 2, and the maximum design strain $\epsilon_{t,d}$ the limit of 7.

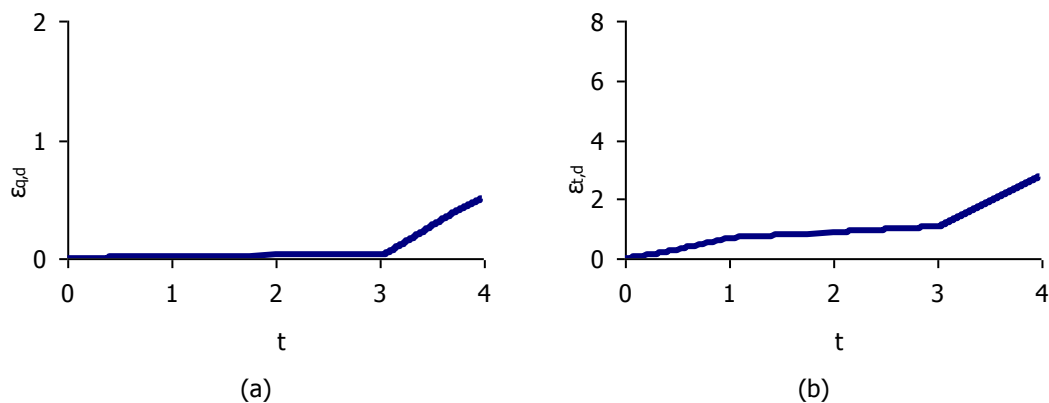


Figure 7.29: Strains of the abutment's bearings: (a) shear strain due to translational movements $\epsilon_{q,d}$, (b) maximum design strain $\epsilon_{t,d}$

Σχήμα 7.29: Παραμορφώσεις εφεδράνων ακροβάθρου: (α) διατμητική παραμόρφωση λόγω μετακίνησης $\epsilon_{q,d}$, (β) συνολική διατμητική παραμόρφωση $\epsilon_{t,d}$

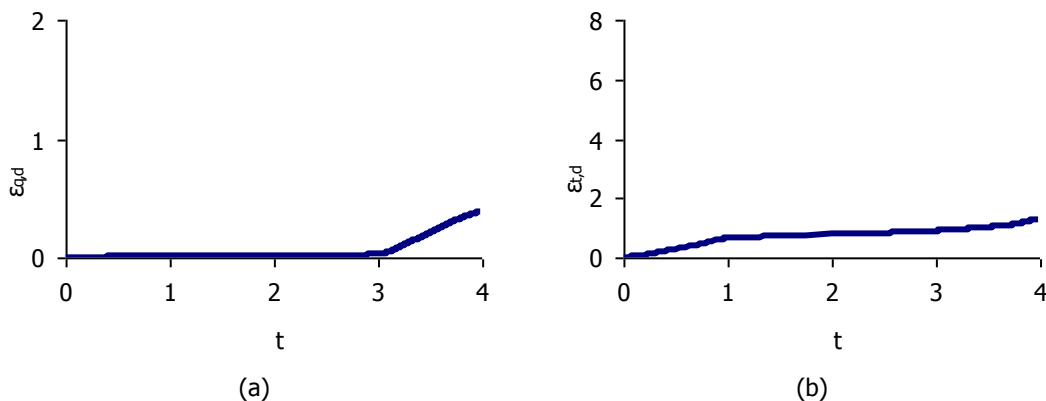


Figure 7.30: Strains of the pier’s bearings: (a) shear strain due to translational movements $\epsilon_{q,d}$, (b) maximum design strain $\epsilon_{t,d}$

Σχήμα 7.30: Παραμορφώσεις εφεδράνων μεσοβάθρου: (α) διατμητική παραμόρφωση λόγω μετακίνησης $\epsilon_{q,d}$, (β) συνολική διατμητική παραμόρφωση $\epsilon_{t,d}$

7.2.6 Permissible rotation and settlement for Combination 2

The diagrams of the longitudinal rotation θ_x (Figure 7.31) and the uniform settlement ρ vs t (Figure 7.32) show that the maximum rotation at failure is $\theta_{x,F}=0.0249\text{rad}=1.43^\circ$ with a corresponding settlement is $\rho_F=28.5\text{cm}$, defining the admissible values. The first yield, shown with dotted lines in the diagrams, occurs at $t=3.613$ and corresponds to a uniform settlement $\rho_Y=17.9\text{cm}$ and a longitudinal rotation $\theta_{x,Y}=0.0156\text{rad}=0.90^\circ$. Taking into account the combination loading factor for LC4, equal to $\xi\gamma_G=0.85\cdot 1.35=1.15$, the maximum permissible values of the settlement and rotation should be equal to $\rho_P=\rho_F/\xi\gamma_G=24.8\text{cm}$ and $\theta_{x,P}=\theta_{x,F}/\xi\gamma_G=0.0217\text{rad}=1.24^\circ$. All values of the calculated settlement and rotation are given in Table 7.8. Comparing with the values of Table 7.5, it is concluded that, both Combinations lead to similar permissible settlements and rotation, although Combination 1 is more crucial for the superstructure.

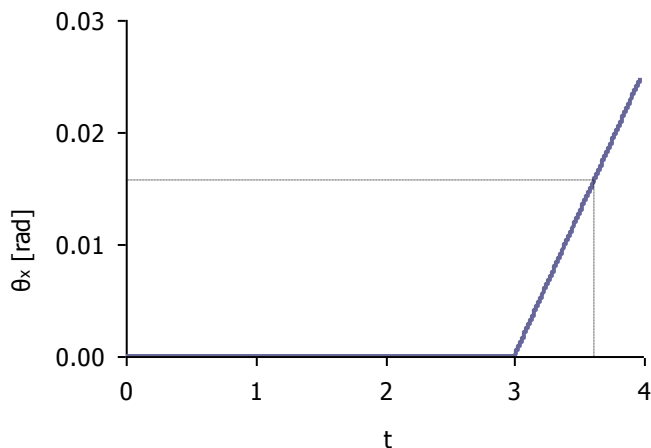


Figure 7.31: Longitudinal rotation θ_x vs t

Σχήμα 7.31: Διαμήκης στροφή θ_x συναρτήσει t

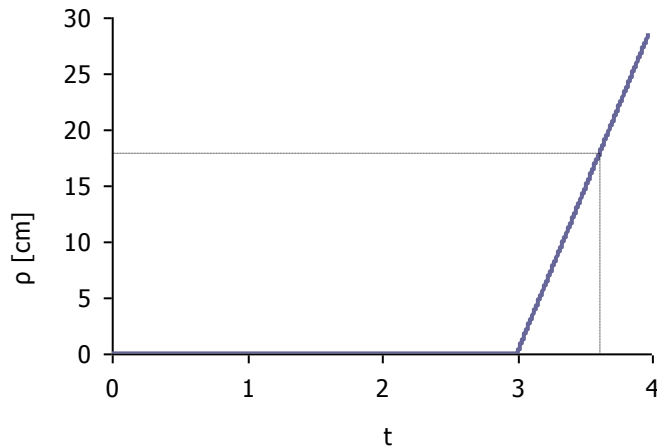


Figure 7.32: Uniform settlement ρ vs t

Σχήμα 7.32: Ομοιόμορφη καθίζηση ρ συναρτήσει t

Table 7.8: Maximum, yield and permissible values of rotation θ_x and uniform settlement ρ

Πίνακας 7.8: Μέγιστη τιμή, τιμή στην πρώτη διαρροή και επιτρεπόμενη τιμή διαμήκους στροφής θ_x και ομοιόμορφης καθίζησης ρ

	t	ρ [cm]	θ_x [rad]	θ_x [degrees]
Yield (Y)	3.613	17.9	0.0156	0.90
Failure (F)	3.975	28.5	0.0249	1.43
Permissible (P=F/1.15)	–	24.8	0.0217	1.24

7.2.7 Inclination angle of the pier for Combination 2

Figure 7.33 gives the diagrams of the inclination angle θ_i of the pier's columns in rad and degrees. At the first yield of the pier's columns, the inclination angle is equal to $\theta_{i,Y}=0.0072\text{rad}=0.41^\circ$, while the one that corresponds to the permissible settlement and rotation is:

$$\theta_{i,P} = \theta_{i,F}/\xi_{\gamma G} = 0.0088\text{rad} = 0.50^\circ < \max\theta_i = 0.04\text{rad} \quad (7-3)$$

where $\theta_{i,F} = 0.0101\text{rad} = 0.58^\circ$.

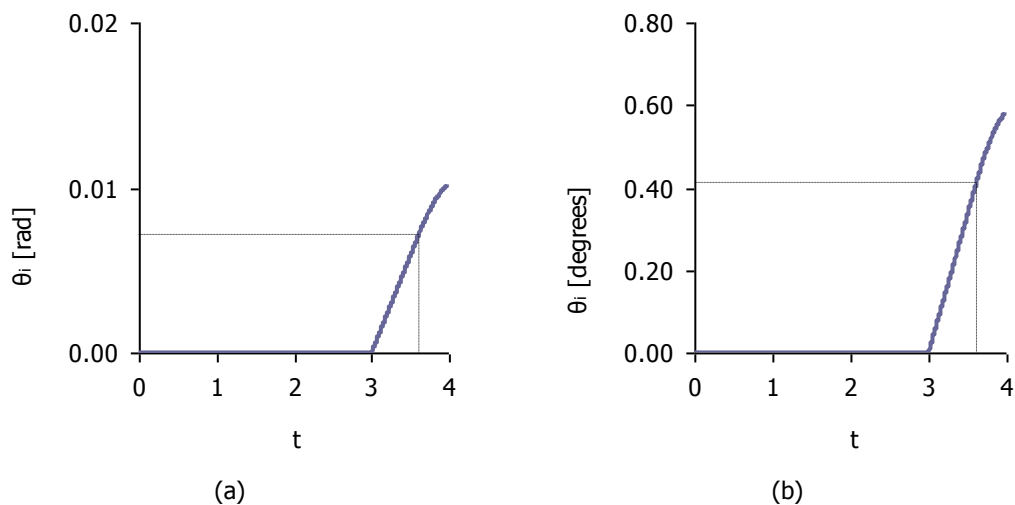


Figure 7.33: Inclination angle of the pier's columns θ_i vs t in (a) [rad] and (b) [degrees]

Σχήμα 7.33: Γωνία κλίσης στύλων μεσοβάθρου θ_i σε σχέση με το χρόνο σε (a) [rad] και (b) [μοίρες]

7.3 Case 2 ($\theta_y + \rho$)

7.3.1 Imposed settlement ρ and rotation θ_y

A rotation at the footing of the pier along the transverse axis y (θ_y) is applied at the base of all three columns. The combined uniform settlement will be equal to:

$$\frac{180}{\pi} \theta_y = 0.05 \cdot 100 \cdot dz \Rightarrow dz = \frac{180}{0.05 \cdot 100 \cdot \pi} \theta_y = 11.459 \theta_y [\text{m}] \quad (7-4)$$

where θ_y is given in [rad]. The imposed rotation and settlement are shown in Figure 7.34.

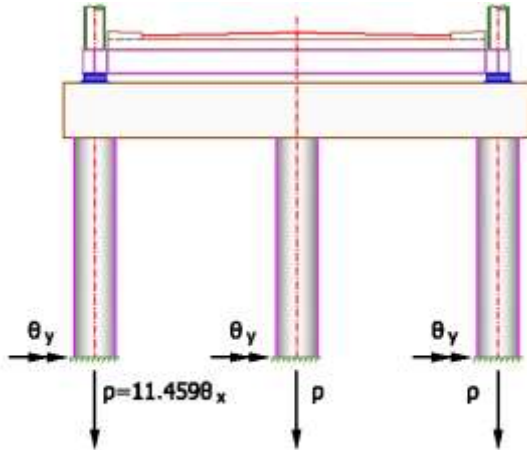


Figure 7.34: Imposed transverse rotation θ_y and settlement ρ

Σχήμα 7.34: Επιβαλλόμενη εγκάρσια στροφή θ_y και καθίζηση ρ

7.3.2 Response of the bridge for Combination 1

Considering the initial imperfections as described in section 6.2, the permanent loads are applied again with loading factor $\xi_{G}=0.85 \times 1.35=1.15$ and 1.35, respectively, as defined in section 5.5 for Combination 1. A maximum rotation θ_y is assumed equal to $\max \theta_y=0.047 \text{ rad}$. The analysis stops when $\theta_y=0.0468 \text{ rad}=2.68^\circ$, at $t=3.995$, because of the bending failure at the base of the outer column 1 and the middle column 2, as shown in Figure 7.35. Although the structure, as well as the imposed rotation and settlement are symmetric, the failure state is not symmetric (with failure at the base of column 1 but not at column 3), due to the initial imperfections. The deformed state at the moment of failure is illustrated in Figure 7.36.

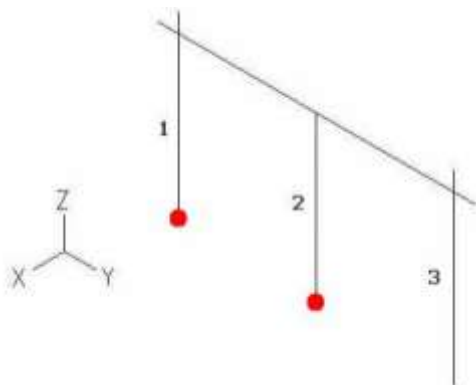


Figure 7.35: Simultaneous failure at the base of columns 1 and 2

Σχήμα 7.35: Ταυτόχρονη αστοχία στην βάση των στύλων 1 και 2

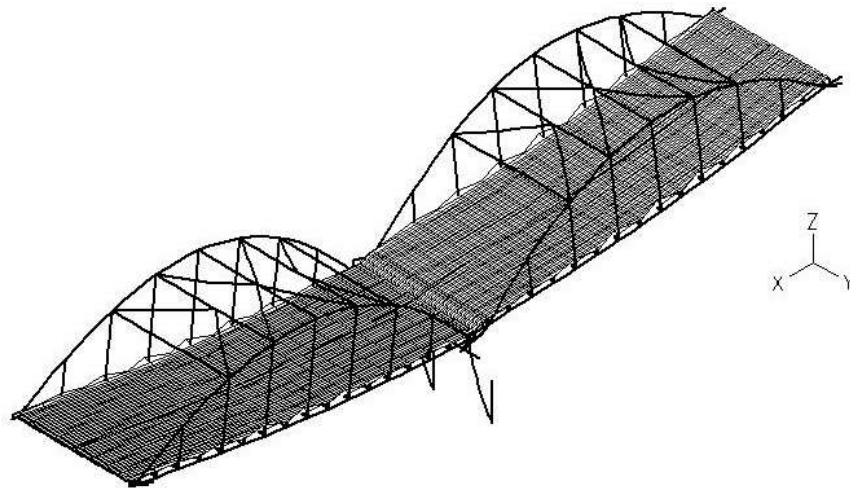


Figure 7.36: Deformed state at failure

Σχήμα 7.36: Παραμορφωμένη κατάσταση στην αστοχία

The diagram M-φ is depicted in Figure 7.37 (a) for the top and (b) for the base of all three columns, where it is noted that the sections at the top of the pier remain in the elastic zone, while significant bending moments are evolved at their base, leading to the failure of the pier. The dotted lines indicate the bending moments that correspond to yield for the section at the base of each column. The outer columns 1 and 3 behave in a similar way, due to the symmetry of the structure and the applied loads. Insignificant differences, between the two columns due to the asymmetric initial imperfections, can be noted in the magnitudes of M and φ that correspond to the yield of each column, listed in Table 7.9. The M-t diagrams are plotted in Figure 7.38, in which the first yield is detected, for t=3.723, occurring at the base of column 3.

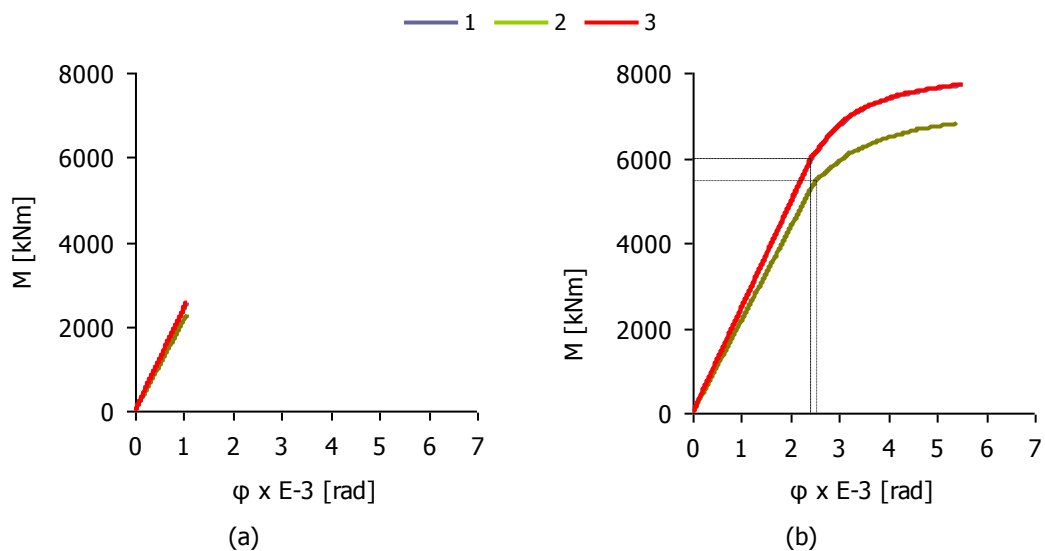


Figure 7.37: M-φ diagrams for (a) the top and (b) the base of the three columns

Σχήμα 7.37: Διαγράμματα M-φ για (a) τις κορυφές και (b) τις βάσεις των τριών στύλων

Table 7.9: Yield at the base of the pier's columns

Πίνακας 7.9: Διαρροή στη βάση των στύλων μεσοβάθρου

Columns	t	M [kNm]	φ E-3 [rad]
1	3.724	5959.98	2.42
2	3.749	5469.71	2.52
3	3.723	5962.90	2.41

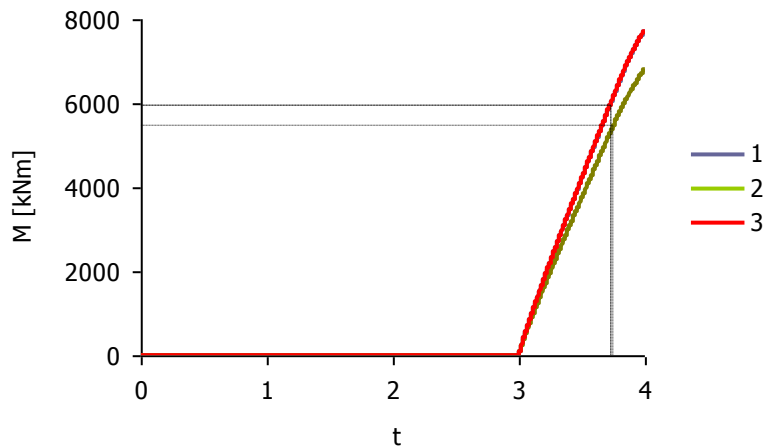


Figure 7.38: M-t diagrams for the base of the three columns

Σχήμα 7.38: Διαγράμματα M-t για τις βάσεις των τριών στύλων

All steel members, at the time of failure, remain in the elastic zone. The response of the steel members at the end of the analysis, as well as at the time of the first yield at the base of the pier's column, is summarized in Table 7.10. The maximum stresses in the steel members of the bridge do not exceed the yield stress. Comparing with the corresponding Table 7.4 of Case 1 it is observed that the longitudinal rotation causes larger stresses in the steel members, except for the secondary beams. Nevertheless, in both cases the steel members of this bridge do not determine the limits of the permissible settlement at the base of the pier.

Table 7.10: Maximum stresses in the steel members at the time of the first yield ($t=3.723$) and the time of failure ($t=3.995$)

Πίνακας 7.10: Μέγιστες τάσεις στα μεταλλικά στοιχεία τη στιγμή της πρώτης διαρροής ($t=3.723$) και τη στιγμή της αστοχίας ($t=3.995$)

Members	t=3.723		t=3.995	
	σ [MPa]	ϵ %	σ [MPa]	ϵ %
Arches	178.21	0.08	179.00	0.09
Main beams	147.91	0.07	152.12	0.07
Secondary beams	134.44	0.06	130.14	0.06
Horizontal bracing	63.21	0.03	63.34	0.03
Diagonal bracing	97.81	0.05	97.94	0.05
Hangers	260.72	0.12	261.72	0.12

Figure 7.39 gives the load – displacement diagram of the horizontal springs in the longitudinal direction of the bridge for the abutment, while the diagram of Figure 7.40 refers to the pier's springs. The springs behave elastically until the end of the analysis. The maximum force and the horizontal displacement of the springs arise at 600kN and 0.17m respectively, for the bearings of the abutment and 638kN and 0.18m, respectively, for the bearings of the pier, showing a larger deformation with respect to the one of Case 1 (Figure 7.18 and Figure 7.19). The diagrams of the shear strains with respect to time t are shown in Figure 7.41 for the abutment's bearings and in Figure 7.42 for the pier's bearings. For both abutment and pier, the shear strain due to translational movements $\epsilon_{q,d}$ remains below the limit of 2, while the maximum design strain $\epsilon_{t,d}$ is smaller than the limit of 7, until the end of the analysis.

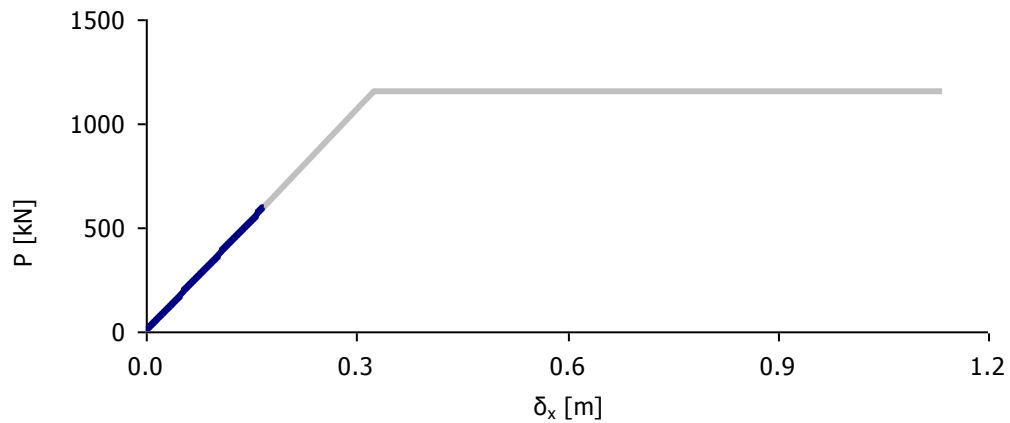


Figure 7.39: Diagram of load – displacement for the abutment’s bearings

Σχήμα 7.39: Διάγραμμα φορτίου – παραμόρφωσης εφεδρώνων ακροβάθρου

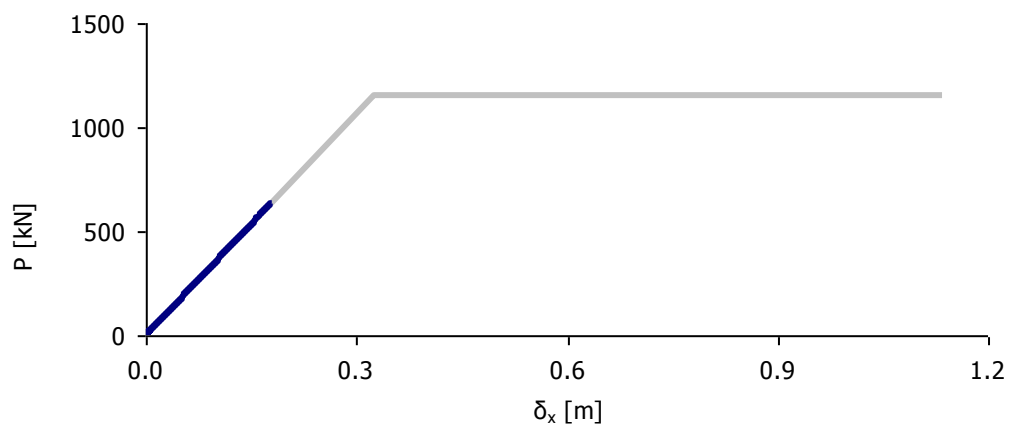


Figure 7.40: Diagram of load – displacement for the pier’s bearings

Σχήμα 7.40: Διάγραμμα φορτίου – παραμόρφωσης εφεδρώνων μεσοβάθρου

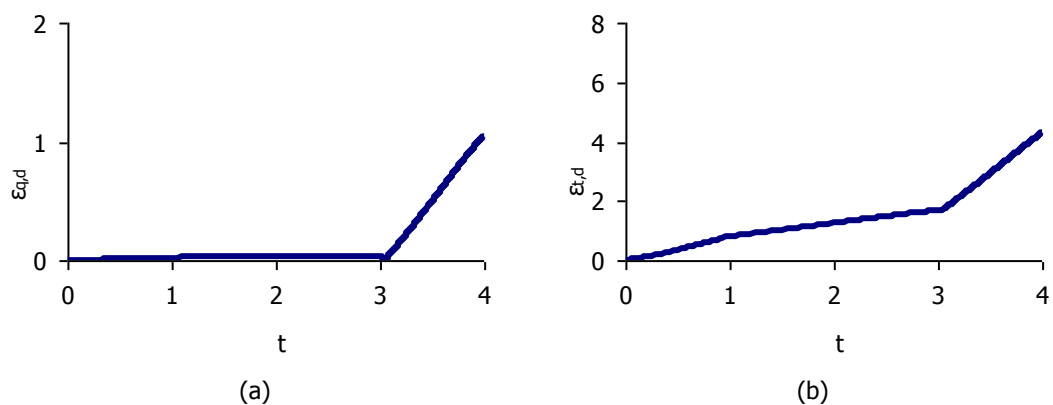


Figure 7.41: Strains of the abutment’s bearings: (a) shear strain due to translational movements $\epsilon_{q,d}$, (b) maximum design strain $\epsilon_{t,d}$

Σχήμα 7.41: Παραμορφώσεις εφεδρώνων ακροβάθρου: (a) διατμητική παραμόρφωση λόγω μετακίνησης $\epsilon_{q,d}$, (b) συνολική διατμητική παραμόρφωση $\epsilon_{t,d}$

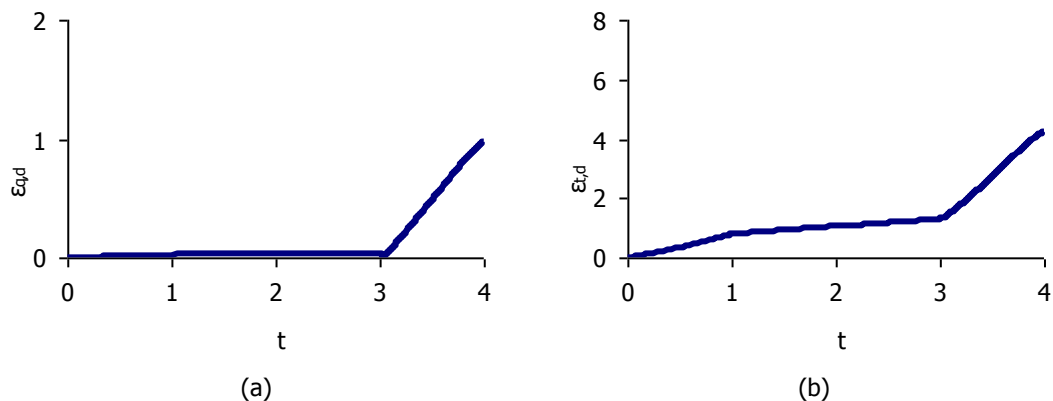


Figure 7.42: Strains of the pier’s bearings: (a) shear strain due to translational movements $\epsilon_{q,d}$, (b) maximum design strain $\epsilon_{t,d}$

Σχήμα 7.42: Παραμορφώσεις εφεδράνων μεσοβάθρου: (α) διατμητική παραμόρφωση λόγω μετακίνησης $\epsilon_{q,d}$, (β) συνολική διατμητική παραμόρφωση $\epsilon_{t,d}$

7.3.3 Permissible rotation and settlement for Combination 1

The evolution of the transverse rotation θ_y is plotted in Figure 7.43 and the uniform settlement ρ in Figure 7.44. The dotted lines refer to the values at the time of the first yield of the pier’s columns. The maximum rotation at failure is $\theta_{y,F}=0.0468\text{rad}=2.68^\circ$ and the corresponding settlement is $\rho_F=53.59\text{cm}$. The settlement at the first yield ($t=3.723$) is $\rho_Y=38.91\text{cm}$, corresponding to a transverse rotation $\theta_{y,Y}=0.034\text{rad}=1.95^\circ$. The maximum permissible values of the settlement and rotation are equal to the Y-values corresponding to first yield, divided by the loading factor 1.15, leading to $\rho_p=33.83\text{cm}$ and $\theta_{x,p}=0.03\text{rad}=1.70^\circ$. The values of the calculated settlement and rotation are given in Table 7.11. Comparing with the ones of Case 1, given in Table 7.5, it is concluded that the longitudinal rotation θ_x is more critical.

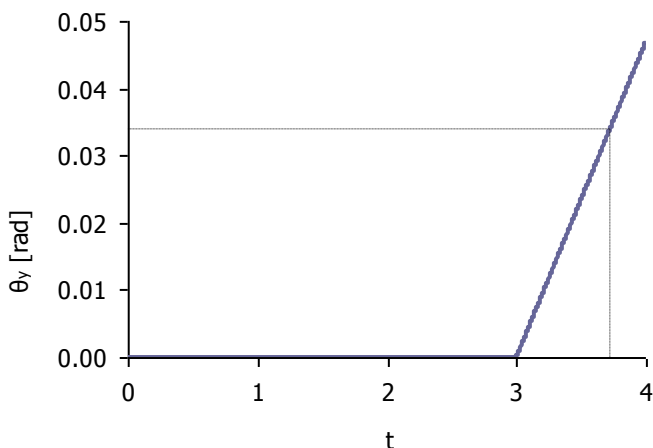


Figure 7.43: Transverse rotation θ_y vs t

Σχήμα 7.43: Εγκάρσια στροφή θ_y συναρτήσει t

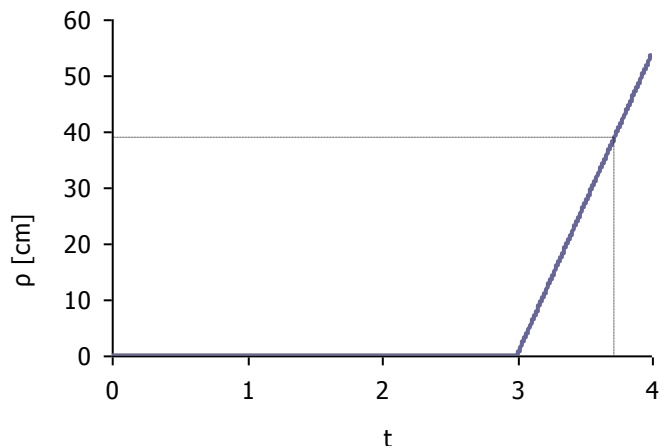


Figure 7.44: Uniform settlement ρ vs t

Σχήμα 7.44: Ομοιόμορφη καθίζηση ρ συναρτήσει t

Table 7.11: Maximum, yield and permissible values of rotation θ_y and uniform settlement ρ

Πίνακας 7.11: Μέγιστη τιμή, τιμή στην πρώτη διαρροή και επιτρεπόμενη τιμή εγκάρσιας στροφής θ_y και ομοιόμορφης καθίζησης ρ

	t	ρ [cm]	θ_y [rad]	θ_y [degrees]
Yield (Y)	3.723	38.9	0.0340	1.95
Failure (F)	3.995	53.6	0.0468	2.68
Permissible (P=Y/1.15)	–	33.8	0.030	1.70

7.3.4 Inclination angle of the pier for Combination 1

The diagram of the inclination angle θ_i of the pier’s columns is plotted in Figure 7.45. At failure, the inclination angle arises at $\theta_{i,F}=0.0352\text{rad}=2.01^\circ$, while the one that corresponds to the permissible settlement and rotation for Combination 1 is:

$$\theta_{i,P} = \theta_{i,Y}/\xi_{YG} = 0.0228\text{rad} = 1.30^\circ < \max\theta_i = 0.04\text{rad} \tag{7-5}$$

where $\theta_{i,Y} = 0.0262\text{rad} = 1.50^\circ$.

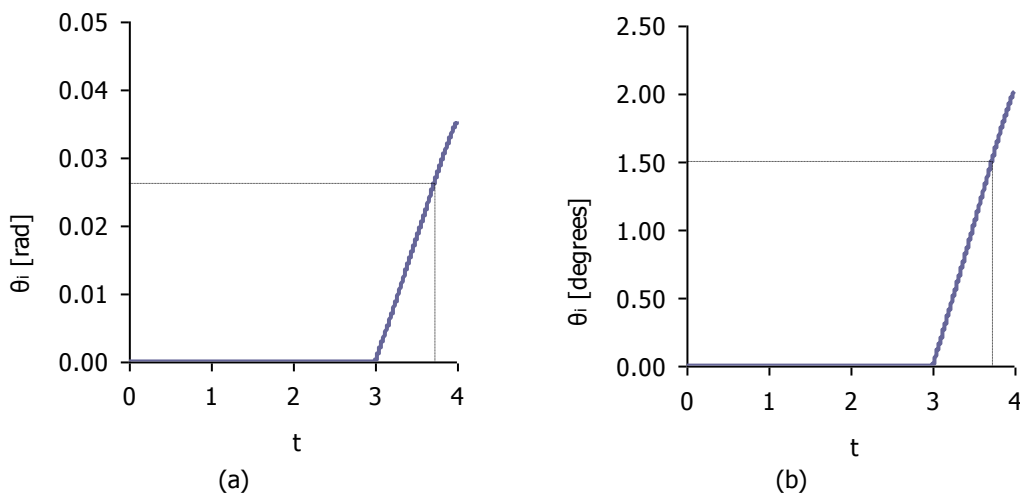


Figure 7.45: Inclination angle of the pier’s columns θ_i vs t in (a) [rad] and (b) [degrees]

Σχήμα 7.45: Γωνία κλίσης στύλων μεσοβάθρου θ_i σε σχέση με το χρόνο σε (a) [rad] και (b) [μοίρες]

7.3.5 Response of the bridge for Combination 2

Taking into account Combination 2, where the initial imperfections as described in section 6.2 are considered and only the permanent loads with a loading factor equal to $\gamma_G=1.00$, a maximum rotation θ_y is imposed equal to $\max\theta_y=0.048\text{rad}$. The analysis continues until $\theta_y=0.0428\text{rad}=2.45^\circ$, at $t= 3.892$, when bending failure occurs at the base of the middle column (column 2), shown in Figure 7.46. The diagrams $M-\phi$ plotted in Figure 7.47 for the top and the base of the three columns, show that the bending moments at the pier's top are small during the analysis, while the ones at the top of them increase significantly, leading to failure. The dotted lines correspond to the magnitudes at the time of the first yield of the pier's columns. The bending moments that correspond to yield are given in Table 7.12 and the $M-t$ diagrams are shown in Figure 7.48, in which the first yield is noted for the middle column 2, for $t=3.625$. In all diagrams it is proved that columns 1 and 3 behave in a similar way.

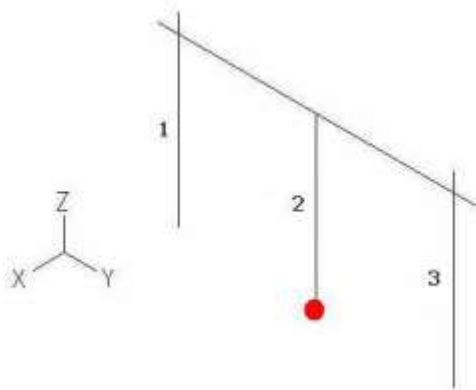


Figure 7.46: Failure at the base of column 2

Σχήμα 7.46: Αστοχία στην βάση του στύλου 2

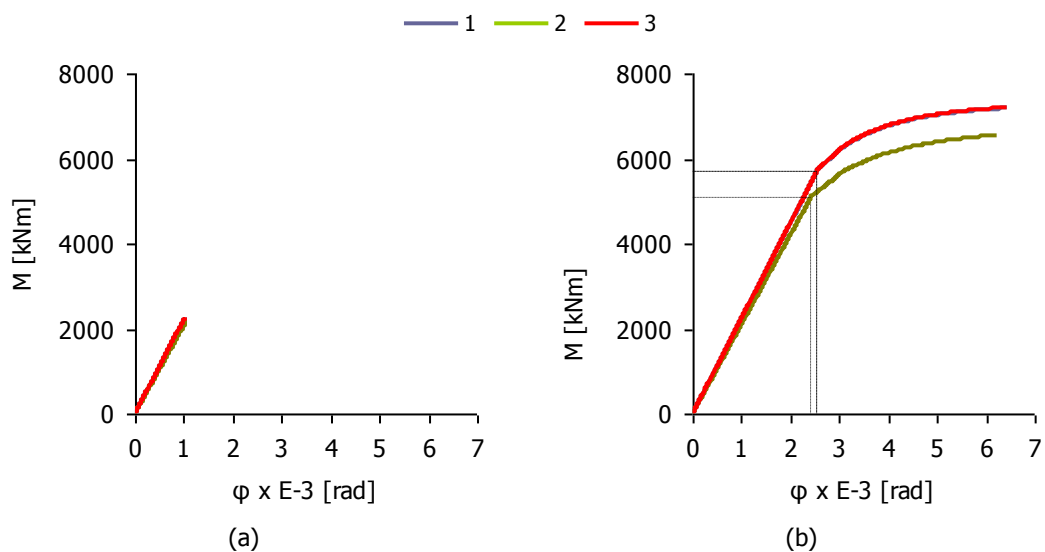


Figure 7.47: $M-\phi$ diagrams for (a) the top and (b) the base of the three columns

Σχήμα 7.47: Διαγράμματα $M-\phi$ για (a) τις κορυφές και (b) τις βάσεις των τριών στύλων

Table 7.12: Yield at the base of the pier's columns

Πίνακας 7.12: Διαρροή στη βάση των στύλων μεσοβάθρου

Columns	t	M [kNm]	ϕ E-3 [rad]
1	3.661	5711.93	2.55
2	3.625	5101.53	2.43
3	3.661	5717.53	2.55

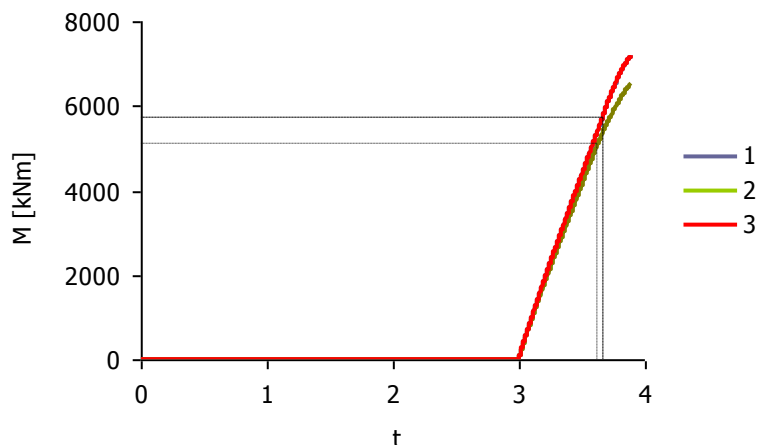


Figure 7.48: M-t diagrams for the base of the three columns

Σχήμα 7.48: Διαγράμματα M-t για τη βάση των τριών στύλων

The maximum stresses in the steel members at the time of the first yield of the pier's column and the time of failure are given in Table 7.13, which remain smaller than the ultimate stress $f_u=510\text{MPa}$. These stresses are larger than the ones of Table 7.10 confirming again that Combination 1 is more unfavorable for the superstructure.

Table 7.13: Maximum stresses in the steel members at the time of the first yield ($t=3.625$) and the time of failure ($t=3.892$)

Πίνακας 7.13: Μέγιστες τάσεις στα μεταλλικά στοιχεία τη στιγμή της πρώτης διαρροής ($t=3.625$) και τη στιγμή της αστοχίας ($t=3.892$)

Members	t=3.625		t=3.892	
	σ [MPa]	ϵ %	σ [MPa]	ϵ %
Arches	112.11	0.05	112.44	0.05
Main beams	103.16	0.05	106.91	0.05
Secondary beams	99.59	0.05	94.53	0.05
Horizontal bracing	60.12	0.03	60.02	0.03
Diagonal bracing	74.82	0.04	74.94	0.04
Hangers	162.12	0.08	162.87	0.08

The load – displacement diagrams of the horizontal springs in the longitudinal direction of the bridge are illustrated in Figure 7.49 for the abutment and in Figure 7.50 for the pier. The springs behave elastically, until the end of the analysis. The maximum force and the horizontal displacement of the springs arise at 520kN and 0.15m respectively, for the bearings of the abutment and 555kN and 0.16m, respectively, for the bearings of the pier, being slightly smaller than the corresponding ones of Combination 1 (see section 7.3.2). The shear strains of the abutment's bearings are given in Figure 7.51, while the ones of the pier's bearings are depicted in Figure 7.52. The shear strain due to translational movements $\epsilon_{q,d}$ does remain smaller than 2, and the maximum design strain $\epsilon_{t,d}$ does not exceed the limit of 7.

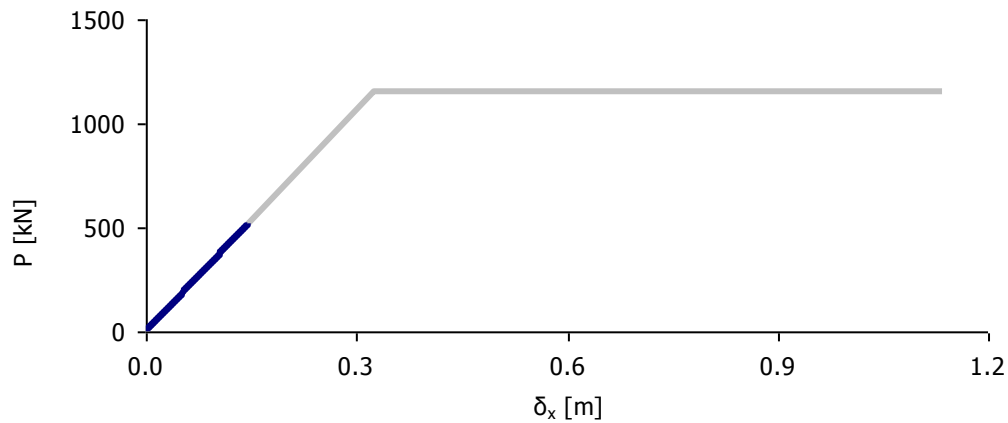


Figure 7.49: Diagram of load – displacement for the abutment’s bearings

Σχήμα 7.49: Διάγραμμα φορτίου – παραμόρφωσης εφεδρώνων ακροβάθρου

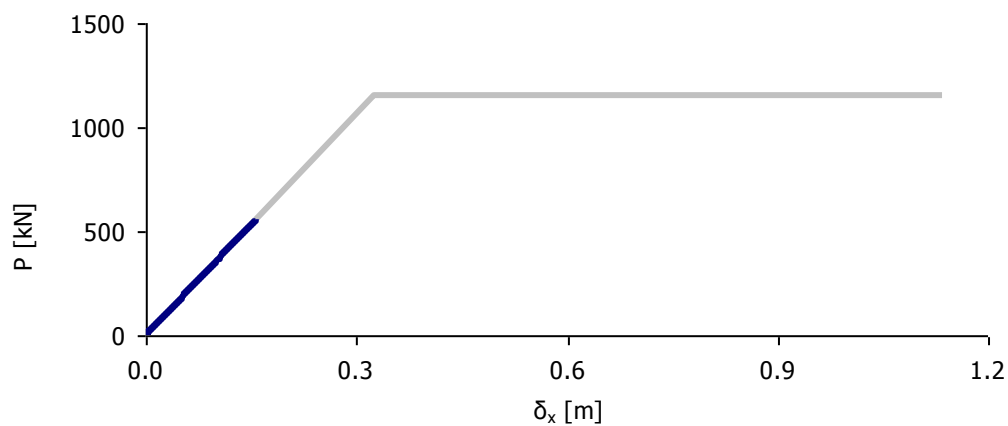


Figure 7.50: Diagram of load – displacement for the pier’s bearings

Σχήμα 7.50: Διάγραμμα φορτίου – παραμόρφωσης εφεδρώνων μεσοβάθρου

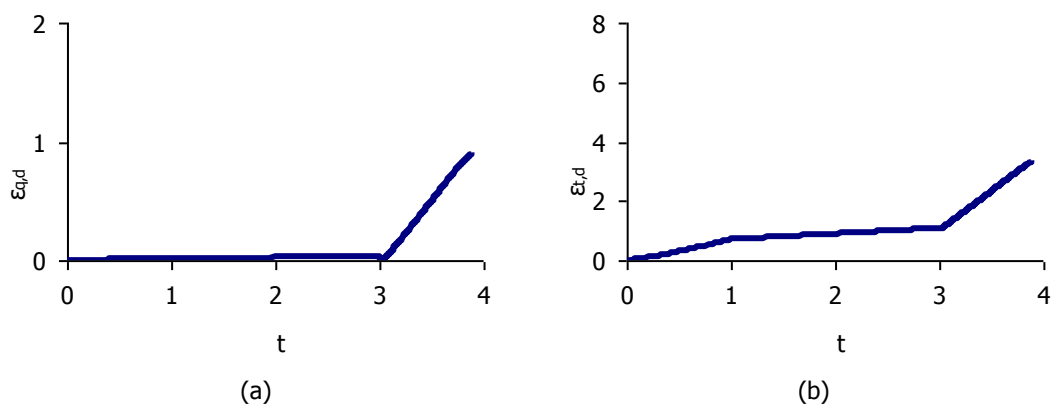


Figure 7.51: Strains of the abutment’s bearings: (a) shear strain due to translational movements $\epsilon_{q,d}$, (b) maximum design strain $\epsilon_{t,d}$

Σχήμα 7.51: Παραμορφώσεις εφεδρώνων ακροβάθρου: (a) διατμητική παραμόρφωση λόγω μετακίνησης $\epsilon_{q,d}$, (b) συνολική διατμητική παραμόρφωση $\epsilon_{t,d}$

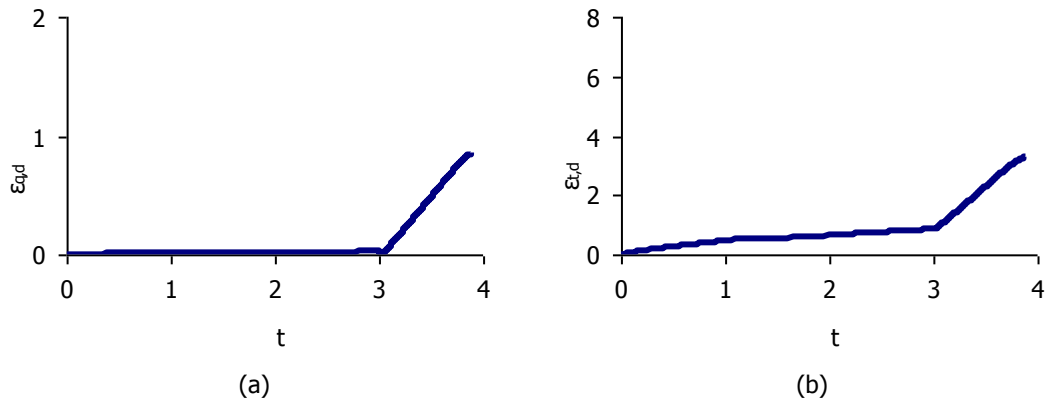


Figure 7.52: Strains of the pier's bearings: (a) shear strain due to translational movements $\epsilon_{q,d}$, (b) maximum design strain $\epsilon_{t,d}$

Σχήμα 7.52: Παραμορφώσεις εφεδράνων μεσοβάθρου: (a) διατμητική παραμόρφωση λόγω μετακίνησης $\epsilon_{q,d}$, (b) συνολική διατμητική παραμόρφωση $\epsilon_{t,d}$

7.3.6 Permissible rotation and settlement for Combination 2

The diagram θ_y vs t is plotted in Figure 7.53 and the uniform settlement ρ vs t in Figure 7.54, with the dotted lines showing the values at the time of the first yield of the pier's columns. The maximum rotation at failure is $\theta_{y,F}=0.0428\text{rad}=2.45^\circ$ and the corresponding settlement is $\rho_F=49.02\text{cm}$. The settlement at first yield ($t=3.625$) is $\rho_Y=34.38\text{cm}$, corresponding to a transverse rotation $\theta_{y,Y}=0.03\text{rad}=1.72^\circ$. The maximum permissible values of the settlement and rotation are equal to the Y-values corresponding to first yield, divided by the loading factor 1.15, leading to $\rho_P=29.90\text{cm}$ and $\theta_{y,P}=0.026\text{rad}=1.50^\circ$. The values of the calculated settlement and rotation are given in Table 7.14, leading again to smaller values, compared with Combination 1 (see Table 7.11). Thus, for both transverse and longitudinal rotations, Combination 1 is more unfavorable for the superstructure, but Combination 2 leads to lower permissible imposed rotation and settlement.

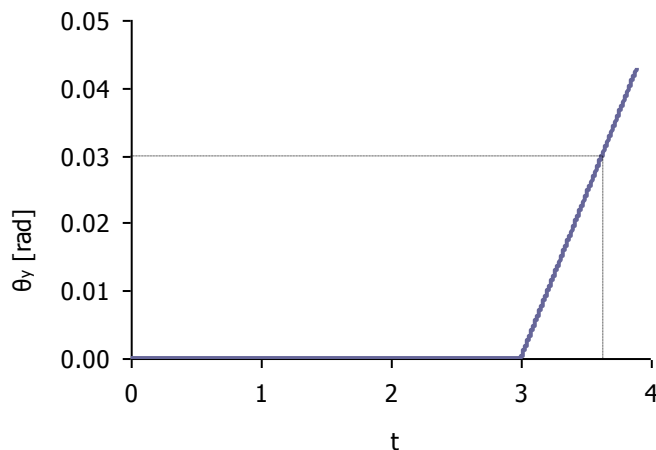


Figure 7.53: Transverse rotation θ_y vs t

Σχήμα 7.53: Εγκάρσια στροφή θ_y συναρτήσει t

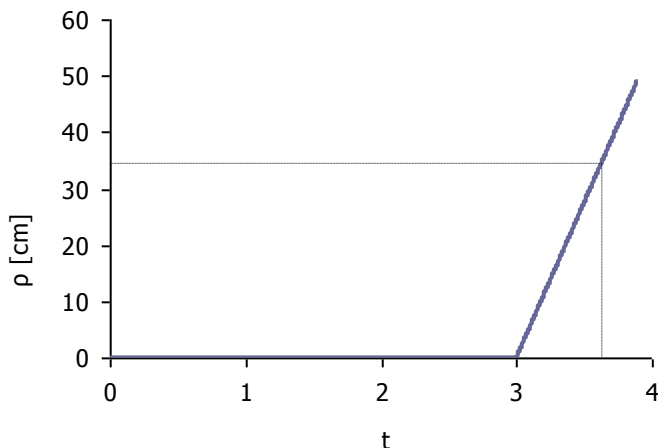


Figure 7.54: Uniform settlement ρ vs t

Σχήμα 7.54: Ομοιόμορφη καθίζηση ρ συναρτήσει t

Table 7.14: Maximum, yield and permissible values of rotation θ_y and uniform settlement ρ

Πίνακας 7.14: Μέγιστη τιμή, τιμή στην πρώτη διαρροή και επιτρεπόμενη τιμή εγκάρσιας στροφής θ_y και ομοιόμορφης καθίζησης ρ

	t	ρ [cm]	θ_y [rad]	θ_y [degrees]
Yield (Y)	3.625	34.4	0.0300	1.72
Failure (F)	3.892	49.0	0.0428	2.45
Permissible (P=Y/1.15)	–	29.9	0.026	1.50

7.3.7 Inclination angle of the pier for Combination 2

At failure, the inclination angle reaches the value of $\theta_{i,F}=0.0307\text{rad}=1.76^\circ$, while the one that corresponds to the permissible settlement and rotation for Combination 2 is:

$$\theta_{i,P} = \theta_{i,Y}/\xi_{YG} = 0.0194\text{rad} = 1.11^\circ < \max\theta_i = 0.04\text{rad} \tag{7-6}$$

where $\theta_{i,Y} = 0.0223\text{rad} = 1.27^\circ$ (Figure 7.55)

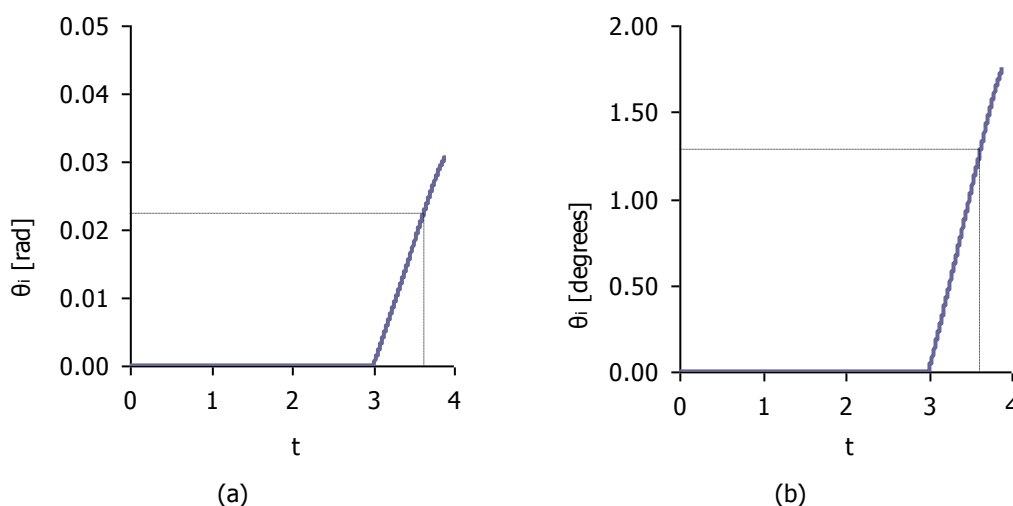


Figure 7.55: Inclination angle of the pier’s columns θ_i vs t in (a) [rad] and (b) [degrees]

Σχήμα 7.55: Γωνία κλίσης στύλων μεσοβάθρου θ_i σε σχέση με το χρόνο σε (a) [rad] και (b) [μοίρες]

7.4 Case 3 ($\theta_x+0.3\theta_y+\rho$)

7.4.1 Imposed settlement ρ and rotations θ_x and θ_y

In this case, the imposed settlements of Figure 7.1d are considered simulating the rotation $\theta_x=\theta$ and the corresponding uniform settlement $\rho=11.459\theta$. A rotation at the footing of the pier along the transverse axis y (θ_y) is also applied at the base of all three columns, with magnitude $\theta_y=0.30\theta$. The imposed rotations and settlement are shown in Figure 7.56.

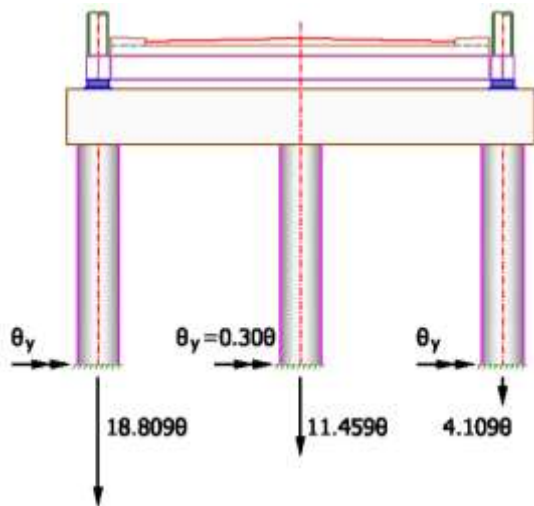


Figure 7.56: Imposed longitudinal rotation $\theta_x=\theta$, transverse rotation $\theta_y=0.30\theta$ and settlement ρ

Σχήμα 7.56: Επιβαλλόμενη διαμήκης στροφή $\theta_x=\theta$, εγκάρσια στροφή $\theta_y=0.30\theta$ και καθίζηση ρ

7.4.2 Response of the bridge for Combination 1

In this Case, in which the longitudinal rotation θ_x prevails, the bridge responds in a similar way as in Case 1, in which only the longitudinal rotation is imposed, while the transverse one is neglected. In this Case, assuming a maximum rotation $\theta_x=\theta$ equal to $\max\theta_x=\max\theta=0.026\text{rad}$ and a corresponding $\max\theta_y=0.30\max\theta=0.0078\text{rad}$, the analysis stops when $\theta_x=\theta=0.0244\text{rad}=1.40^\circ$, and $\theta_y=0.30\theta=0.0073\text{rad}=0.42^\circ$, at $t=3.94$, due to failure at the top of columns 2 and 3 (Figure 7.57). The deformed state at the moment of failure is illustrated in Figure 7.58.

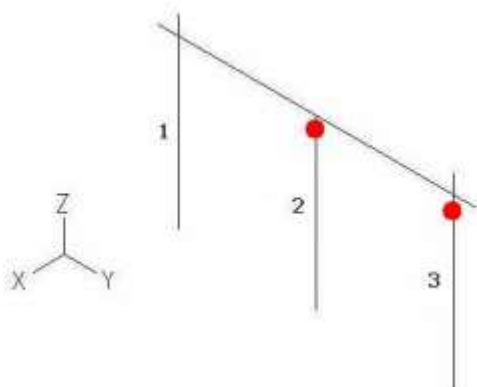


Figure 7.57: Simultaneous failure at the top of columns 2 and 3

Σχήμα 7.57: Ταυτόχρονη αστοχία στην κορυφή των στύλων 2 και 3

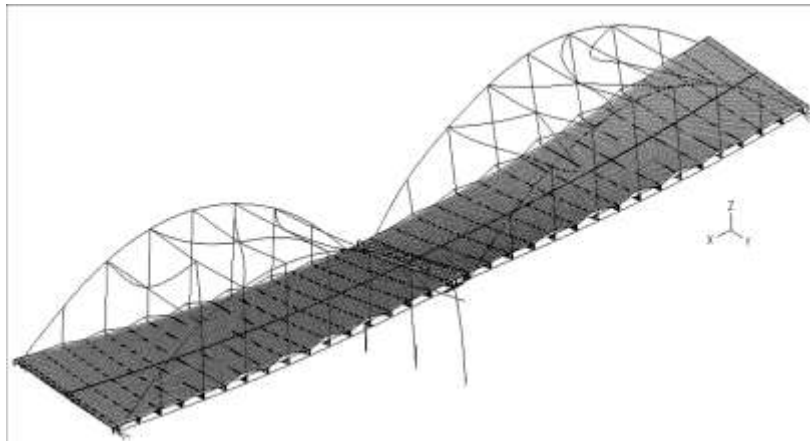


Figure 7.58: Deformed state at failure

Σχήμα 7.58: Παραμορφωμένη κατάσταση στην αστοχία

The diagrams $M-\phi$ (a) for the top and (b) for the base of all three columns are plotted in Figure 7.59. The base of all three columns remains in the elastic zone, as in Case 1, while failure takes place at the top of them. In the $M-\phi$ diagrams, the dotted lines indicate the bending moments that correspond to yield for the section at the top of each column. The magnitudes M and ϕ that correspond to the yield of each column are given in Table 7.15, while the $M-t$ diagrams are shown in Figure 7.60, in which the first yield is detected, occurring simultaneously at $t=3.641$ at the top of columns 1 and 2.

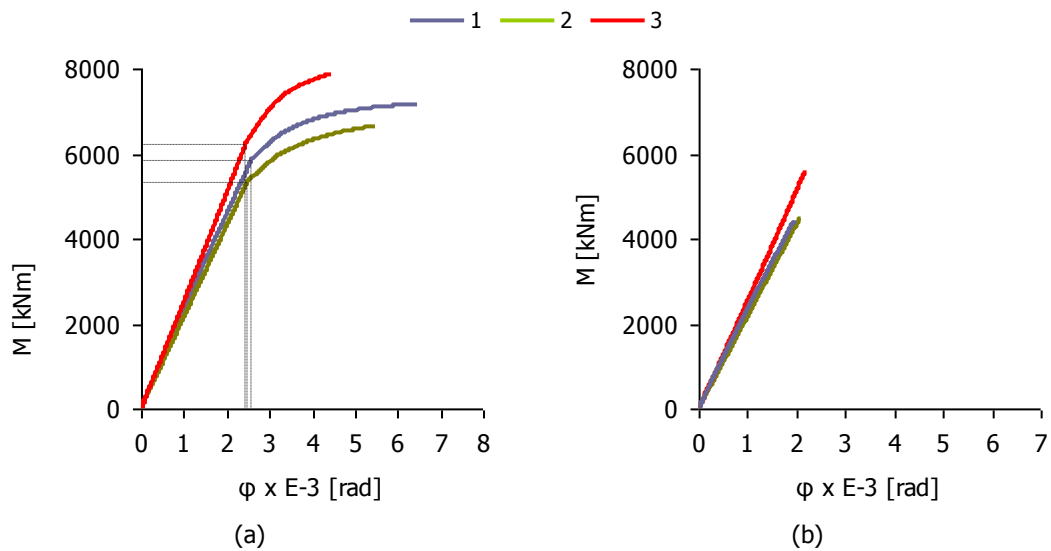


Figure 7.59: $M-\phi$ diagrams for (a) the top and (b) the base of the three columns

Σχήμα 7.59: Διαγράμματα $M-\phi$ για (a) τις κορυφές και (b) τις βάσεις των τριών στύλων

Table 7.15: Yield at the top of the pier's columns

Πίνακας 7.15: Διαρροή στην κορυφή των στύλων μεσοβάθρου

Columns	t	M [kNm]	ϕ E-3 [rad]
1	3.641	5836.79	2.58
2	3.641	5324.33	2.48
3	3.706	6214.99	2.44

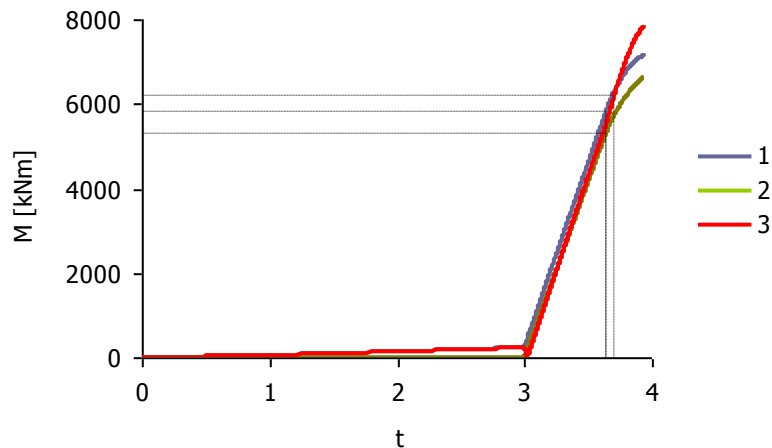


Figure 7.60: M-t diagrams for the top of the three columns

Σχήμα 7.60: Διαγράμματα M-t για τις κορυφές των τριών στύλων

As noticed also in Case 1, all steel members, at the time of failure, remain in the elastic zone, except of the diagonal bracing members, which exceed the yield stress due to buckling, but being replaceable, do not determine the permissible settlement, since they do not reach the ultimate stress $f_u=510\text{MPa}$. The response of the steel members at the end of the analysis, as well as at the time of the first yield at the base of the pier's column, is summarized in Table 7.16. The maximum stresses in the steel members are comparable with the ones of Table 7.4 referring to Case 1.

Table 7.16: Maximum stresses in the steel members at the time of the first yield ($t=3.641$) and the time of failure ($t=3.94$)

Πίνακας 7.16: Μέγιστες τάσεις στα μεταλλικά στοιχεία τη στιγμή της πρώτης διαρροής ($t=3.641$) και τη στιγμή της αστοχίας ($t=3.94$)

Members	t=3.641		t=3.94	
	σ [MPa]	ϵ %	σ [MPa]	ϵ %
Arches	225.68	0.11	249.95	0.12
Main beams	168.52	0.08	183.52	0.09
Secondary beams	116.76	0.06	121.61	0.06
Horizontal bracing	186.03	0.09	264.99	0.13
Diagonal bracing	358.61	0.76	363.04	1.30
Hangers	273.06	0.13	277.10	0.13

The load – displacement diagrams of the horizontal springs in the transverse and longitudinal direction of the bridge are given in Figure 7.61 for the abutment and in Figure 7.62 for the pier. The springs behave elastically until the end of the analysis. The maximum force and the horizontal displacement of the springs in the longitudinal direction arise at 288kN and 0.08m, for both abutment and pier, which are the same as in Case 1 (Figure 7.18 and Figure 7.19). The diagrams of the shear strains with respect to time t are shown in Figure 7.63 for the abutment's bearings and in Figure 7.64 for the pier's bearings. For both abutment and pier, the shear strain due to translational movements $\epsilon_{q,d}$ remains below the limit of 2, while the maximum design strain $\epsilon_{t,d}$ is smaller than the limit of 7, until the end of the analysis, confirming their elastic behavior.

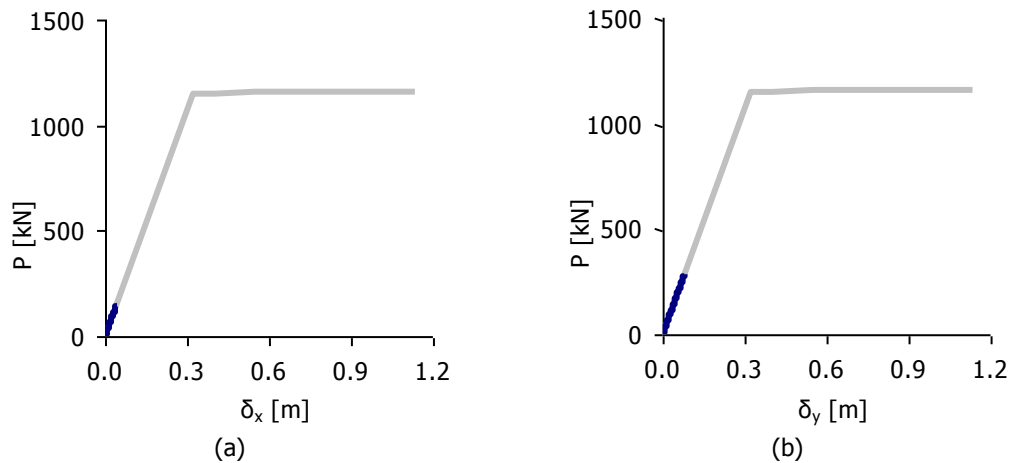


Figure 7.61: Diagram of load – displacement for the abutment’s bearings (a) in the longitudinal and (b) transverse direction

Σχήμα 7.61: Διάγραμμα φορτίου – παραμόρφωσης εφεδράνων ακροβάθρου (a) στη διαμήκη και (b) στην εγκάρσια έννοια

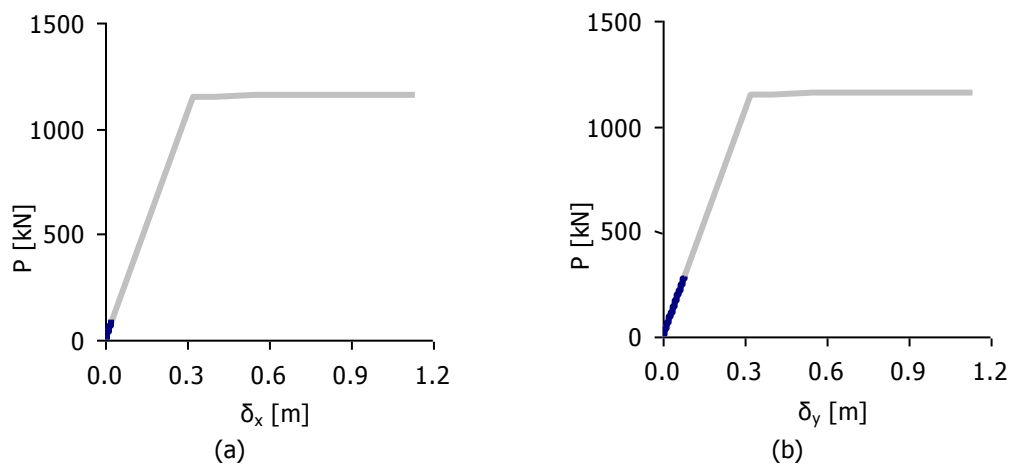


Figure 7.62: Diagram of load – displacement for the pier’s bearings (a) in the longitudinal and (b) transverse direction

Σχήμα 7.62: Διάγραμμα φορτίου – παραμόρφωσης εφεδράνων μεσοβάθρου (a) στη διαμήκη και (b) στην εγκάρσια έννοια

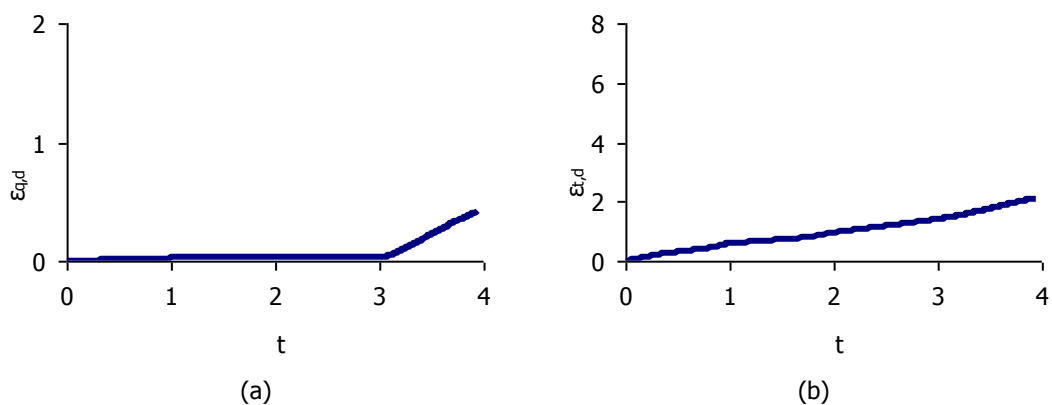


Figure 7.63: Strains of the abutment’s bearings: (a) shear strain due to translational movements $\epsilon_{q,d}$, (b) maximum design strain $\epsilon_{t,d}$

Σχήμα 7.63: Παραμορφώσεις εφεδράνων ακροβάθρου: (a) διαμητική παραμόρφωση λόγω μετακίνησης $\epsilon_{q,d}$, (b) συνολική διαμητική παραμόρφωση $\epsilon_{t,d}$

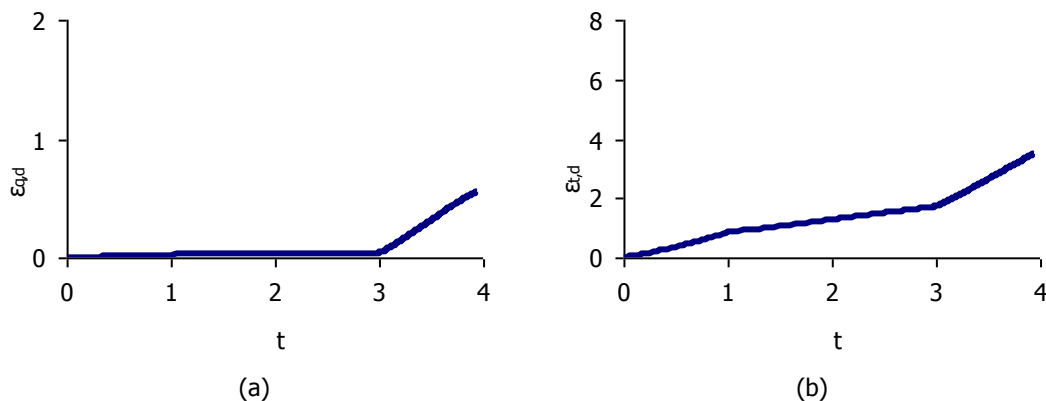


Figure 7.64: Strains of the pier’s bearings: (a) shear strain due to translational movements $\epsilon_{q,d}$, (b) maximum design strain $\epsilon_{t,d}$

Σχήμα 7.64: Παραμορφώσεις εφεδράνων μεσοβάθρου: (a) διατμητική παραμόρφωση λόγω μετακίνησης $\epsilon_{q,d}$, (b) συνολική διατμητική παραμόρφωση $\epsilon_{t,d}$

7.4.3 Permissible rotation and settlement for Combination 1

The evolution of the rotation’s components in the longitudinal and transverse direction of the bridge, θ_x and θ_y respectively, is plotted in Figure 7.65, while the resultant rotation and the uniform settlement ρ are shown in Figure 7.66, with the dotted lines referring to the values at the time of the first yield of the pier’s columns. The values of the calculated rotations are given in Table 7.17, while the values of the total rotation and settlement are listed in Table 7.18, which are close to the ones of Case 1, given in Table 7.5.

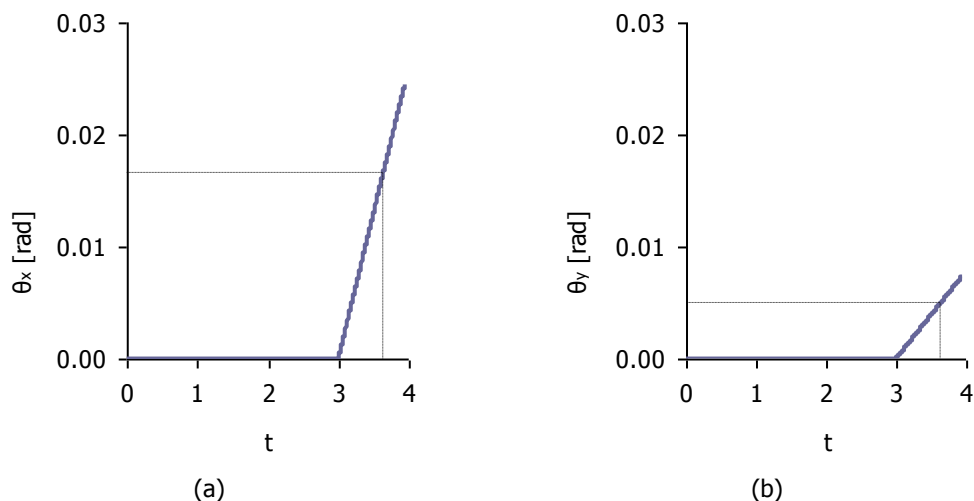


Figure 7.65: Components of the rotation vs t: (a) longitudinal θ_x , (b) transverse θ_y

Σχήμα 7.65: Συνιστώσες της στροφής συναρτήσει t: (a) διαμήκης θ_x , (b) εγκάρσια θ_y

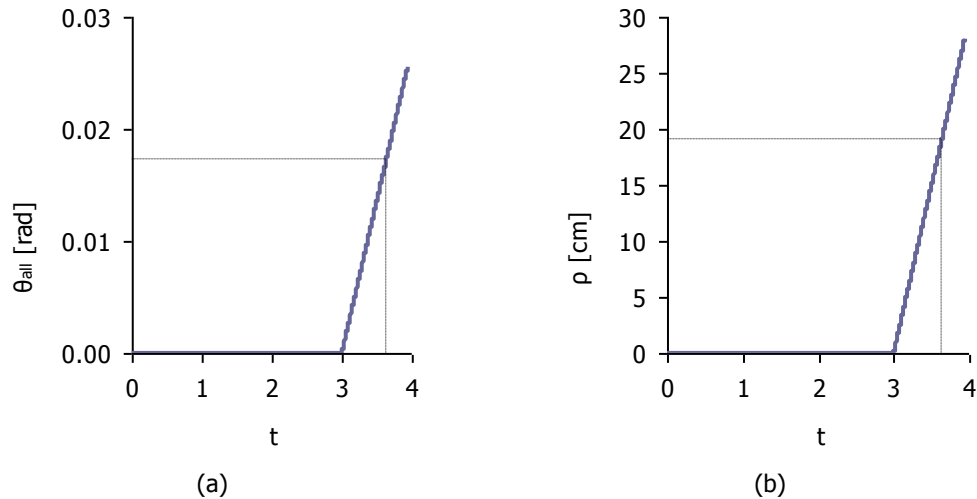


Figure 7.66: (a) Resultant rotation vs t, (b) Uniform settlement ρ vs t

Σχήμα 7.66: (a) Συνισταμένη στροφή συναρτήσει t, (b) Ομοιόμορφη καθίζηση ρ συναρτήσει t

Table 7.17: Maximum and yield values of rotations $\theta_x=\theta$ and $\theta_y=0.30\theta$

Πίνακας 7.17: Μέγιστη τιμή και τιμή στην πρώτη διαρροή διαμήκους στροφής $\theta_x=\theta$, εγκάρσιας στροφής $\theta_y=0.30\theta$

	t	θ_x [rad]	θ_x [degrees]	θ_y [rad]	θ_y [degrees]
Yield (Y)	3.641	0.0167	0.96	0.0050	0.29
Failure (F)	3.940	0.0244	1.40	0.0073	0.42

Table 7.18: Maximum, yield and permissible values of total rotation and uniform settlement ρ

Πίνακας 7.18: Μέγιστη τιμή, τιμή στην πρώτη διαρροή και επιτρεπόμενη τιμή συνολικής στροφής και ομοιόμορφης καθίζησης ρ

	t	ρ [cm]	θ_{all} [rad]	θ_{all} [degrees]
Yield (Y)	3.641	19.1	0.0174	1.00
Failure (F)	3.940	28.0	0.0255	1.46
Permissible (P=F/1.15)	–	24.3	0.022	1.27

7.4.4 Inclination angle of the pier for Combination 1

Figure 7.67 shows the diagram of the inclination angle θ_i of the pier's columns vs t. At failure, the inclination angle arises at $\theta_{i,F}=0.0119\text{rad}=0.68^\circ$, the one at the first yield is $\theta_{i,Y}=0.0087\text{rad}=0.50^\circ$, and the one that corresponds to the permissible settlement and rotation is:

$$\theta_{i,P} = \theta_{i,F}/\xi_{YG} = 0.0103\text{rad} = 0.59^\circ < \max\theta_i = 0.04\text{rad} \quad (7-7)$$

Comparing with the corresponding inclination angle of Case 1 for Combination 1, calculated in section 7.2.4, Case 3 leads to larger inclination angles of the pier, while the permissible settlement is the same.

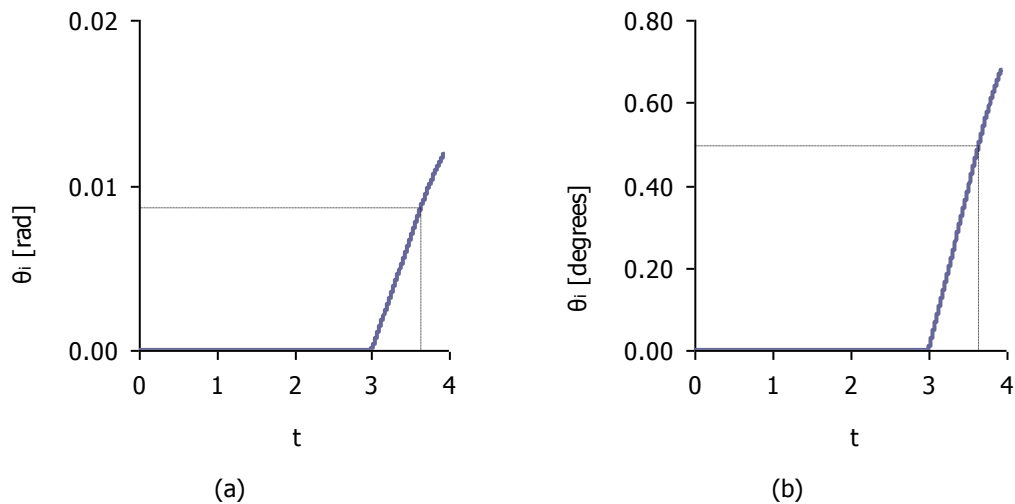


Figure 7.67: Inclination angle of the pier's columns θ_i vs t in (a) [rad] and (b) [degrees]

Σχήμα 7.67: Γωνία κλίσης στύλων μεσοβάθρου θ_i σε σχέση με το χρόνο σε (a) [rad] και (b) [μοίρες]

7.4.5 Response of the bridge for Combination 2

For Combination 2, a maximum rotation $\theta_x = \theta$ is assumed equal to $\max\theta_x = \max\theta = 0.026\text{rad}$ and $\max\theta_y = 0.30\max\theta = 0.0078\text{rad}$. The analysis stops when $\theta_x = \theta = 0.0249\text{rad} = 1.42^\circ$, and $\theta_y = 0.30\theta = 0.0075\text{rad} = 0.43^\circ$, at $t = 3.956$, because of the bending failure at the top of the column 1 (Figure 7.68). The diagram $M-\varphi$ is plotted in Figure 7.69 for the top and the base of the three columns. As in Case 1, the bending moments at the pier's base remain at low levels, while large bending moments at the top of them cause the failure of the pier. The $M-t$ diagrams are depicted in Figure 7.70, in which the first yield is detected for the outer column 1, for $t = 3.601$. It is reminded that the dotted lines denote the bending moments that correspond to the first yield of each column. The bending moments and curvatures, corresponding to the yield of each column, are listed in Table 7.19. Comparing with the magnitudes of bending moments of Case 1 (Table 7.6), it is noticed that the bridge exhibits a very similar behavior.

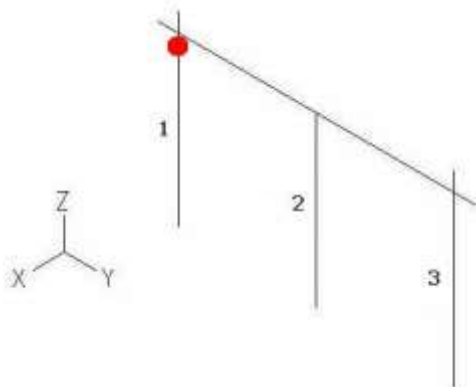


Figure 7.68: Failure at the top of column 1

Σχήμα 7.68: Αστοχία στην κορυφή του στύλου 1

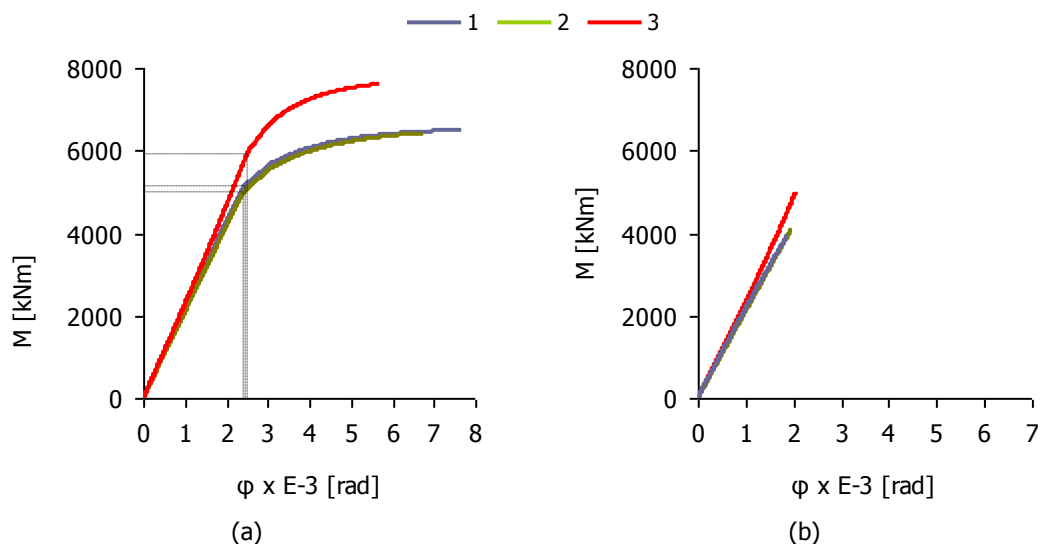


Figure 7.69: M-φ diagrams for (a) the top and (b) the base of the three columns

Σχήμα 7.69: Διαγράμματα M-φ για (a) τις κορυφές και (b) τις βάσεις των τριών στύλων

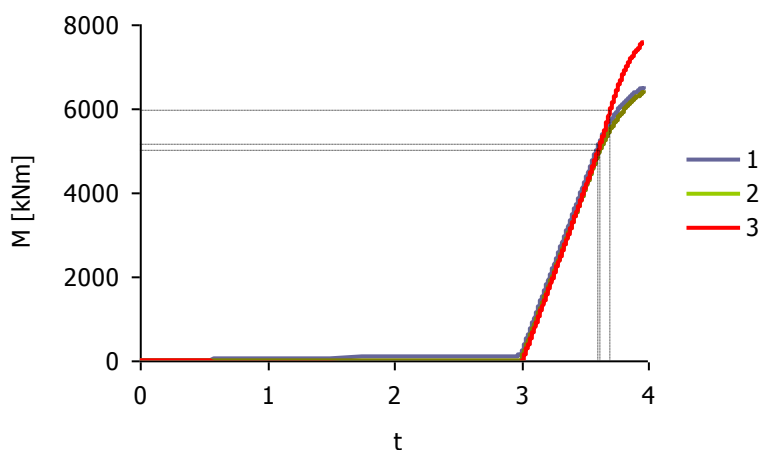


Figure 7.70: M-t diagrams for the top of the three columns

Σχήμα 7.70: Διαγράμματα M-t για τις κορυφές των τριών στύλων

Table 7.19: Yield at the top of the pier’s columns

Πίνακας 7.19: Διαρροή στην κορυφή των στύλων μεσοβάθρου

Columns	t	M [kNm]	φ E-3 [rad]
1	3.601	5134.58	2.43
2	3.622	4985.87	2.41
3	3.704	5895.70	2.50

As noted in Case 1 all steel members remain in the elastic zone, except of the diagonal bracing members, which buckle. The response of the steel members at the end of the analysis, as well as at the time of the first yield, is listed in Table 7.20 in terms of maximum stresses and strains. Until the end of the analysis, corresponding to the bridge’s failure the steel members’ stresses remain smaller than the ultimate stress $f_u=510\text{MPa}$. As first mentioned in section 7.2.2, the diagonal bracing members that experience buckling, are considered replaceable. Thus, their failure does not indicate a bridge failure.

Table 7.20: Maximum stresses in the steel members at the time of the first yield ($t=3.601$) and the time of failure ($t=3.956$)

Πίνακας 7.20: Μέγιστες τάσεις στα μεταλλικά στοιχεία τη στιγμή της πρώτης διαρροής ($t=3.601$) και τη στιγμή της αστοχίας ($t=3.956$)

Members	t=3.601		t=3.956	
	σ [MPa]	ϵ %	σ [MPa]	ϵ %
Arches	158.73	0.08	191.77	0.09
Main beams	135.47	0.06	158.86	0.08
Secondary beams	72.63	0.03	81.00	0.04
Horizontal bracing	142.28	0.07	222.00	0.11
Diagonal bracing	356.83	0.43	361.85	1.13
Hangers	171.54	0.08	174.84	0.08

The behavior of the horizontal springs in the transverse and longitudinal direction of the bridge is denoted by the load – displacement diagrams, given in Figure 7.71 for the abutment and in Figure 7.72 for the pier. The springs always behave elastically until the end of the analysis. The maximum force and the horizontal displacement of the springs in the longitudinal direction arise at 287kN and 0.08m, for both abutment and pier, which are the same as in Case 1 for Combination 2 (Figure 7.27 and Figure 7.28). The diagrams of the shear strains with respect to time t are shown in Figure 7.73 for the abutment's bearings and in Figure 7.74 for the pier's bearings. For both abutment and pier, the shear strain due to translational movements $\epsilon_{q,d}$ remains smaller than 2, and the maximum design strain $\epsilon_{t,d}$ smaller than 7, until the end of the analysis, confirming their elastic behavior.

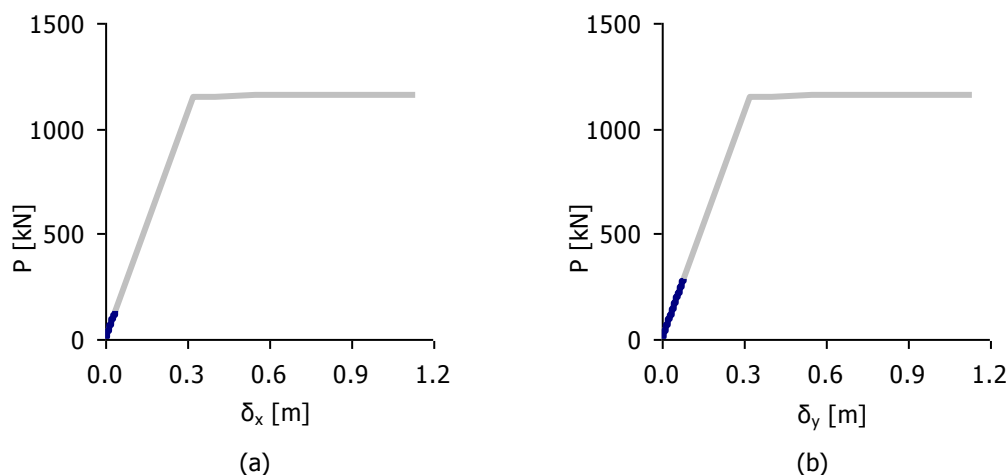


Figure 7.71: Diagram of load – displacement for the abutment's bearings (a) in the longitudinal and (b) transverse direction

Σχήμα 7.71: Διάγραμμα φορτίου – παραμόρφωσης εφεδράνων ακροβάθρου (α) στη διαμήκη και (β) στην εγκάρσια έννοια

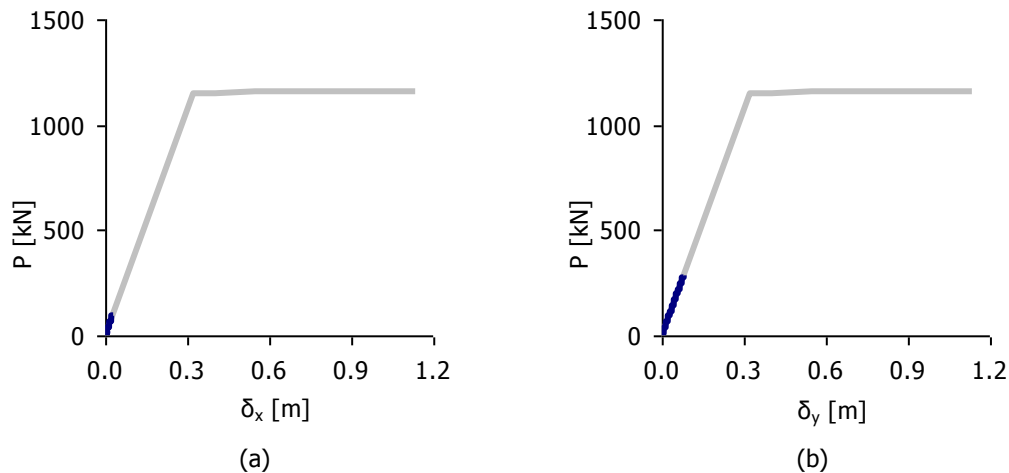


Figure 7.72: Diagram of load – displacement for the pier’s bearings (a) in the longitudinal and (b) transverse direction

Σχήμα 7.72: Διάγραμμα φορτίου – παραμόρφωσης εφεδράνων μεσοβάθρου (a) στη διαμήκη και (b) στην εγκάρσια έννοια

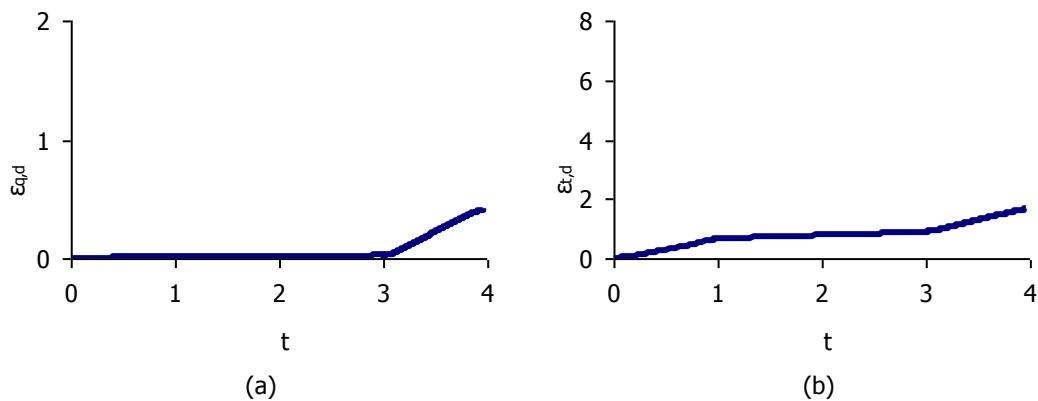


Figure 7.73: Strains of the abutment’s bearings: (a) shear strain due to translational movements $\epsilon_{q,d}$, (b) maximum design strain $\epsilon_{t,d}$

Σχήμα 7.73: Παραμορφώσεις εφεδράνων ακροβάθρου: (a) διατμητική παραμόρφωση λόγω μετακίνησης $\epsilon_{q,d}$, (b) συνολική διατμητική παραμόρφωση $\epsilon_{t,d}$

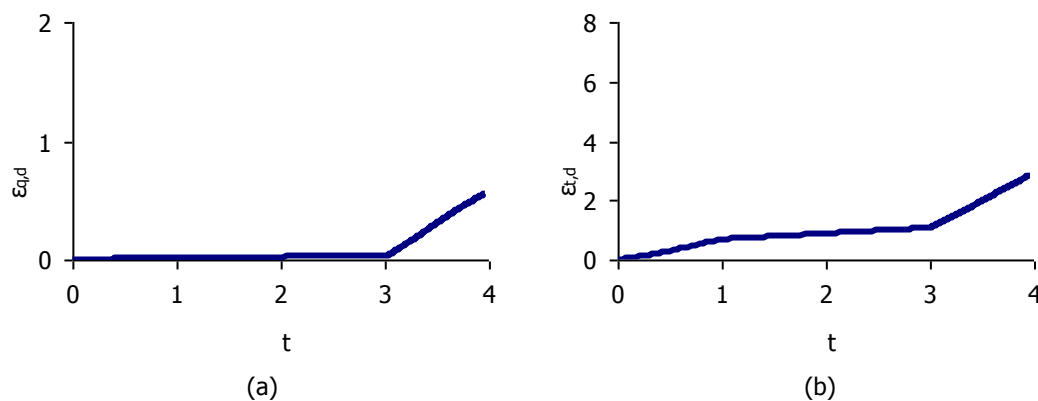


Figure 7.74: Strains of the pier’s bearings: (a) shear strain due to translational movements $\epsilon_{q,d,r}$, (b) maximum design strain $\epsilon_{t,d}$

Σχήμα 7.74: Παραμορφώσεις εφεδράνων μεσοβάθρου: (a) διατμητική παραμόρφωση λόγω μετακίνησης $\epsilon_{q,d,r}$, (b) συνολική διατμητική παραμόρφωση $\epsilon_{t,d}$

7.4.6 Permissible rotation and settlement for Combination 2

The diagram of the rotation's components θ_x and θ_y , in the longitudinal and transverse direction of the bridge, respectively, with respect to t , is plotted in Figure 7.75. The corresponding one of the resultant rotation and the uniform settlement ρ are shown in Figure 7.76. The dotted lines refer to the values at the time $t=3.601$, which corresponds to the first yield of the pier's columns. The values of the calculated rotations are given in Table 7.21, while the values of the total rotation and settlement are listed in Table 7.22, which are similar to the ones of Case 1 – Combination 2, given in Table 7.8.

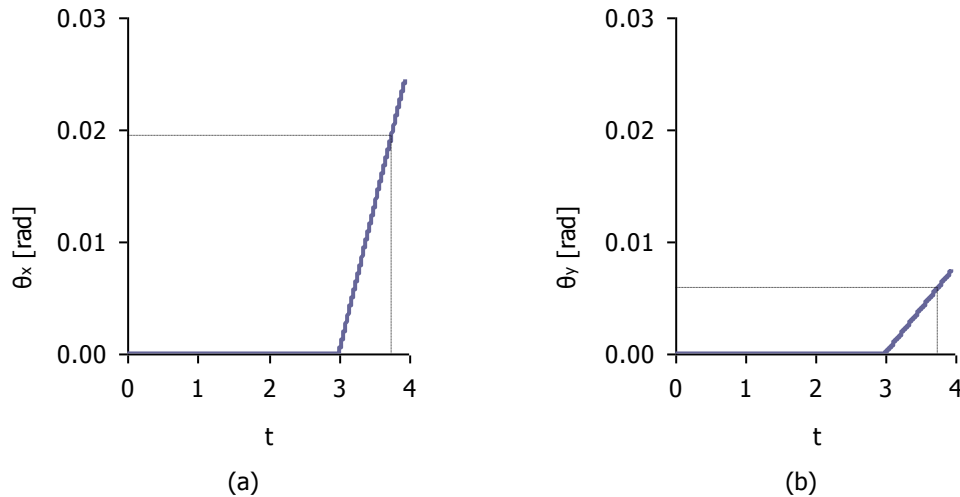


Figure 7.75: Components of the rotation vs t: (a) longitudinal θ_x , (b) transverse θ_y

Σχήμα 7.75: Συνιστώσες της στροφής συναρτήσει t: (a) διαμήκης θ_x , (b) εγκάρσια θ_y

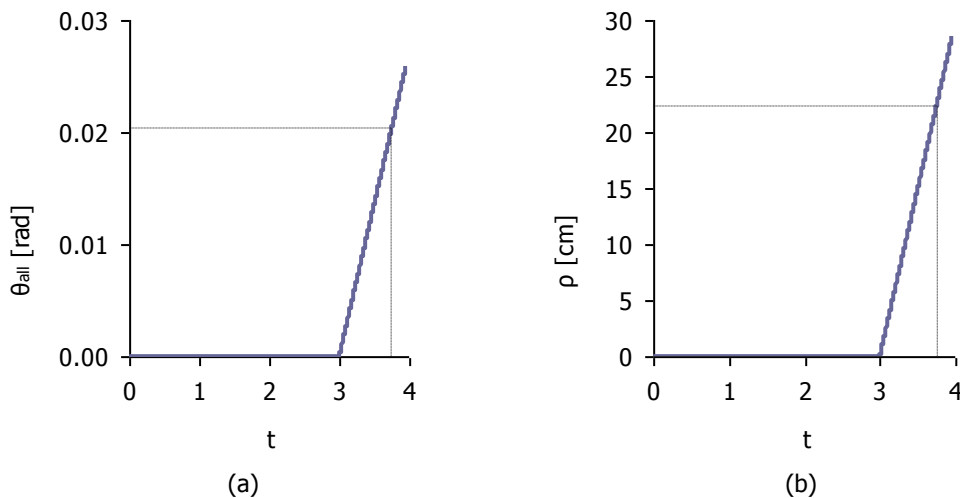


Figure 7.76: (a) Resultant rotation vs t, (b) Uniform settlement ρ vs t

Σχήμα 7.76: (a) Συνισταμένη στροφή συναρτήσει t, (b) Ομοιόμορφη καθίζηση ρ συναρτήσει t

Table 7.21: Maximum and yield values of rotations $\theta_x=\theta$ and $\theta_y=0.30\theta$

Πίνακας 7.21: Μέγιστη τιμή και τιμή στην πρώτη διαρροή διαμήκους στροφής $\theta_x=\theta$, εγκάρσιας στροφής $\theta_y=0.30\theta$

	t	θ_x [rad]	θ_x [degrees]	θ_y [rad]	θ_y [degrees]
Yield (Y)	3.601	0.0133	0.76	0.0040	0.22
Failure (F)	3.956	0.0249	1.42	0.0075	0.43

Table 7.22: Maximum, yield and permissible values of total rotation and uniform settlement ρ

Πίνακας 7.22: Μέγιστη τιμή, τιμή στην πρώτη διαρροή και επιτρεπόμενη τιμή συνολικής στροφής και ομοιόμορφης καθίζησης ρ

	t	ρ [cm]	θ_{all} [rad]	θ_{all} [degrees]
Yield (Y)	3.601	15.3	0.0139	0.80
Failure (F)	3.956	28.5	0.0260	1.49
Permissible (P=F/1.15)	–	24.8	0.023	1.30

7.4.7 Inclination angle of the pier for Combination 2

Figure 7.77 shows the evolution of the inclination angle θ_i of the pier's columns. At failure, the inclination angle arises at $\theta_{i,F}=0.0116\text{rad}=0.67^\circ$, the one at the first yield is $\theta_{i,Y}=0.008\text{rad}=0.46^\circ$, and the one that corresponds to the permissible settlement and rotation is:

$$\theta_{i,P} = \theta_{i,F}/\xi_{YG} = 0.0101\text{rad} = 0.58^\circ < \max\theta_i = 0.04\text{rad} \quad (7-8)$$

Comparing with the corresponding inclination angle of Case 1 for Combination 2, calculated in section 7.2.7, Case 3 leads to larger inclination angles of the pier for smaller permissible settlement.

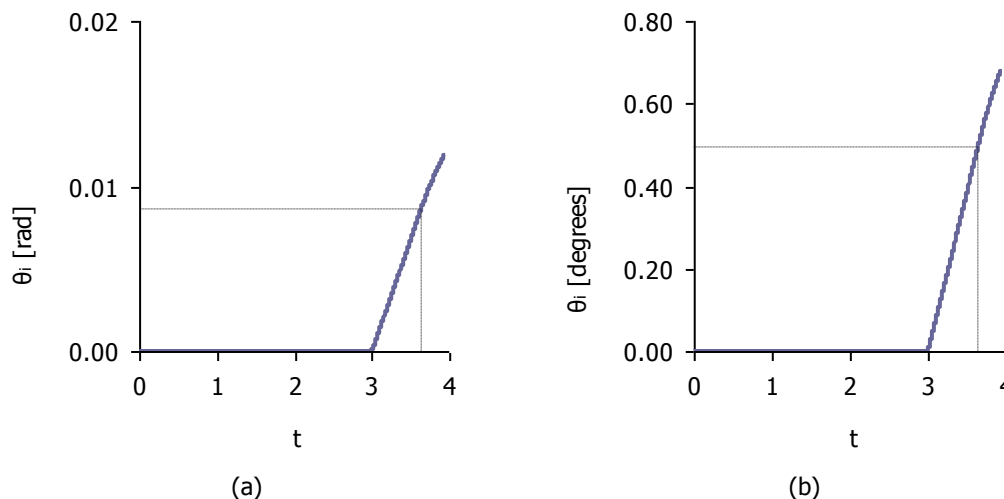


Figure 7.77: Inclination angle of the pier's columns θ_i vs t in (a) [rad] and (b) [degrees]

Σχήμα 7.77: Γωνία κλίσης στύλων μεσοβάθρου θ_i σε σχέση με το χρόνο σε (a) [rad] και (b) [μπίρες]

7.5 Case 4 ($0.30x+\theta_y+\rho$)

7.5.1 Imposed settlement ρ and rotations θ_x and θ_y

A rotation at the footing of the pier along the transverse axis y (θ_y) is applied at the base of all three columns, with magnitude $\theta_y=\theta$. Another rotation along the longitudinal axis x (θ_x) with magnitude $\theta_x=0.30\theta$, is also considered as a differential settlement at the outer columns, equal to:

$$\rho^\theta = \pm L_y \theta_x = \pm 7.35 \cdot 0.30 \cdot \theta = \pm 2.205\theta \text{ [m]} \quad (7-9)$$

where θ is measured in [rad], while ρ in [m]. The combined uniform settlement is equal to:

$$\rho = 11.459\theta \text{ [m]} \quad (7-10)$$

The sum of imposed rotations and settlements at the pier's columns is shown in Figure 7.78.

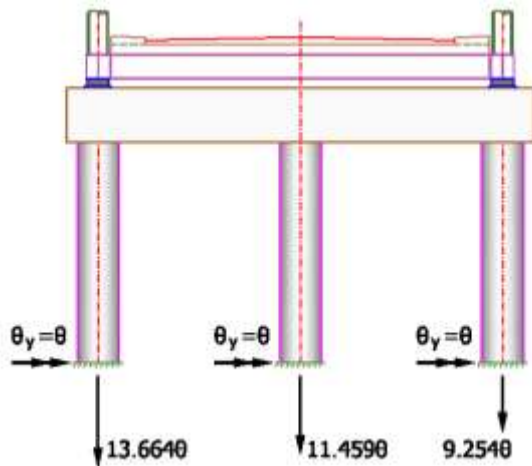


Figure 7.78: Imposed longitudinal rotation $\theta_x=0.30\theta$, transverse rotation $\theta_y=\theta$ and settlement ρ

Σχήμα 7.78: Επιβαλλόμενη διαμήκης στροφή $\theta_x=0.30\theta$, εγκάρσια στροφή $\theta_y=\theta$ και καθίζηση ρ

7.5.2 Response of the bridge for Combination 1

For Combination 1, a maximum rotation $\theta_y=\theta$ is imposed equal to $\max\theta_y=\max\theta=0.047\text{rad}$, while the corresponding longitudinal maximum rotation is $\theta_x=0.0141\text{rad}$. The analysis stops when $\theta_y=\theta=0.0466\text{rad}=2.67^\circ$, at $t=3.991$, when bending failure occurs at the base of the middle and the outer columns (columns 2 and 3), as shown in Figure 7.79. The deformed state at the time of failure is illustrated in Figure 7.80. In the diagrams $M-\phi$ shown in Figure 7.81, referring to the top and the base of the three columns, it is noted that the bending moments at the pier's top are small during the analysis, while the ones at the top of them, increased significantly as the rotation and settlement increase, lead to failure. The dotted lines correspond to the magnitudes at the time of the first yield of the pier's columns. The bending moments that correspond to yield are given in Table 7.23 and the $M-t$ diagrams, plotted in Figure 7.82, show that the first yield takes place at the outer column 1, for $t=3.734$.

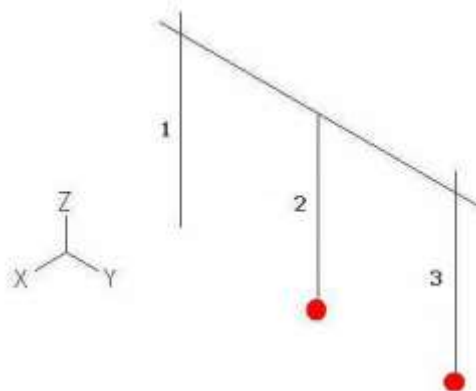


Figure 7.79: Simultaneous failure at the base of columns 2 and 3

Σχήμα 7.79: Ταυτόχρονη αστοχία στην βάση των στύλων 2 και 3

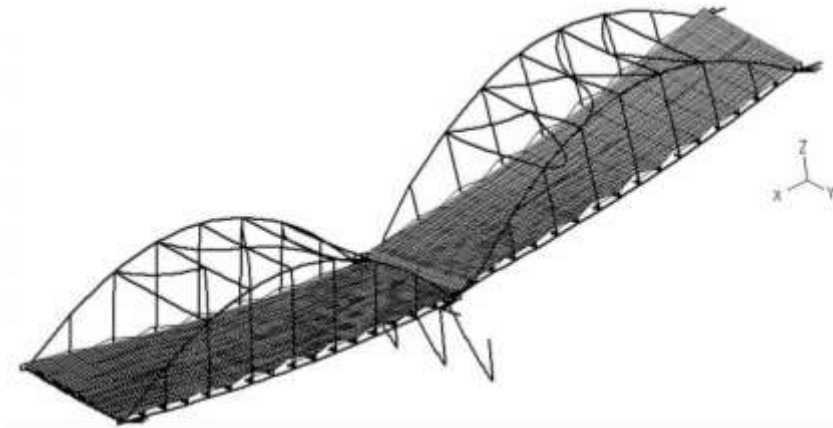


Figure 7.80: Deformed state at failure

Σχήμα 7.80: Παραμορφωμένη κατάσταση στην αστοχία

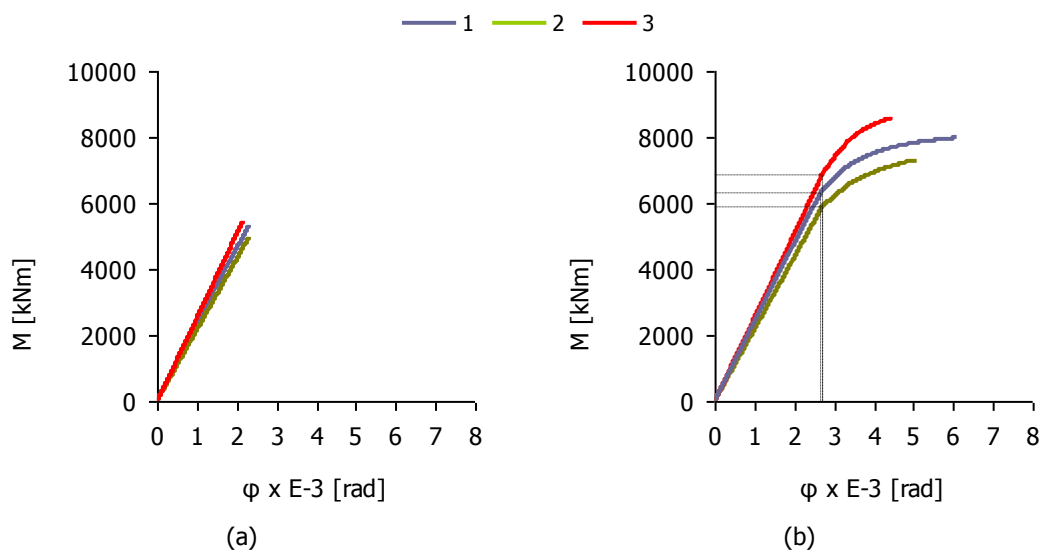


Figure 7.81: M-φ diagrams for (a) the top and (b) the base of the three columns

Σχήμα 7.81: Διαγράμματα M-φ για (a) τις κορυφές και (b) τις βάσεις των τριών στύλων

Table 7.23: Yield at the base of the pier's columns

Πίνακας 7.23: Διαρροή στη βάση των στύλων μεσοβάθρου

Columns	t	M [kNm]	φ E-3 [rad]
1	3.734	6327.24	2.67
2	3.760	5870.57	2.70
3	3.786	6864.16	2.71

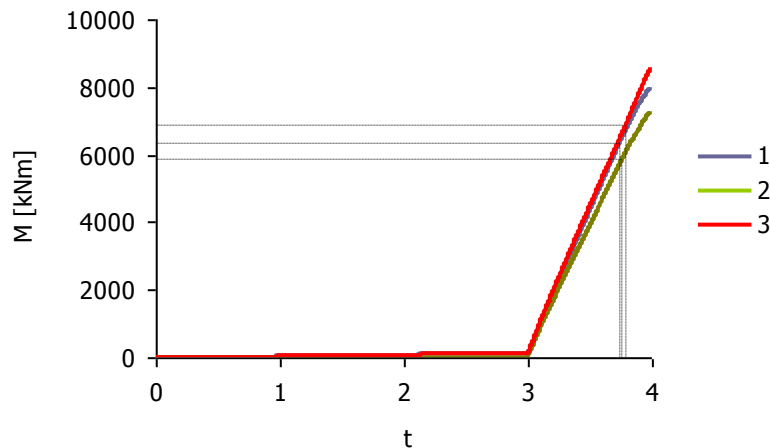


Figure 7.82: M-t diagrams for the base of the three columns

Σχήμα 7.82: Διαγράμματα M-t για τις βάσεις των τριών στύλων

As far as the steel members are concerned, at the time of failure, they all behave elastically. The response of the steel members at the time of the first yield at the base of the pier's columns, as well as at the end of the analysis, is given in Table 7.24. The maximum stresses in the steel members of the bridge do not exceed the yield stress. The stresses are larger than the ones presented in Table 7.10 of Case 2 for the same Combination, but they are comparable, with the ones of Combination 1 of Case 3, given in Table 7.16. Nevertheless, the Case 3 gives larger values of stresses for the arches and the diagonal bracing members. From these analyses it is concluded that the longitudinal rotation θ_x results in large response of the bridge.

Table 7.24: Maximum stresses in the steel members at the time of the first yield ($t=3.734$) and the time of failure ($t=3.991$)

Πίνακας 7.24: Μέγιστες τάσεις στα μεταλλικά στοιχεία τη στιγμή της πρώτης διαρροής ($t=3.734$) και τη στιγμή της αστοχίας ($t=3.991$)

Members	t=3.734		t=3.991	
	σ [MPa]	ϵ %	σ [MPa]	ϵ %
Arches	222.72	0.11	235.52	0.11
Main beams	176.17	0.08	188.68	0.09
Secondary beams	125.24	0.06	124.05	0.06
Horizontal bracing	104.39	0.05	146.40	0.07
Diagonal bracing	355.42	0.23	356.84	0.43
Hangers	273.21	0.13	275.49	0.13

Regarding the bearings, the load – displacement diagrams of the horizontal springs in the transverse and longitudinal direction of the bridge are plotted in Figure 7.83 for the abutment and in Figure 7.84 for the pier. Even in this Case, the springs behave elastically until the end of the analysis. The maximum force and the horizontal displacement of the springs in the longitudinal direction reach the values of 677kN and 0.18m, for the abutment and 651kN and 0.18m, for the pier, which are larger than the ones of Case 2 for the same Combination (Figure 7.39 and Figure 7.40). The evolution of the shear strains is illustrated in Figure 7.85 for the abutment's bearings and in Figure 7.86 for the pier's bearings. For both abutment and pier, the shear strain due to translational movements $\epsilon_{a,d}$ remains below the limit of 2, while the maximum design strain $\epsilon_{t,d}$ is smaller than the limit of 7, until the end of the analysis, confirming their elastic behavior.

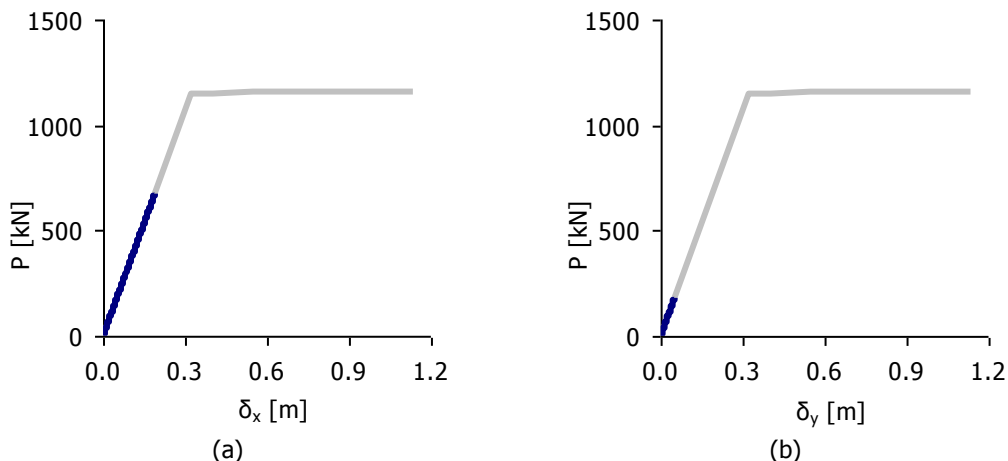


Figure 7.83: Diagram of load – displacement for the abutment’s bearings (a) in the longitudinal and (b) transverse direction

Σχήμα 7.83: Διάγραμμα φορτίου – παραμόρφωσης εφεδράνων ακροβάθρου (a) στη διαμήκη και (b) στην εγκάρσια έννοια

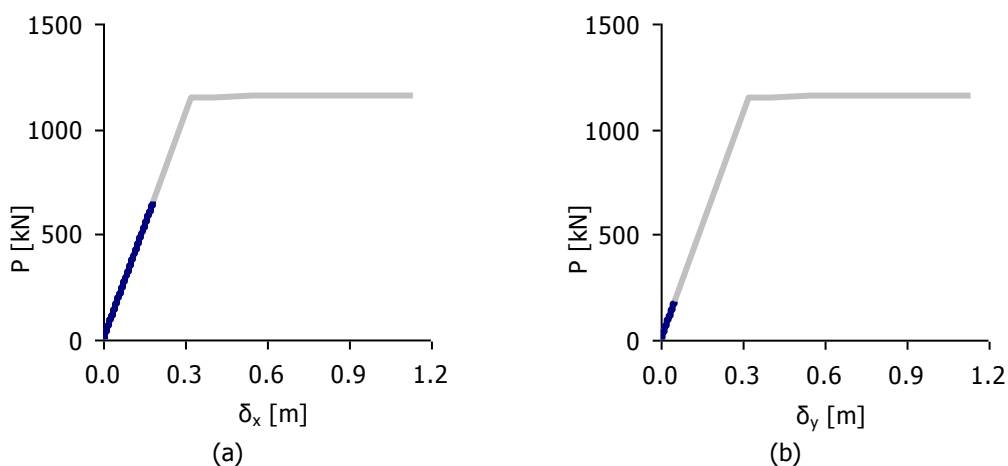


Figure 7.84: Diagram of load – displacement for the pier’s bearings (a) in the longitudinal and (b) transverse direction

Σχήμα 7.84: Διάγραμμα φορτίου – παραμόρφωσης εφεδράνων μεσοβάθρου (a) στη διαμήκη και (b) στην εγκάρσια έννοια

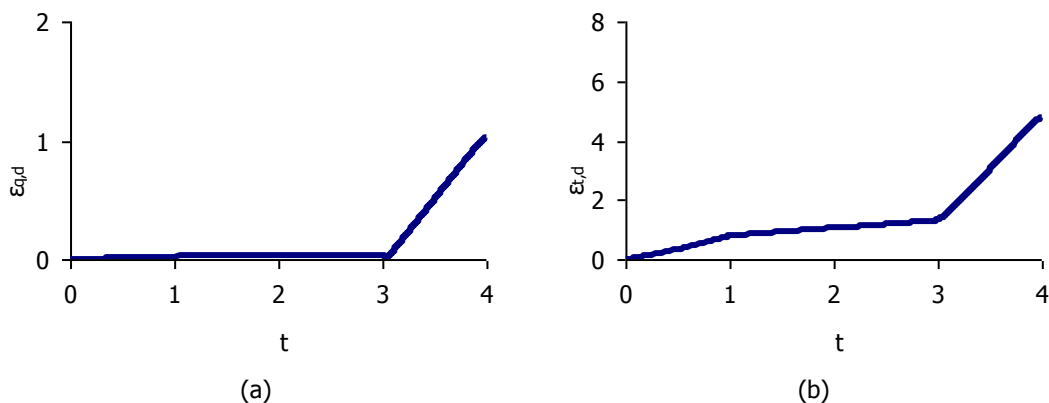


Figure 7.85: Strains of the abutment’s bearings: (a) shear strain due to translational movements $\epsilon_{q,d}$, (b) maximum design strain $\epsilon_{t,d}$

Σχήμα 7.85: Παραμορφώσεις εφεδράνων ακροβάθρου: (a) διαμητική παραμόρφωση λόγω μετακίνησης $\epsilon_{q,d}$, (b) συνολική διαμητική παραμόρφωση $\epsilon_{t,d}$

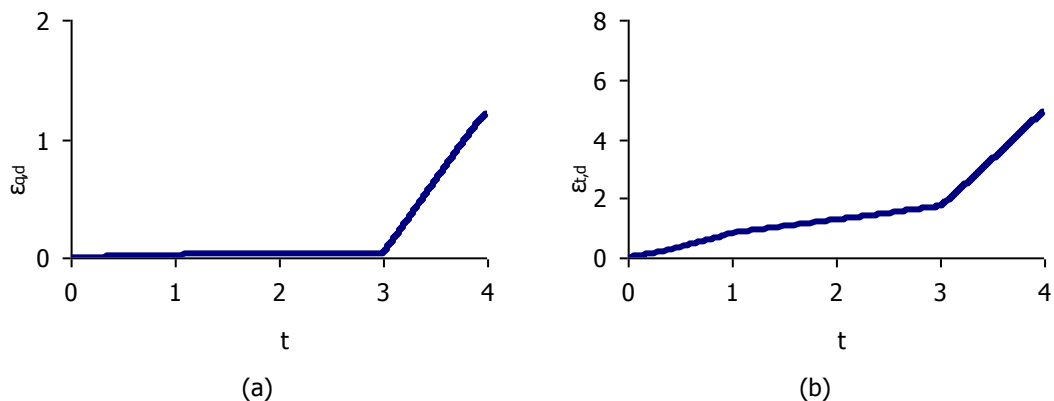


Figure 7.86: Strains of the pier’s bearings: (a) shear strain due to translational movements $\epsilon_{q,d}$, (b) maximum design strain $\epsilon_{t,d}$

Σχήμα 7.86: Παραμορφώσεις εφεδράνων μεσοβάθρου: (a) διατμητική παραμόρφωση λόγω μετακίνησης $\epsilon_{q,d}$, (b) συνολική διατμητική παραμόρφωση $\epsilon_{t,d}$

7.5.3 Permissible rotation and settlement for Combination 1

The diagrams of the rotation’s components in the longitudinal and transverse direction of the bridge, θ_x and θ_y respectively, with respect of t , are plotted in Figure 7.87, while the ones of the resultant rotation and the uniform settlement ρ are shown in Figure 7.88, with the dotted lines referring to the values at the time of the first yield of the pier’s columns. The values of the calculated rotations are given in Table 7.25, while the values of the total rotation and settlement are listed in Table 7.26, which are close to the ones of Case 2, given in Table 7.11.

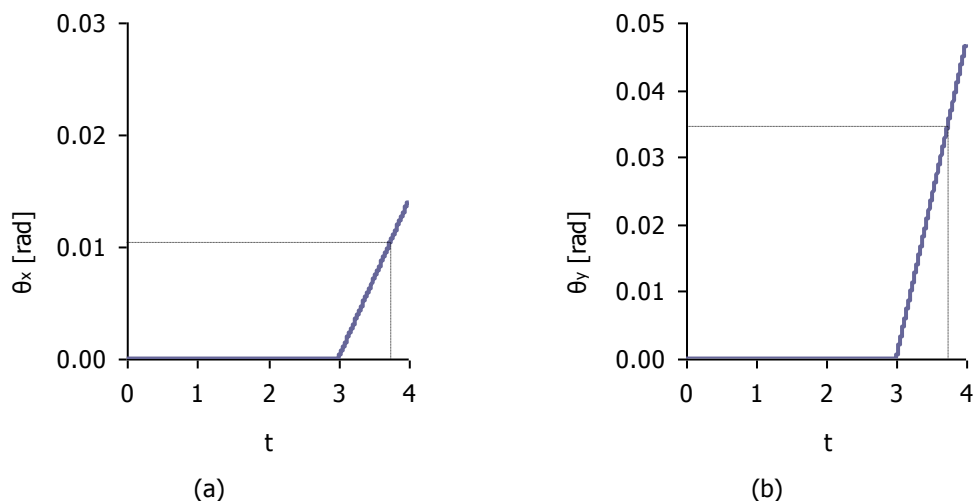


Figure 7.87: Components of the rotation vs t: (a) longitudinal θ_x , (b) transverse θ_y

Σχήμα 7.87: Συνιστώσες της στροφής συναρτήσει t: (a) διαμήκης θ_x , (b) εγκάρσια θ_y

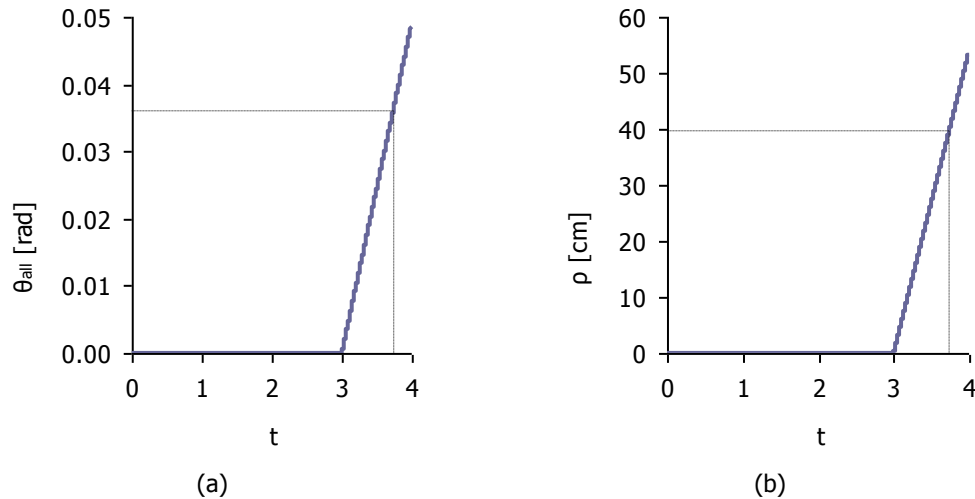


Figure 7.88: (a) Resultant rotation vs t, (b) Uniform settlement ρ vs t

Σχήμα 7.88: (a) Συνισταμένη στροφή συναρτήσει t, (b) Ομοιόμορφη καθίζηση ρ συναρτήσει t

Table 7.25: Maximum and yield values of rotations $\theta_x=0.30\theta$ and $\theta_y=\theta$

Πίνακας 7.25: Μέγιστη τιμή και τιμή στην πρώτη διαρροή διαμήκους στροφής $\theta_x=0.30\theta$, εγκάρσιας στροφής $\theta_y=\theta$

	t	θ_x [rad]	θ_x [degrees]	θ_y [rad]	θ_y [degrees]
Yield (Y)	3.734	0.0103	0.59	0.0345	1.98
Failure (F)	3.991	0.0139	0.80	0.0465	2.67

Table 7.26: Maximum, yield and permissible values of total rotation and uniform settlement ρ

Πίνακας 7.26: Μέγιστη τιμή, τιμή στην πρώτη διαρροή και επιτρεπόμενη τιμή συνολικής στροφής και ομοιόμορφης καθίζησης ρ

	t	ρ [cm]	θ_{all} [rad]	θ_{all} [degrees]
Yield (Y)	3.734	39.6	0.0360	2.06
Failure (F)	3.991	53.4	0.0486	2.79
Permissible (P=Y/1.15)	–	34.4	0.031	1.80

7.5.4 Inclination angle of the pier for Combination 1

Figure 7.89 shows the evolution of the inclination angle θ_i of the pier's columns. At failure, the inclination angle reaches the value of $\theta_{i,F}=0.0365\text{rad}=2.09^\circ$, the one at the first yield is $\theta_{i,Y}=0.0275\text{rad}=1.57^\circ$, and the one that corresponds to the permissible settlement and rotation is:

$$\theta_{i,P} = \theta_{i,Y}/\xi_{YG} = 0.0239\text{rad} = 1.36^\circ < \max\theta_i = 0.04\text{rad} \quad (7-11)$$

The values are comparable with the ones of Case 2 for Combination 1, given in Figure 7.45. Nevertheless, this Case is not the most unfavorable for the bridge, as it results in larger permissible settlements than Case 3.

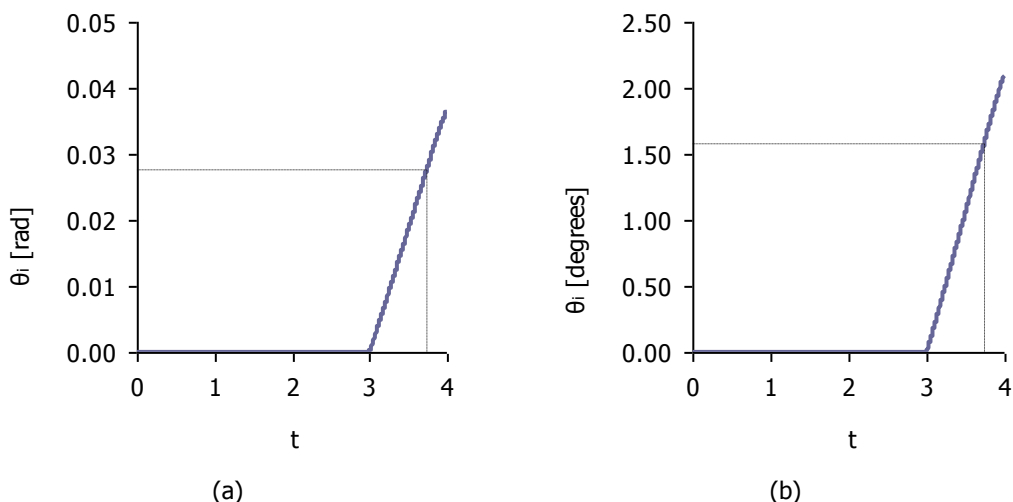


Figure 7.89: Inclination angle of the pier’s columns θ_i vs t in (a) [rad] and (b) [degrees]

Σχήμα 7.89: Γωνία κλίσης στύλων μεσοβάθρου θ_i σε σχέση με το χρόνο σε (a) [rad] και (b) [μοίρες]

7.5.5 Response of the bridge for Combination 2

Taking into account only the permanent loads for Combination 2, a maximum rotation $\theta_y = \theta$ is imposed $\max \theta_y = \max \theta = 0.046 \text{ rad}$, and a corresponding maximum longitudinal rotation $\theta_x = 0.0138 \text{ rad}$. Bending failure occurs at the base of the two outer columns (columns 1 and 3), as shown in Figure 7.90 and the analysis stops when $\theta_y = \theta = 0.0426 \text{ rad} = 2.44^\circ$, at $t = 3.926$. In the diagrams $M-\phi$ are given in Figure 7.91, referring to the top and the base of the three columns. The bending moments at the pier’s top remain small, while the ones at the top of them, increase significantly as the rotation and settlement evolve, leading to failure. The dotted lines correspond to the magnitudes at the time of the first yield of the pier’s columns. The bending moments that correspond to yield are given in Table 7.27 and the $M-t$ diagrams, plotted in Figure 7.92, show that the first yield takes place at the outer column 1 and middle column 2, for $t = 3.664$.

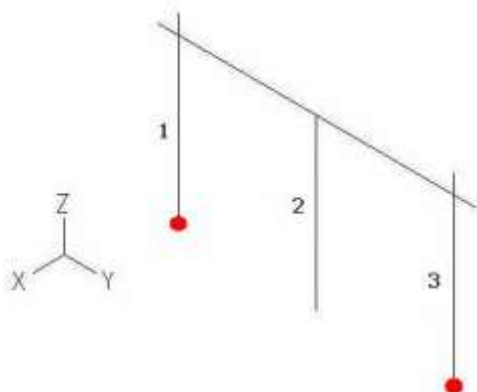


Figure 7.90: Simultaneous failure at the base of columns 1 and 3

Σχήμα 7.90: Ταυτόχρονη αστοχία στην βάση των στύλων 1 και 3

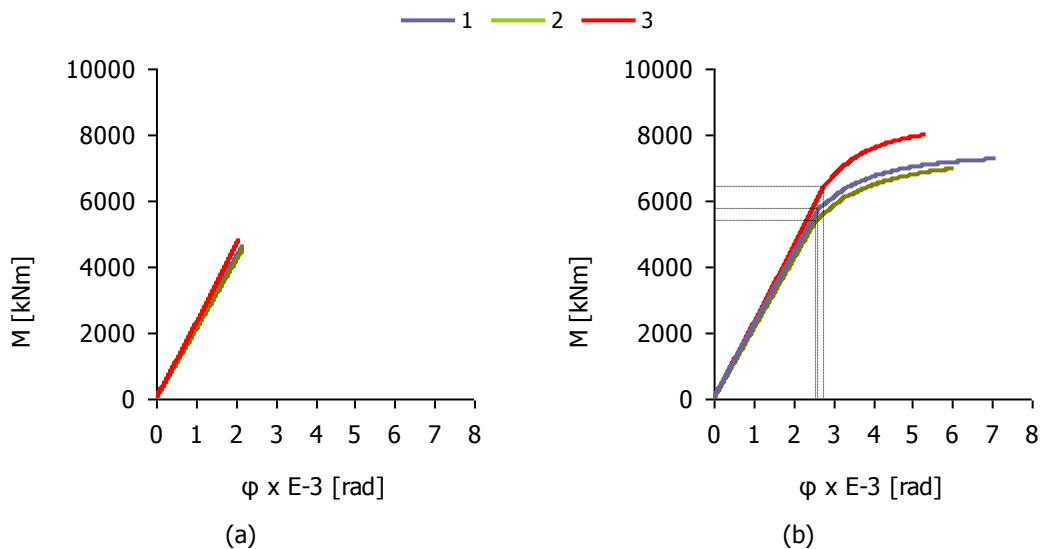


Figure 7.91: M-φ diagrams for (a) the top and (b) the base of the three columns

Σχήμα 7.91: Διαγράμματα M-φ για (a) τις κορυφές και (b) τις βάσεις των τριών στύλων

Table 7.27: Yield at the base of the pier's columns

Πίνακας 7.27: Διαρροή στη βάση των στύλων μεσοβάθρου

Columns	t	M [kNm]	φ E-3 [rad]
1	3.664	6406.82	2.76
2	3.664	5408.64	2.58
3	3.731	6864.16	2.64

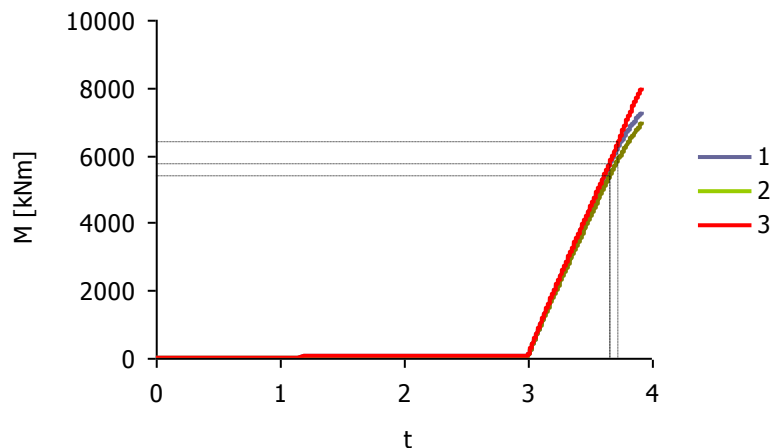


Figure 7.92: M-t diagrams for the base of the three columns

Σχήμα 7.92: Διαγράμματα M-t για τις βάσεις των τριών στύλων

Regarding the steel members, at the time of failure, they all behave elastically. The diagonal bracing members reach and slightly exceed the yield stress. The response of the steel members at the time of the first yield at the base of the pier's columns, as well as at the time of failure, is given in Table 7.28. With this final analysis, it is concluded that the steel members are not crucial for the bridge, thus, they do not determine the permissible settlement.

Table 7.28: Maximum stresses in the steel members at the time of the first yield ($t=3.664$) and the time of failure ($t=3.926$)

Πίνακας 7.28: Μέγιστες τάσεις στα μεταλλικά στοιχεία τη στιγμή της πρώτης διαρροής ($t=3.664$) και τη στιγμή της αστοχίας ($t=3.926$)

Members	t=3.664		t=3.926	
	σ [MPa]	ϵ %	σ [MPa]	ϵ %
Arches	146.14	0.07	159.75	0.08
Main beams	123.35	0.06	135.80	0.06
Secondary beams	90.62	0.04	88.57	0.04
Horizontal bracing	83.17	0.04	117.39	0.06
Diagonal bracing	355.02	0.17	355.72	0.27
Hangers	169.34	0.08	172.06	0.08

As far as the bearings are concerned, the load – displacement diagrams of the horizontal springs in the transverse and longitudinal direction of the bridge are shown in Figure 7.93 for the abutment and in Figure 7.94 for the pier. The springs always behave elastically, with maximum force and horizontal displacement of the springs in the longitudinal direction equal to 581kN and 0.16m, for the abutment and 564kN and 0.16m, for the pier.

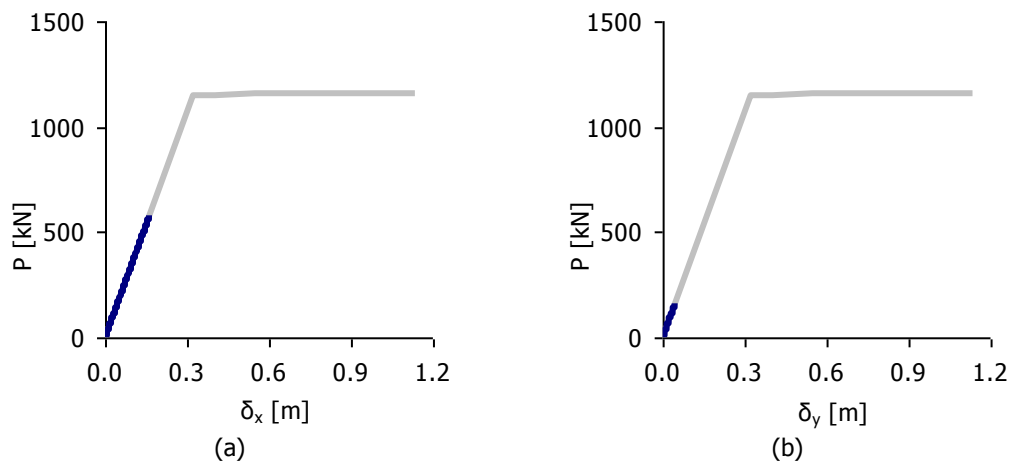


Figure 7.93: Diagram of load – displacement for the abutment's bearings (a) in the longitudinal and (b) transverse direction

Σχήμα 7.93: Διάγραμμα φορτίου – παραμόρφωσης εφεδράνων ακροβάθρου (α) στη διαμήκη και (β) στην εγκάρσια έννοια

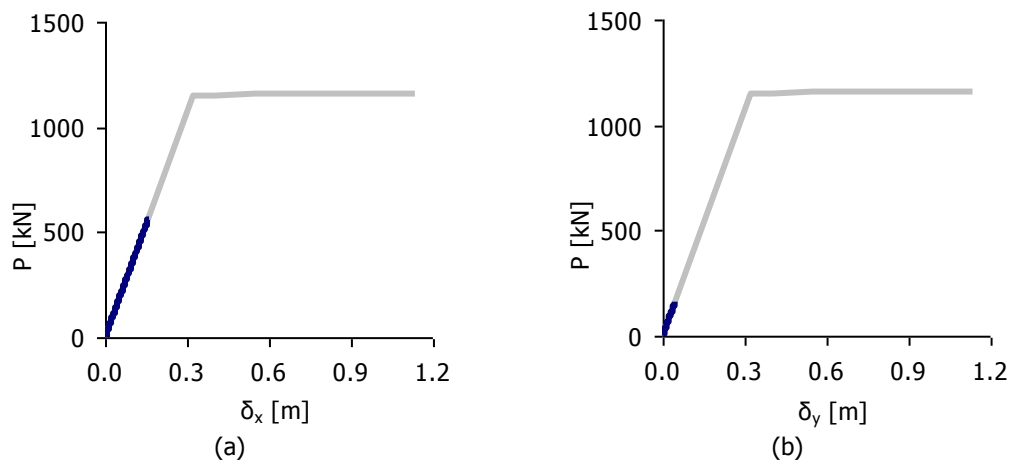


Figure 7.94: Diagram of load – displacement for the pier's bearings (a) in the longitudinal and (b) transverse direction

Σχήμα 7.94: Διάγραμμα φορτίου – παραμόρφωσης εφεδράνων μεσοβάθρου (α) στη διαμήκη και (β) στην εγκάρσια έννοια

The diagram of the shear strains with respect to t is illustrated in Figure 7.95 for the abutment's bearings and in Figure 7.96 for the pier's bearings. The shear strain due to translational movements $\epsilon_{q,d}$ remains smaller than 2, and the maximum design strain $\epsilon_{t,d}$ is smaller than 7, until the end of the analysis, for both abutment and pier, confirming their elastic behavior. Concluding with this analysis it is proved that in all cases the bearings are not critical components of the bridge.

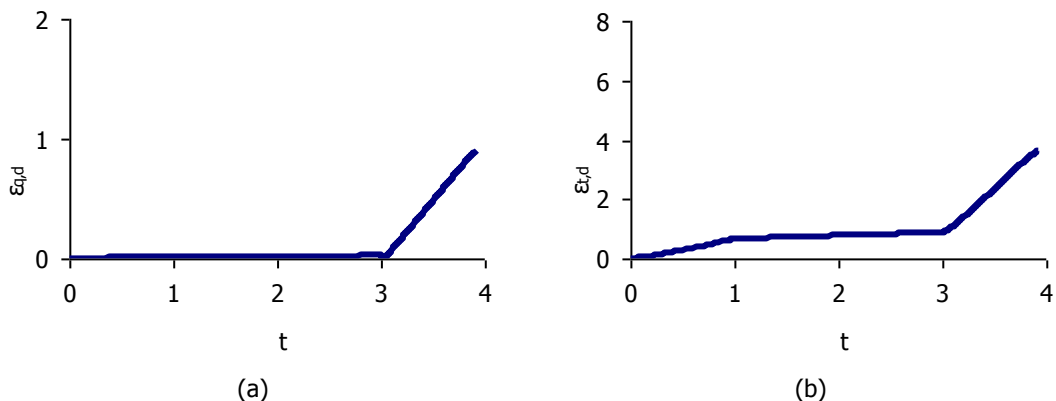


Figure 7.95: Strains of the abutment's bearings: (a) shear strain due to translatory movements $\epsilon_{q,d}$, (b) maximum design strain $\epsilon_{t,d}$

Σχήμα 7.95: Παραμορφώσεις εφεδράνων ακροβάθρου: (α) διατμητική παραμόρφωση λόγω μετακίνησης $\epsilon_{q,d}$, (β) συνολική διατμητική παραμόρφωση $\epsilon_{t,d}$

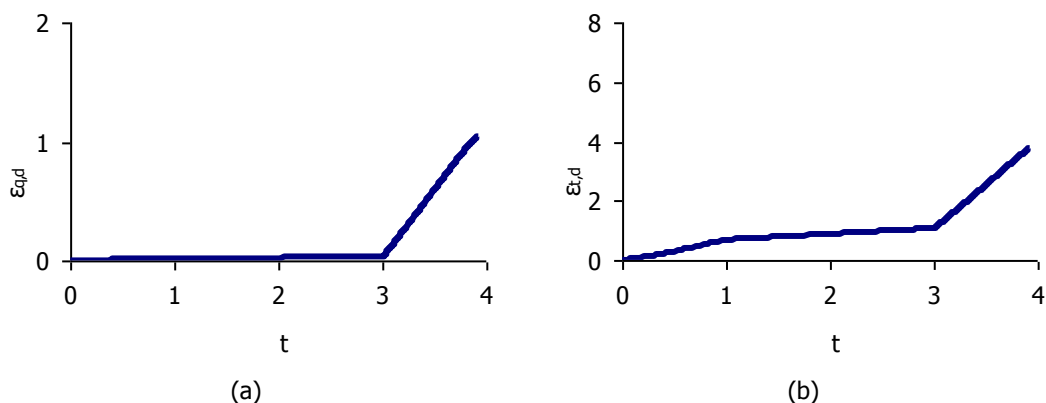


Figure 7.96: Strains of the pier's bearings: (a) shear strain due to translatory movements $\epsilon_{q,d}$, (b) maximum design strain $\epsilon_{t,d}$

Σχήμα 7.96: Παραμορφώσεις εφεδράνων μεσοβάθρου: (α) διατμητική παραμόρφωση λόγω μετακίνησης $\epsilon_{q,d}$, (β) συνολική διατμητική παραμόρφωση $\epsilon_{t,d}$

7.5.6 Permissible rotation and settlement for Combination 2

The evolution of the rotation's components in the longitudinal and transverse direction of the bridge, θ_x and θ_y respectively, are shown in Figure 7.97, while the ones of the resultant rotation and the uniform settlement ρ are illustrated in Figure 7.98. The dotted lines refer to the values at the time of the first yield of the pier's columns. Table 7.29 summarizes the values of the calculated rotations, while the values of the total rotation and settlement are listed in Table 7.30. In the cases in which the transverse rotation is dominant, the permissible settlement are close to 30cm, exceeding the limit of 28cm defined in section 3.3 for the ULS. Thus, the tolerable longitudinal rotation constitutes the most severe criterion for the design of the pier's footing.

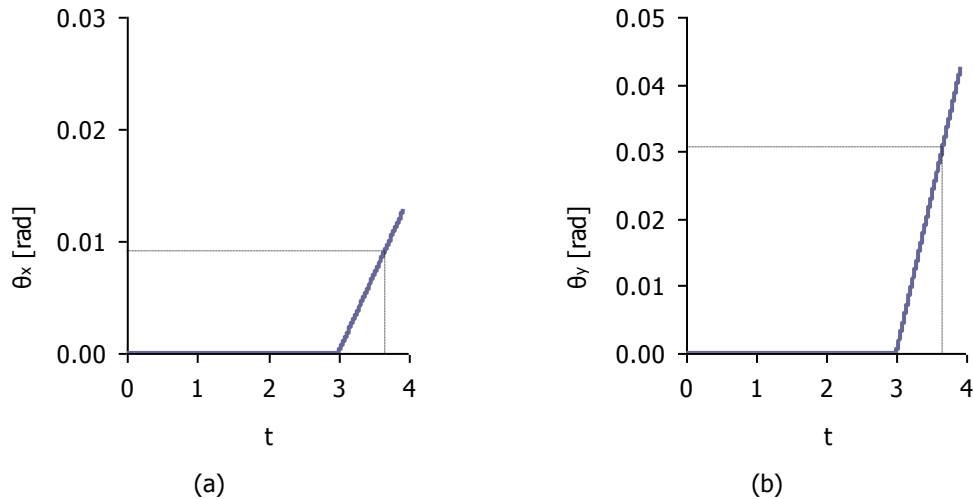


Figure 7.97: Components of the rotation vs t: (a) longitudinal θ_x , (b) transverse θ_y

Σχήμα 7.97: Συνιστώσες της στροφής συναρτήσει t: (a) διαμήκης θ_x , (b) εγκάρσια θ_y

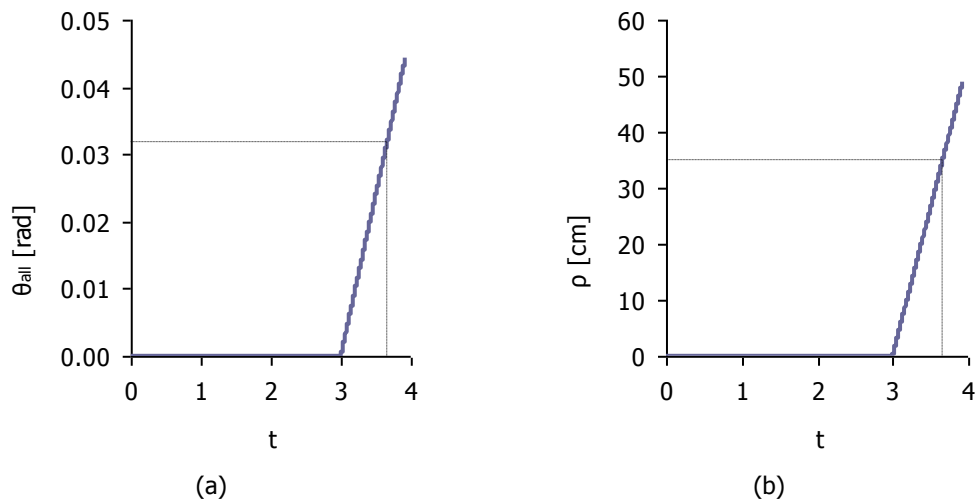


Figure 7.98: (a) Resultant rotation vs t, (b) Uniform settlement ρ vs t

Σχήμα 7.98: (a) Συνισταμένη στροφή συναρτήσει t, (b) Ομοιόμορφη καθίζηση ρ συναρτήσει t

Table 7.29: Maximum and yield values of rotations $\theta_x=0.30\theta$ and $\theta_y=\theta$

Πίνακας 7.29: Μέγιστη τιμή και τιμή στην πρώτη διαρροή διαμήκους στροφής $\theta_x=0.30\theta$, εγκάρσιας στροφής $\theta_y=\theta$

	t	θ_x [rad]	θ_x [degrees]	θ_y [rad]	θ_y [degrees]
Yield (Y)	3.664	0.0092	0.53	0.0305	1.75
Failure (F)	3.926	0.0128	0.73	0.0425	2.44

Table 7.30: Maximum, yield and permissible values of total rotation and uniform settlement ρ

Πίνακας 7.30: Μέγιστη τιμή, τιμή στην πρώτη διαρροή και επιτρεπόμενη τιμή συνολικής στροφής και ομοιόμορφης καθίζησης ρ

	t	ρ [cm]	θ_{all} [rad]	θ_{all} [degrees]
Yield (Y)	3.664	35.0	0.0319	1.83
Failure (F)	3.926	48.8	0.0445	2.55
Permissible (P=Y/1.15)	–	30.4	0.028	1.59

7.5.7 Inclination angle of the pier for Combination 2

The evolution of the inclination angle θ_i of the pier's columns is shown in Figure 7.99. At failure, the inclination angle reaches the value of $\theta_{i,F}=0.0317\text{rad}=1.82^\circ$, the one at the first yield is $\theta_{i,Y}=0.0234\text{rad}=1.34^\circ$, and the one that corresponds to the permissible settlement and rotation is:

$$\theta_{i,P} = \theta_{i,Y}/\xi\gamma_G = 0.0203\text{rad} = 1.17^\circ < \max\theta_i = 0.04\text{rad} \quad (7-12)$$

The inclination angle of the pier results in all cases smaller than the max permissible angle, defined in section 3.3, thus, this criterion is not the most crucial for the design of the bridge's footing.

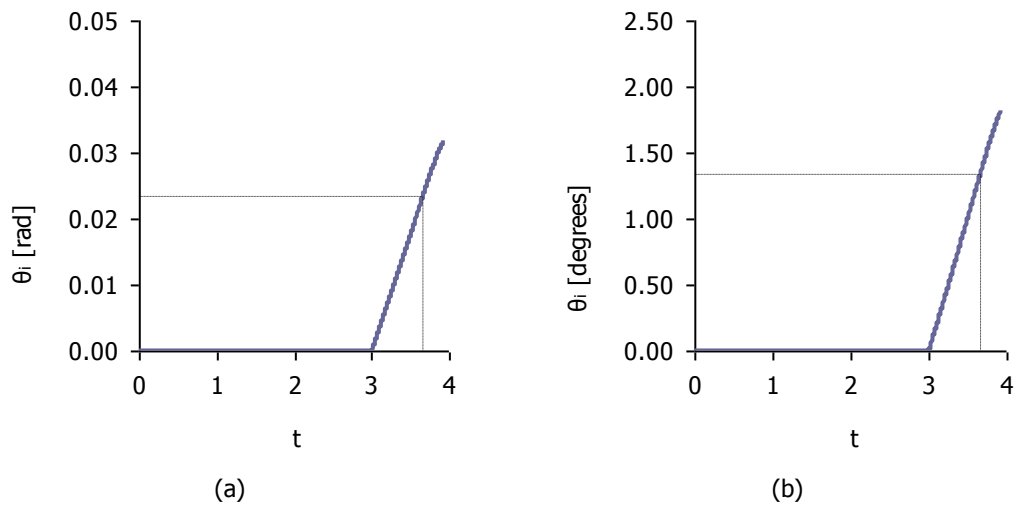


Figure 7.99: Inclination angle of the pier's columns θ_i vs t in (a) [rad] and (b) [degrees]

Σχήμα 7.99: Γωνία κλίσης στύλων μεσοβάθρου θ_i σε σχέση με το χρόνο σε (a) [rad] και (b) [μοίρες]

Chapter 8

SUMMARY AND CONCLUSIONS

The bridge under investigation is a steel arch road bridge with two simply supported spans, with total length 87.60m. The steel members of each span include two main beams, seventeen transverse beams, two arches connected with transverse and diagonal bracing members. Each main beam is suspended by each arch with seven hangers. A composite deck is formed using trapezoidal profiles and a concrete slab. The concrete slab is connected with the transverse and main beams through steel shear connectors in order to ensure composite action. The pier consists of three circular reinforced concrete columns. They are connected at the top with a concrete beam, forming thus a frame in the transverse direction of the bridge. Fixed supports are considered at the base of the columns.

The bridge is founded on liquefaction susceptible soil using spread footings. Additional permanent ground movements, by means of settlements and rotations may evolve after a major earthquake event. The behavior of the bridge is investigated in order to determine the permissible ground movements without loss of its serviceability and resistance. These permissible settlements and rotations will be used for the design of the pier's footing.

Rotations about the transverse and longitudinal axes of the bridge are considered, as well as a combination of these two rotations. Corresponding settlements are always taken into account combined with these rotations. Hence, four cases of rotation and settlement combination are considered, each for two loading combinations. In all cases, the first combination which takes into account both permanent and live loads was proved to be the most unfavorable for the superstructure, i.e. the steel members, while the second one, including only the permanent loads, was the most unfavorable for the pier's columns, leading to smaller values of axial forces and thus flexural resistance. In any case, the steel members never reach failure. In some cases the diagonal bracing members exceed the yield stress $f_y=355\text{MPa}$, due to inelastic buckling, but considering them replaceable, they do not denote a total failure of the bridge.

In all cases, failure occurs at the pier's columns, but, since a simply supported bridge is investigated, plastic hinges at the base of the columns are not allowed, because they would lead to the collapse of the bridge. Thus, when imposed rotations about the transverse axis of the bridge prevail, large values of bending moments evolve at the base of the pier. In these cases, the first yield defines the permissible settlements. Nevertheless, plastic hinges at the top of the columns are permitted, caused by dominant longitudinal rotations imposed at the pier's foundation. In these cases, the formation of the first flexural failure determines the permissible settlements, while plastic hinges are formed at the top of all three columns of the pier. This investigation proves that, for the specific pier consisting of three circular columns, the longitudinal rotation at the foundation is more critical than the transverse one. For all cases and load combinations considered, the permissible settlements are summarized in Table 8.1. In the cases in which the transverse rotation prevails the permissible settlement are close to 30cm, which is larger than the limit of 28cm for the ULS. The smallest value of the permissible settlements, which defines the allowable p for the design of the pier's footing, is

for the cases in which the longitudinal rotation prevails. The design of the pier's foundation will be based on a permissible settlement equal to 24cm.

Table 8.1: Permissible values of rotation θ and uniform settlement ρ and corresponding inclination angles of the pier's columns θ_i

Πίνακας 8.1: Επιτρεπόμενη τιμή στροφής θ και ομοιόμορφης καθίζησης ρ και αντίστοιχες γωνίες κλίσης των στύλων μεσοβάθρου θ_i

Case	Combination	ρ [cm]	θ [rad]	θ [degrees]	θ_i [rad]	θ_i [degrees]
1 ($\theta_x + \rho$)	1	24.4	0.021	1.22	0.0090	0.52
	2	24.8	0.022	1.24	0.0088	0.50
2 ($\theta_y + \rho$)	1	33.8	0.030	1.70	0.0228	1.30
	2	29.9	0.026	1.50	0.0194	1.11
3 ($\theta_x + 0.3\theta_y + \rho$)	1	24.3	0.022	1.27	0.0103	0.59
	2	24.8	0.023	1.30	0.0101	0.58
4 ($0.3\theta_x + \theta_y + \rho$)	1	34.4	0.031	1.80	0.0239	1.36
	2	30.4	0.028	1.59	0.0203	1.17

Chapter 9

REFERENCES

- [1] Barker R.M., Duncan J.M., Rojiani K.B., Ooi P.S.K., Tan C.K., and Kim S. G. "Manuals for the Design of Bridge Foundations", NCHRP Report 343, Transportation Research Board, National Research Council, Washington D.C., 1991.
- [2] Wahls H.E. "Synthesis of Highway Practice 159: Design and Construction of Bridge Approaches", Transportation Research Board, National Research Council, Washington, D.C., 1990.
- [3] Naresh C., Samtani N.C., Nowatzki E.A. and Mertz D. "Selection of Spread Footings on Soils to Support Highway Bridge Structures", Report No. FHWA RD/TD-10-001, Federal Highway Administration, U.S. Department of Transportation, 2010.
- [4] Moulton L.K., GangaRao H.V.S. and Halvorsen G.T. "Tolerable Movement Criteria for Highway Bridges", Report No. FHWA RD-85-107, Federal Highway Administration, U.S. Department of Transportation, 1985.
- [5] Bozozuk M. "Bridge foundations move", TRB Research Record, Vol. 678, pp. 17-21, 1978.
- [6] Walkinshaw J.L. "Survey of bridge movements in the Western United States", TRB Research Record, Vol. 678, pp. 6-12, 1978.
- [7] Grover R.A. "Movements of bridge abutments and settlements of approach pavements in Ohio", TRB Research Record, Vol. 678, pp. 12-17, 1978.
- [8] DiMillio A.F. "Performance of Highway Bridge Abutments on Spread Footings on Compacted Fill", Report No. FHWA RD-81-184, Federal Highway Administration, U.S. Department of Transportation, 1982.
- [9] Wahls H.E. "Shallow Foundations for Highway Structures", NCHRP Report 107, Transportation Research Board, National Research Council, Washington, D.C., 1983.
- [10] Stark T.D., Olson S.M. and Long J.H. "Differential Movement at the Embankment / Structure Interface - Mitigation and Rehabilitation", Report No. IAB-H1 FY93, Illinois DOT, Springfield, Illinois, 1995.
- [11] AASHTO "Standard Specifications for Highway Bridges" American Association of State Highway and Transportation Officials, Washington, D.C., 2002.
- [12] AASHTO ". AASHTO LRFD Bridge Design Specifications" 4th Edition, American Association of State Highway and Transportation Officials, Washington, D.C., 2007 with 2009 Interims.

- [13] EN 1992-2 "Design of concrete structures – Part 2: Concrete bridges" European Committee for Standardization, Brussels, 2005
- [14] EN 1997-1 "Geotechnical design – Part 1: General rules" European Committee for Standardization, Brussels, 2004
- [15] EN 1998-2 "Design of structures for earthquake resistance - Part 2: Bridges" European Committee for Standardization, Brussels, 2005
- [16] Rossetto T., Kappos A.J., Kouris L.A., Indirli M., Borg R.P., Lloyd T.O. and Sword-Daniels V. "Comparison of damage assessment methodologies for different natural hazards", Proceedings of COST Action C26 Final International Conference on Urban habitat construction under catastrophic events, Naples, Italy, 2010.
- [17] FEMA-356 "Prestandard and Commentary for the Seismic Rehabilitation of Buildings" ASCE, FEMA, Washington, D.C., 2000.
- [18] ADINA R & D Inc. "Theory and Modeling Guide. Volume I: ADINA, Report ARD 08-7", 2006.
- [19] SOFiSTiK v.23, Finite Element Software, SOFiSTiK AG, Germany, 2006.
- [20] Response-2000 v.1.0.5, Reinforced Concrete Sectional Analysis using the Modified Compression Field Theory, Evan C. Bentz and Michael P. Collins, 2000.
- [21] MyBiAxial v. 2.0.37, Charalampakis A.E. and Koumoussis V.K., National Technical University of Athens (NTUA), Department of Civil Engineering, Institute of Structural Analysis and Aseismic Research, 2005.
- [22] Charalampakis A.E. and Koumoussis V.K. "Ultimate strength analysis of composite sections under biaxial bending and axial load", Advances in Engineering Software, Vol. 39, pp. 923–936, 2008.